Characterization of a new virulence factor secreted by the plant pathogenic bacteria Dickeya dadantii

Lulu Liu

N°d'ordre NNT : 2019LYSEI020

THESE de DOCTORAT DE L'UNIVERSITE DE LYON
opérée au sein de
INSA de Lyon

Ecole Doctorale N° ED341
ÉVOLUTION, ÉCOSYSTÈME, MICROBIOLOGIE, MODÉLISATION

Spécialité / discipline de doctorat :

Microbiologie moléculaire

Soutenue publiquement le 05/04/2019, par :

Lulu LIU

Characterization of a new virulence factor secreted by the plant pathogenic bacteria *Dickeya dadantii*

Devant le jury composé de :

SCHALK, Isabelle	Directeur de Recherche	Université de Strasbourg
BARNY, Marie-Anne	Directeur de Recherche	Sorbonne Université
JAFRA, Sylwia	Professeur	Université de Gdansk
LEJEUNE, Philippe	Professeur	INSA-LYON
CONDEMINE, Guy	Directeur de Recherche	Université Lyon1

Directeur de thèse

Acknowledgements

This research was worked on in the co-operation project of China Scholarship Council with the UT-INSA of France. Thanks for the grant supported by China Scholarship Council and the opportunity provided by the UT-INSA program.

I am really grateful to my supervisor Dr. Guy Condemine for giving me the occasion to complete the thesis in France, for picking me up at the airport when I arrived in France alone, and for his academic guidance and help in cultivating my experimental thinking and valuable suggestions for conducting scientific experiments. Thanks for all that he did for my study and life during the past 42 months.

I really appreciate that the director of UMR5240 Dr. William Nasser, and Dr. Sylvie gave me their continuous encouragement and helped when I encountered barriers in my research.

Also, I owe special thanks to Dr. Agnès Rodrigue for her help and guidance in many of my experiments.

I would like to extend my deep gratitude to Dr. Nicole Cotte-Pattat, for her help and corrections in my manuscript. I also want to thank Dr. Vladimir Shevchik for his advice given on the normative experimental operation in the beginning of my research in the lab of MAP.

Thanks Florence Ruaudel and Natalia Guschinskaya for giving me a lot of technical support and helping me practice French speaking. Thanks to the preparation of experimental materials by Véronique Utzinger and Jean-Michel Prost. I am also very grateful to the secretary of the laboratory Isabelle Thevenoux.

Thanks for the help of Shiheng Zhang and all my friends in China and France who gave me a lot of encouragement and support.

Last but not least, I am deeply indebted to my family and those who love me, who have been accompanying me all the way and shared with me all my worries, frustrations, and happiness.

Table of contents

List of abbreviations

ABC: ATP binding cassette

Amp: Ampicillin

AS: Specific activity

ATD: Amino terminal domain

ATP: Adenosine triphosphate

BCSA: Bathocuproine disulfonic acid

Cm: Chloramphenicol

CWDE: Cell wall-degrading enzymes

DAMP: Damage-Associated Molecular Pattern

DNA: Deoxyribonucleic acid

EDTA: Ethylenediaminetetraacetic acid

EF-Tu: Elongation factor thermo unstable

EHEC: Enterohaemorrhagic *Escherichia coli*

ETEC: Enterotoxigenic *Escherichia coli*

ETI: Effector-Triggered Immunity

GPCR: G-protein coupled receptor

GST: Glutathione S-transferase

GUS: β-glucuronidase

HC-toxin: *Helminthosporium carbonum* toxin

HR: Hypersensitive cell death response

IM: Inner membrane

IPTG: Isopropyl β-D-Thiogalactoside

MDR: Multidrug resistance protein

MES: 2-(N-morpholino) ethanesulfonic acid

MFS: Major facilitator superfamily

MRP: Multidrug resistance-associated protein

NBD: Nucleotide-binding domain

NLP: Nep-1 like protein

NLS: Nuclear localization signal

OD: Optical density

OM: Outer membrane

ONP: Ortho-nitrophenol

ONPG: Ortho-nitrophenyl-β-galactoside

PAMPs: Pathogen-Associated Molecular Patterns

PCR: Polymerase chain reaction

PRR: Pattern recognition receptor

PTI: Pattern-Triggered Immunity

PVDF: Polyvinylidene fluoride

RLK: Receptor-like kinase

RLP: Receptor-like protein

ROS: Reactive oxygen species

SA: Salicylic acid

SAR: Systemic Acquired Resistance

SBD: Substrate-binding domain

SDS: Sodium dodecyl sulfate

JA: Jasmonic acid

LAR: Localized Acquired Resistance

LB: Luria Bertani

LCG: Medium L Glucose Calcium

LPS: Lipopolysaccharide

LRR: Leucine-rich repeat

MAMP: Microbe-Associated Molecular Pattern

MAP: Mitogen-activated protein

MAPK: Mitogen-activated protein kinase

SDS-PAGE: Sodium dodecyl sulfate polyacrylamide gel electrophoresis

T2SS: Type II secretion system

T3SS: Type III secretion system

Tat: Twin arginine translocation

TBDR: TonB-Dependent Receptor

TCA: Tricarboxylic acid

TMD: Transmembrane domain

TRAP: Tripartite ATP-independent periplasmic transporter

TTT: Tripartite tricarboxylate transporter

List of figures and tables

List of figures

List of tables

Summary

Few secreted proteins involved in plant infection common to necrotrophic bacteria, fungi and oomycetes have been identified except for plant cell wall-degrading enzymes. Herein, we have characterized the structure and properties of a protein (IbpS) secreted by the plant pathogenic bacterial necrotroph *Dickeya dadantii*. Homologs of this protein are present in not only $Gram^+$ bacteria but also in fungi, oomycetes, most phytopathogens, and some animals. The gene originating from bacteria was transferred once in oomycetes and most likely several times in fungi. IbpS is capable of binding the redox-active metals iron and copper and has a classical Venus Fly trap fold with some original characteristics: it forms dimers in solution and has a novel metal binding site. IbpS is involved in *D. dadantii* and of the *Botrytis cinerea*, a fungal necrotroph, infection process. We propose that secreted IbpS binds exogenous iron and copper, reducing their intracellular concentrations of these metals and ROS formation in the microorganisms. Secretion of this metal scavenging protein appears to be a common antioxidant protection mechanism shared by necrotrophic phytopathogens and required during infection.

Key words : *Dickeya dadantii*, necrotrophic phytopathogens, type II secretion system, IbpS, reactive oxygen species (ROS), virulence, Venus Fly trap

Résumé

Peu de protéines nécessaires à l'infection des plantes communes aux bactéries, aux champignons et aux oomycètes ont été identifiées à part les enzymes dégradant les parois des cellules végétales. Nous avons caractérisé la structure et les propriétés d'une protéine, IbpS, sécrétée par la bactérie phytopathogène nécrotrophe *Dickeya dadantii*. Des homologues de cette protéine sont présents non seulement chez des bactéries à $Gram^+$ mais aussi chez des champignons, des oomycètes et quelques animaux. Ce gène d'origine bactérienne a été transféré une fois chez les oomycètes et probablement plusieurs fois chez les champignons. IbpS peut fixer le fer et le cuivre, des métaux à activité redox. Elle a une structure en Venus Fly Trap classique mais avec des caractéristiques originales : elle forme des dimères en solution et possède un nouveau mode de fixation du métal. IbpS est impliquée dans le processus infectieux de *D. dadantii* et de *Botrytis cinerea*, un champignon phytopathogène nécrotrophe. Nous proposons qu'IbpS, une fois sécrétée, fixe le fer et le cuivre exogène, réduisant ainsi leur concentration intracellulaire et la formation de ROS dans le microorganisme. La sécrétion de cette protéine fixant les métaux semble être un mécanisme de protection contre l'oxydation requis pendant l'infection partagé par des phytopathogènes nécrotrophes.

Mots clés : *Dickeya dadantii*, phytopathogènes nécrotrophes, système de sécrétion de type II, IbpS, espèces d'oxygène réactif (ROS), virulence, Venus Fly trap

General introduction

I The infectious cycle of phytopathogenic microbes

Plants are constantly attacked by a variety of pathogens, including bacteria, fungi and viruses. Depending on their lifestyle, plant pathogens can be divided into two major categories – Biotrophs and Necrotrophs. Biotrophs are pathogens that acquire nutrients from living host tissues, while necrotrophs are pathogens that acquire nutrients from dead or dying cells (Agrios, 1997). Most bacteria and viruses are considered to be biotrophic organisms, and most fungi adopt necrotrophic lifestyle (Glazebrook, 2005). However, many others which behave as both biotrophs and necrotrophs are called hemi-biotrophs, depending on the conditions in which they find themselves or the stages of their life cycles. Many fungi that are generally considered necrotrophs may really be hemi-biotrophs because they have a biotrophic stage in the early infection process. Bacterial plant pathogens cause relatively less damage and economic costs worldwide compared to fungi and viruses (Laluk and Mengiste, 2010). Bacteria may be present on plants with or without any signs of developing symptom. Bacteria belonging to biotrophs or hemi-biotrophs pathogens interact with host plants through specialized genes and mechanisms to infect or colonize plants. The association of bacteria with plants may be harmful or beneficial. Some bacterial species, such as saprophytic bacteria do not cause disease in plants, so they are considered to be non-pathogens (Glazebrook, 2005) (Figure 1).

I.1 Biotrophs

Biotrophs develop on living tissues and feed on them by maintaining a tightly regulated interaction where the microbe does not kill its host (Ökmen and Doehlemann, 2014). Biotrophy is a pervasive trait that evolved independently in plant pathogenic

fungi and oomycetes (Figure 1). Biotrophic pathogens have coevolved pathogenesis mechanisms that maneuver host physiology to maintain host viability and thrive on nutrients from live host cells (Mendgen and Hahn, 2002). They secrete limited amounts of CWDEs and generally lack toxin production. Highly developed infection-related structures, such as haustoria, which are specialized hyphae for nutrient absorption and metabolism, also distinguish most obligate biotrophs.

The obligate oomycte pathogen *Phytophthora parasitica* is perhaps the clearest example of an *Arabidopsis* biotroph. Compatible infection begins with germination of conidia on the leaf surface (Glazebrook, 2005). Appressoria form, resulting in hyphal penetration of epidermal cells and formation of haustoria within these cells. Haustoria are separated from the host cytoplasm by a host membrane that is continuous with the plasma membrane. Hyphae subsequently grow throughout the leaf, penetrating mesophyll cells and forming additional haustoria there. Conidiophores emerge from stomata, and mature conidia are formed after about one week. Then the oospores are formed through sexual reproduction. The infected plant cells remain alive throughout this process. Heavily infected seedlings sometimes die, but only after sporulation is complete (Koch and Slusarenko, 1990). The ascomycete fungi *Erysiphe orontii* and *Erysiphe cichoracearum* are also good examples of obligate biotrophs. Compatible isolates of these fungi infect epidermal cells, develop haustoria, and sporulate profusely, without causing host cell death (Reuber *et al*., 1998; Vogel and Somerville, 2000).

The bacterial pathogen *Pseudomonas syringae* is often considered a biotroph, occasionally a necrotroph (Butt *et al*., 1998), and should probably be considered a hemi-biotroph (Glazebrook, 2005). The bacteria infect through wounds and stomata and multiply in the intercellular spaces. Host cells keep alive in the early stages of compatible infections, but it is associated with host tissue chlorosis and necrosis in the later stages of infection. Many strains, including *P. syringae pv. tomato* DC3000, which infects *Arabidopsis*, produce toxins that contribute to pathogenicity (Preston, 2000). Like many bacterial pathogens of animals, *P. syringae* actively transports dozens of proteins into host cells through a specialized system known as type III secretion. These

proteins are called type III effectors and are thought to contribute to virulence. Several of them have been shown to contribute to virulence in *Arabidopsis* (Alfano and Collmer, 2004; Espinosa and Alfano, 2004).

I.2 Necrotrophs

Necrotrophs are bacterial, fungal and oomycete species that extract nutrients from dead cells killed prior to or during colonization, resulting in extensive necrosis, tissue maceration, and plant rots. When the host fails to constrain initial necrosis, diseases culminate in the death and decay of the entire plant. By contrast, biotrophic pathogens deploy complex and co-evolved biological strategies to exploit their hosts while keeping them alive in order to complete their life cycle. To cause disease, bacterial necrotrophs secrete virulence factors into host tissue both prior to and during colonization, with primary infection involving the formation of expanding necrotic lesions (Alfano and Collmer, 1996; Walton, 1996). Some of these factors include phytotoxins, cell wall degrading enzymes (CWDEs), and other necrosis inducing proteins resulting in soft rot diseases (Alfano and Collmer, 1996; Pemberton and Salmond, 2004). Additionally, bacteria are not able to actively penetrate the leaf surface, relying instead on natural openings and wounds to gain entrance into the intracellular space. Some bacteria also utilize quorum sensing to enhance disease and evade host defenses (Alfano and Collmer, 1996). In quorum sensing, bacteria use cell to cell signaling to induce virulence gene expression only when the population density has reached a level high enough to overwhelm host responses.

Necrotrophs are further divided into host-specific and broad host-range species. Host-specific necrotrophs produce essential host-specific toxins for their pathogenicity and virulence on their hosts (Wolpert *et al*., 2002). For example, the fungal pathogen *Cochliobolus carbonum* produces HC-toxin, and its infection is limited to susceptible genotypes on which it causes the Northern corn leaf spot (Walton, 1996). The fungal pathogens *Botrytis cinerea*, *Alternaria brassicicola*, *Plectosphaerella cucumerina*, and

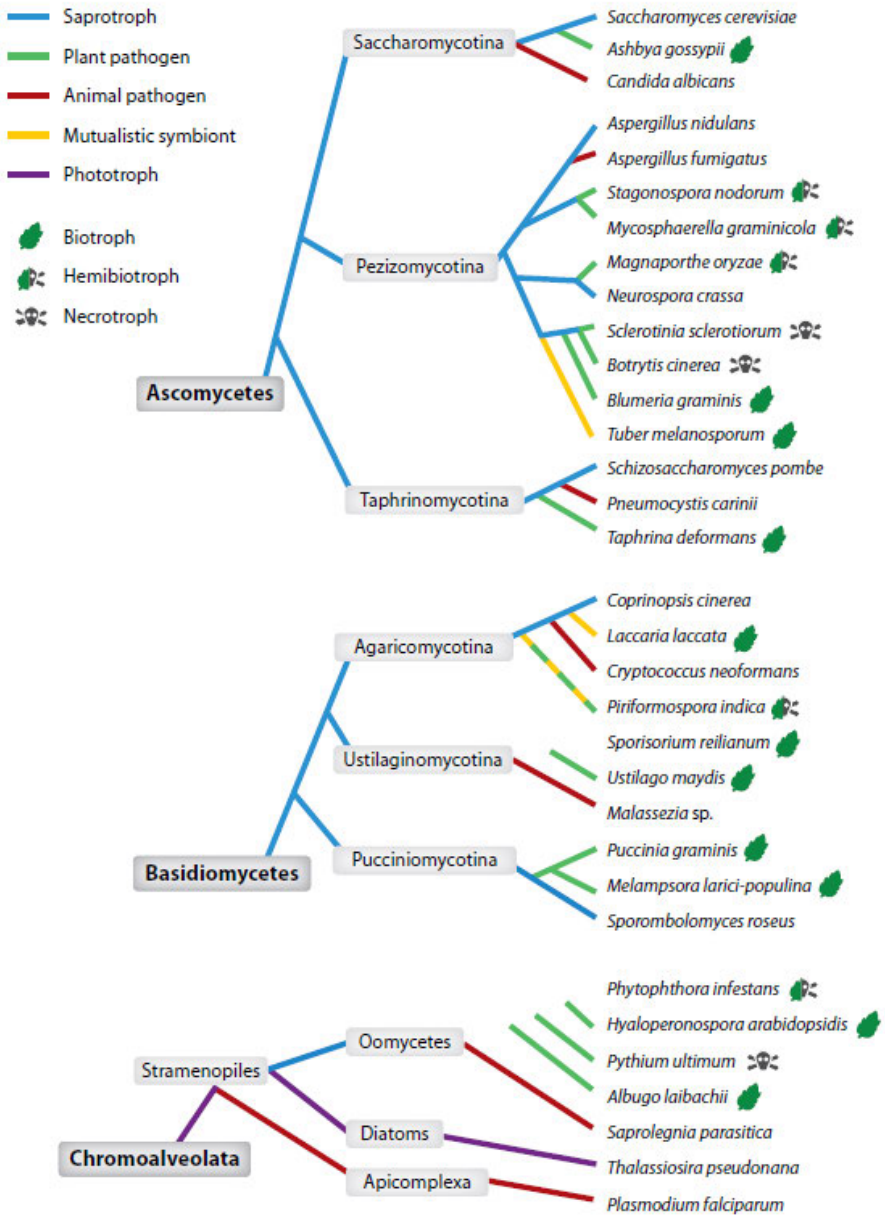

Figure 1 Pathogenesis is polyphyletic.

Phylogenies of eukaryotic microbes show how plant (green) and animal (red) pathogenic lifestyles have evolved independently and repeatedly from saprotrophic (blue) or photosynthetic (purple) lineages. Biotrophy and necrotrophy are also polyphyletic. (Spanu, 2012)

Sclerotinia sclerotiorum and the bacterial pathogen *Pectobacterium carotovorum* are archetypical broad host-range necrotrophs (Amselem *et al*., 2011; Laluk and Mengiste, 2010; Mbengue *et al*., 2016). Broadly, the necrotrophic mode of nutrition is linked to pro-death virulence strategies. Immune responses to different necrotrophs vary depending on the primary determinant of virulence, which in turn influence the nature of effective host immune responses that have evolved to counter infection. Regardless the lifestyle of pathogens, there exists overlapping immune responses and interwoven genetic regulators. The multiplicity of virulence mechanisms targeting diverse host cellular processes matches the complexity of the host immune system (Mengiste, 2012).

I.3 Hemi-biotrophs

Hemibiotrophs have an initial biotroph lifestyle followed by necrotrophy. *M. graminicola*, also known as *Septoria tritici*, which causes wheat leaf blotch is an ascomycete of the Dothideomycetes (Spanu, 2012). The outbreaks of this disease are capable of reducing yields by 30–40% to wheat (Palmer and Skinner, 2002). This class includes many other plant pathogenic fungi (e.g., *Venturia inequalis*, *Cochliobolus heterostrophus*, *Mycosperella fijiensis*, *Cladosporium fulvum*, and *Stagonospora nodorum*). *Colletotrichum* spp. or *Magnaporthe oryzae*, initially develop an intracellular bulged hypha encased by the plant plasma membrane which does not kill the plant cell, and later switch to a thin intracellular necrotrophic hypha and cause extensive tissue death (Kraepiel and Barny, 2016). Whole-genome sequences and comparative analyses have started to reveal the genetic bases of obligate biotrophy (Baxter *et al*., 2010; Duplessis *et al*., 2011; Spanu *et al*., 2010), from necrotrophy (Amselem *et al*., 2011) to complete saprotrophy (Espagne *et al*., 2008; Soanes *et al*., 2008) which will undoubtedly expedite molecular and genetic dissection of plant immunity to pathogens and provide newer avenues for more imaginative crop protection approaches.

II *Dickeya dadantii*

II.1 The *Pectobacterium* and *Dickeya* genera

A recent reanalysis of the enterobacteriales order defined seven families among which the pectobacteriaceae family that contains the plant pathogenic bacteria *Pectobacterium*, *Dickeya*, *Brenneria*, *Lonsdalea* and *Sodalis* (Adeolu, 2016). Pectinolytic enterobacteria were at a time grouped in the genus *Pectobacterium* which was later divided into the two genera *Pectobacterium* and *Dickeya* (Samson *et al*., 2005). Six *Dickeya* species (Table 1) were first described: *D. dadantii*, *D. dieffenbacchiae*, *D. chrysanthemi*, *D. zeae, D. paradisiaca* and *D. dianthicola*. Subsequently, *Dickeya dieffenbachiae* has been reclassified as *D. dadantii* subsp. *dieffenbachiae* (Brady *et al*., 2012). Recently new species have been described: *D. solani*, a highly virulent pathogen of potato, *D. aquatica*, found in freshwater rivers (Parkinson *et al*., 2014), *D. fangzhongdai* that infects pear trees (Tian *et al*., 2016) and very recently *D. lacustris* found in a pound in the Dombes region (Hugouvieux-Cotte-Pattat *et al*., 2019), *D. poaceaphila* and *D. undicola* identified after a reanalysis of *Dickeya* phylogeny (Reverchon, communication personnelle**)**.

Dickeya provoke soft rot disease, caused primarily by secreted pectinases that degrade pectin in the middle lamella of plant cell walls, in a wide range of crop plants summarized in Table 1 (Charkowski, 2018). They can also cause decay diseases named blackleg in potato (Figure 2), foot rot in rice and bleeding cancer in pear tree. In Europe, the main economical damages are provoked on potato by *D. dianthicola* and *D. solani*. The primary pathogen species present in potato-growing regions differs over time and space, further complicating disease management. *D. dadantii*, the most studied *Dickeya* strain (Glasner *et al*., 2011) is mainly found in tropical and sub-tropical countries. The *D. dadantii* strain 3937 used in this study was isolated in the 80s on a saintpaulia plant.

Name	Hosts
D. dadantii,	*Pelargonium*, *Dianthus* spp., pineapple, potato, *Euphorbia*, sweet potato, banana, maize, *Philodendron*, *Saintpaulia*
D. dadantii subsp. *dieffenbachiae*	*Dieffenbachia*, tomato, banana
D. chrysanthemi	*Chrysanthemum spp*., potato, chicory, tomato, sunflower
D. zeae	Maize, rice, potato, pineapple, banana, tobacco, *Brachiaria, Chrysanthemum spp.*
D. paradisiaca	Banana
D. dianthicola	*Dianthus spp.*, potato, tomato, chicory, artichoke, *Dahlia*, *Kalanchoe*
D. solani	Potato, muscari
D. aquatica	-
D. fangzhongdai	Pear, *Phalaenopsis colocasia aglaonema*
D. lacustris	-
D. poaceaphila	Sugar cane
D. undicola	-

Table 1 Currently named members of the genus *Dickeya*, their synonyms and main hosts.

adapted from Samson *et al* (Samson *et al*., 2005)

II.2 Pathogenic mechanisms of *D. dadantii*

II.2.1 The virulence factors secreted by *D. dadantii*

Many factors important for *D. dadantii* virulence have been identified and characterized. The main virulence factor is the Out type II secretion system and the proteins it secretes. These proteins are mostly CWDEs, including a full set of pectinases. Most of these pectinases are active on the homogalacturanate part of pectin: the pectin methylesterase PemA, the pectin acetylesterase PaeY, the pectate lyases PelA, PelB, PelC, PelD, PelE, PelI, PelL, PelN and PelZ. RhiE is an endorhamnogalacturonate lyase that cleaves the rhamnogalacturonate I chain of pectin (Hugouvieux‐Cotte‐Pattat *et al.*, 2014). In addition, the feruloylesterase FaeD cleaves side chains of pectin (Hassan and Hugouvieux-Cotte-Pattat, 2011). The cellulase Cel5 cleaves the cellulose chains. Other proteins with no known enzymatic activity have been detected in the Out-dependent supernatant of *D. dadantii*: the necrosis inducing toxin NipE, and two proteins similar to avirulence proteins of *Xanthomonas*, AvrL and AvrM (Kazemi‐Pour *et al.*, 2004). *D. dadantii* possesses a type I secretion system that secretes 4 proteases, PrtA, PrtB, PrtC and PrtG. Mutants in this secretion system display delayed symptoms. Type III secretion systems are the main responsible of biotrophic bacteria virulence. They often secrete multiple effectors inside the plant host. In *D. dadantii*, only three proteins that could be secreted by the T3SS have been identified: the effector DspE and two harpins, HrpN and HrpW. *D. dadantii* possesses 2 type V and 3 type VI secretion systems, but these systems are involved in killing of other microorganisms and they do not seem to play a role in plant virulence.

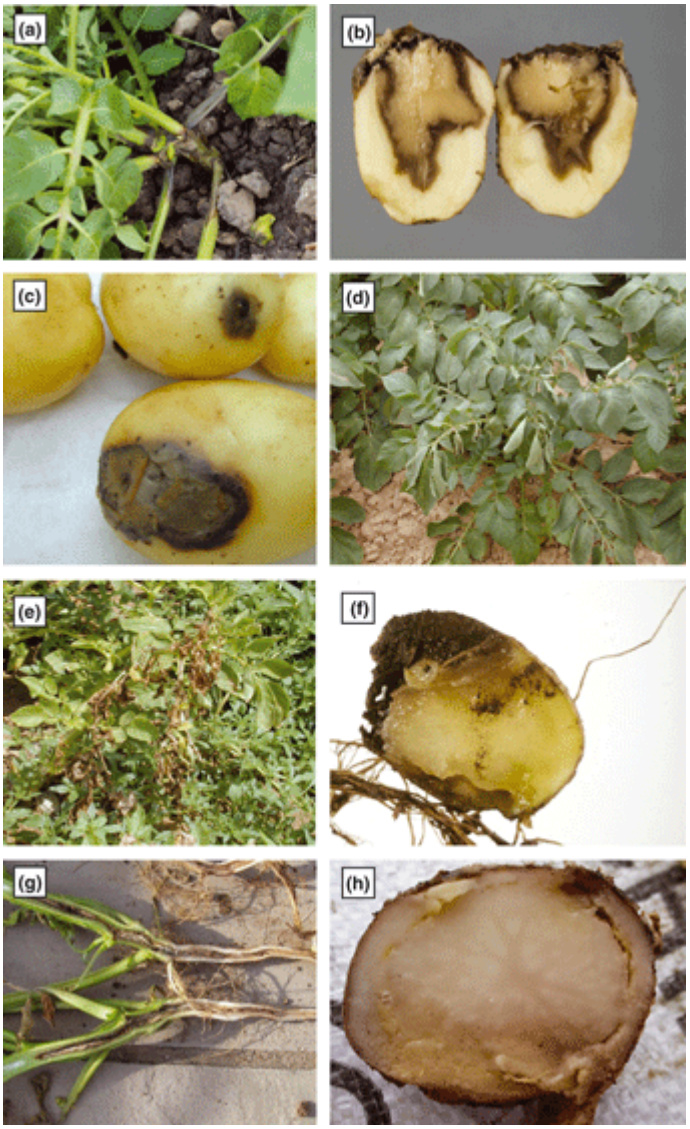

Figure 2 Disease symptoms in potato tubers and stems caused by *Dickeya* species.

(a) typical blackleg symptoms caused by '*Dickeya solani*'; (b) '*Dickeya solani*' soft rot of developing progeny tuber extending from the stolon; (c) soft rot of daughter tubers developing from the stolon; (d) initial wilt in upper leaves; (e) increased levels of necrosis in the upper leaves and wilt and desiccation in the lower leaves; (f) *D. dianthicola* rotting mother tuber; (g) internal stem necrosis or rotting extending from the stem base, but with the stem base appearing externally healthy; (h) '*Dickeya solani*' on imported potato causing cheesy rot and break down of the vascular ring similar to ring rot or brown rot. (Toth *et al*., 2011)

II.2.2 Type II secretion system (T2SS)

II.2.2.1 The T2SS pathway

Gram-negative bacteria use the T2SS to transport a large number of proteins from the periplasmic space into the extracellular environment. Many of the secreted proteins are major virulence factors in plants and animals (Johnson *et al*., 2006). However, it can be found in non-pathogenic species. Human pathogens with one or more T2SSs include *Vibrio cholerae*, enterotoxigenic and enterohaemorrhagic *Escherichia coli* (ETEC and EHEC, respectively), *Pseudomonas aeruginosa*, *Klebsiella* spp., *Legionella pneumophila* and *Yersinia enterocolitica*. *Aeromonas hydrophila*, a pathogen of fish and amphibia, also contains a T2SS. Plant pathogens that contain a T2SS include *D. dadantii*, *P. carotovorum, P. atrosepticum* and *Xanthomonas campestris* (which causes black rot in crucifers), among others. Non-pathogens with a T2SS gene cluster include metal-reducing bacteria such as *Shewanella oneidensis*.

T2SSs have a broad specificity and are capable of secreting a diverse array of substrates outside of the bacterial cell, some of which contribute to the virulence of bacterial pathogens (Korotkov *et al*., 2012). In some bacterial species, such as *D. dadantii*, the T2SS is required for the secretion of multiple substrates, while in others, such as *K. oxytoca*, it is only used to transport a single protein (Cianciotto, 2005). These secreted proteins have a range of biological functions, but are generally enzymes, such as proteases, lipases, and phosphatases, as well as several proteins that process carbohydrates such as CWDEs (Korotkov *et al*., 2012).

In Gram-negative bacteria, proteins secreted by a T2SS are synthesized with a sequence signal which is cleaved by the signal peptidases LepB or LspA for lipoproteins, when the proteins cross the inner membrane (Bos *et al*., 2007; Pugsley, 1993). These proteins first cross the inner membrane by the Sec or the Tat pathway (Pugsley, 1993; Voulhoux *et al*., 2001) (Figure 3). Once they are folded in the periplasm, they then

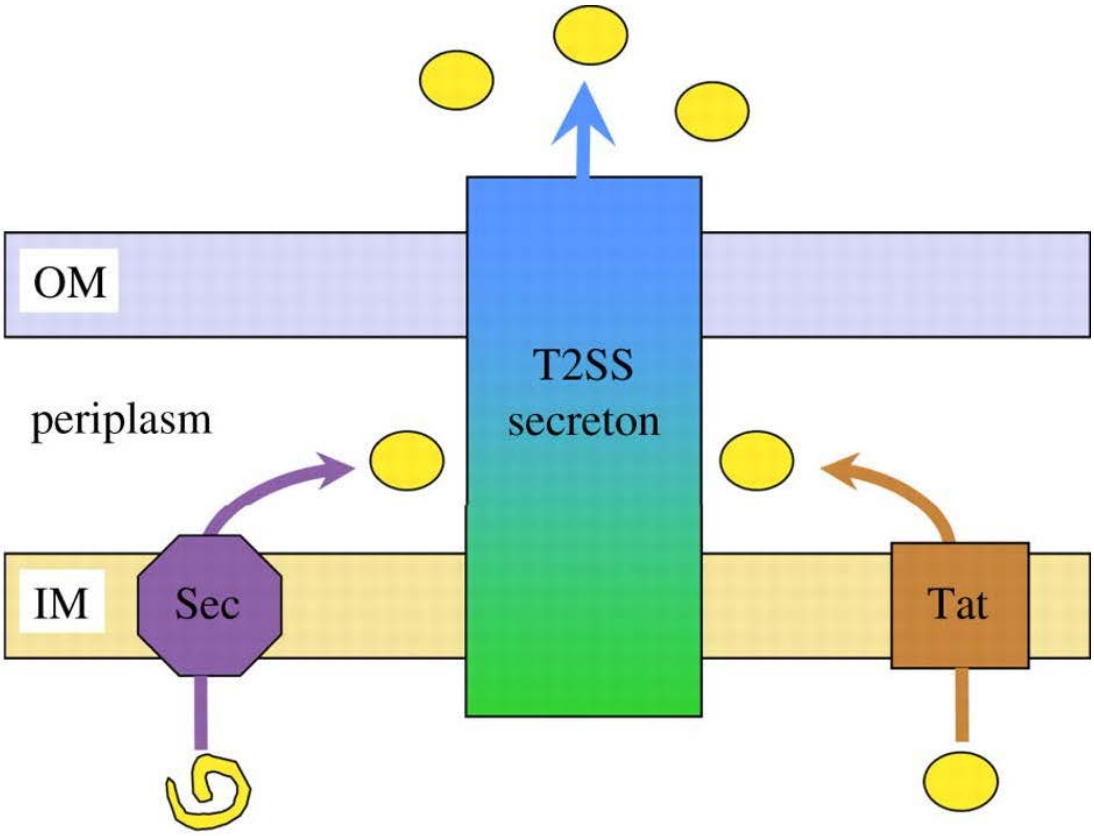

Figure 3 Sec and Tat pathway model in Gram-negative bacteria.

The T2SS-dependent exoproteins, shown as yellow circles, are first exported across the IM via the Sec (purple) or Tat (brown) machineries. The exoproteins are subsequently recognized and transported across the OM by the secreton (blue/green). (Douzi *et al*., 2012)

interact with the T2SS to cross the outer membrane (Bouley *et al*., 2001; Shevchik *et al*., 1997). The final destination of the secreted proteins is generally the outer medium, but some proteins like the *K. oxytoca* lipoprotein PulA or the *D. dadantii* PnlH remain anchored to the outer face of the outer membrane (Pugsley *et al*., 1986; Rondelet and Condemine, 2013).

This secretion system was originally called the main terminal branch of the Sec secretion pathway due to its ability to export proteins transported across the inner membrane by the Sec secretion system (Korotkov *et al*., 2012). Hence, a Gsp prefix followed by a capital letter has been proposed for the names of all T2SS proteins (Table 2). However, species specific nomenclatures still remain in use like Out for *D. dadantii*, Pul for *K. oxytoca* or Xcp for *P. aeruginosa*.

II.2.2.2 Genetic organization of T2SS

T2SSs are encoded by a set of 12 to 16 *gsp* genes organized into large operons including the genes denoted *gspC* to *O* which are highly conserved and in some bacterial species extra *gsp* genes such as *gspAB*, *gspN* or *gspS* (Figure 4). The genetic organization of the T2SS clusters is remarkably conserved. However, the position of the *gspCD* genes is peculiar in some species (Figure 4). In the *P. aeruginosa xcp* cluster, these two genes form an operon divergent from the operon containing the *gspE-M* genes. In *X. campestris*, the *gspCD* genes are found after *gspM* at the end of the *gsp* operon (Figure 4). Exceptions are with the T2SS genes in *Burkholderia pseudomallei* and *L. pneumophila*, where *gspC* and *gspD* are not next to each other.

II.2.2.3 Structure and function of T2SS

The components of the T2SS are located in both the inner and outer membranes where they assemble into a multi-protein, cell-envelope spanning, complex

Protein function	ETEC	*Vibrio cholerae*	*Aeromonas hydrophila*	*Dickeya dadantii*[‡]	*Klebsiella oxytoca*	*Pseudomonas aeruginosa*[§]	*Xanthomonas campestris*
Peptidoglycan binding		EpsA	ExeA				
Unknown function		EpsB	ExeB	OutB	PulB		
Inner-membrane platform protein, interaction with secretin	GspC	EpsC	ExeC	OutC	PulC	XcpP	XpsC[‖]
Outer-membrane secretin	GspD	EpsD	ExeD	OutD	PulD	XcpQ	XpsD
Secretion ATPase	GspE	EpsE	ExeE	OutE	PulE	XcpR	XpsE
Inner-membrane platform protein	GspF	EpsF	ExeF	OutF	PulF	XcpS	XpsF
Major pseudopilin	GspG	EpsG	ExeG	OutG	PulG	XcpT	XpsG
Minor pseudopilin	GspH	EpsH	ExeH	OutH	PulH	XcpU	XpsH
Minor pseudopilin	GspI	EpsI	ExeI	OutI	PulI	XcpV	XpsI
Minor pseudopilin	GspJ	EpsJ	ExeJ	OutJ	PulJ	XcpW	XpsJ
Minor pseudopilin	GspK	EpsK	ExeK	OutK	PulK	XcpX	XpsK
Inner-membrane platform protein	GspL	EpsL	ExeL	OutL	PulL	XcpY	XpsL
Inner-membrane platform protein	GspM	EpsM	ExeM	OutM	PulM	XcpZ	XpsM
Unknown function		EpsN	ExeN		PulN		
Prepilin peptidase	GspO	VcpD	TapD	OutO	PulO	XcpA (also known as PilD)	XpsO
Pilotin	YghG[¶]			OutS	PulS		

Table 2 Composition and species-specific nomenclature of the T2SS.

(Korotkov *et al.*, 2012)

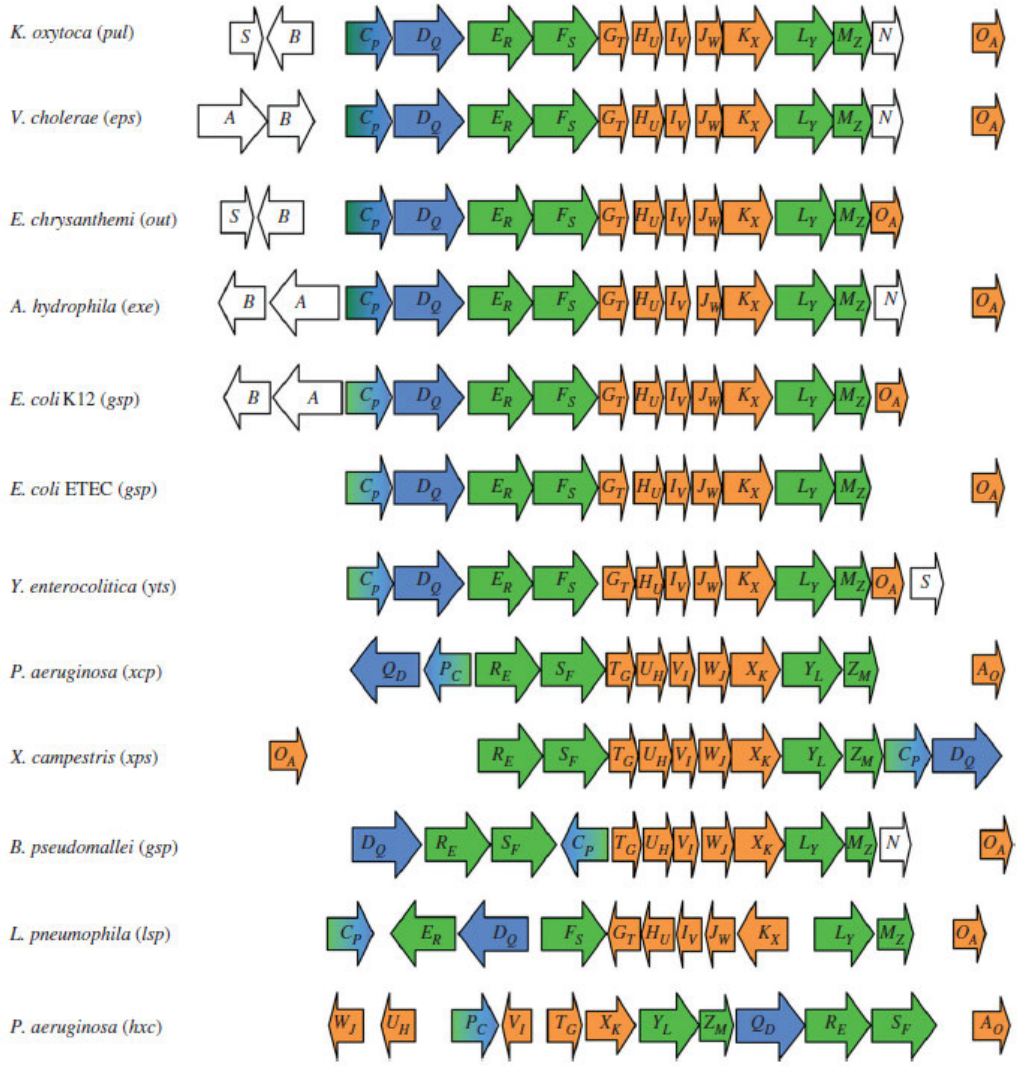

Figure 4 Genetic organization of the T2SS clusters.

The name of each T2SS gene cluster is shown in brackets beside the name of the bacterial species. Each gene is represented by an arrow and 'core' genes present in all T2SS clusters are represented in colour. The *gspE*, *F*, *L* and *M* genes encoding components of the inner membrane platform are shown in green; the *gspG*, *H*, *I*, *J* and *K* genes encoding pseudopilins and *gspO* gene encoding the prepilin peptidase are shown in orange; the *gspD* gene encoding the secretin is shown in blue; the *gspC* gene encoding the trans-periplasmic protein is represented in shaded green and blue tones because GspC is a component of the inner membrane surface interacting with secretin. The *gspA*, *B*, *N* and *S* genes that are not considered to be core components of the T2SS are represented in white. (Douzi *et al*., 2012)

(Johnson et al., 2006). T2SSs complexes consist of as many as 15 different proteins, which can be broken into four subassemblies: the outer-membrane complex, the inner-membrane platform, the secretion ATPase, and the pseudopilus (Korotkov *et al*., 2012). The outer-membrane complex resides in the outer membrane, where it serves as the channel through which folded periplasmic T2SS substrates are translocated (Korotkov *et al*., 2011). This channel is composed of GspD, a multimeric protein called the secretin (Figure 5, blue) (Brok *et al*., 1999; Nouwen *et al*., 1999). The secretin has a long N terminus, which is believed to extend all the way to the periplasm to make contact with other T2SS proteins in the inner membrane (Korotkov *et al*., 2011). The secretin often interacts with the pilotin GspS which helps its insertion in the outer membrane. The inner membrane platform (Figure 5, green) which is composed of the GspC, F, L and M IM proteins, is embedded in the inner membrane and extends into the periplasm, contacting the secretin. This platform plays a crucial role in the secretion process, by communicating with the secretin, pseudopilus, and the ATPase to coordinate export of substrates (Korotkov *et al*., 2012). The secreton also contains five proteins that display homologies with the type IV pilin PilA and are designated pseudopilins (Bally *et al*., 1992; Nunn, 1999; Nunn and Lory, 1993). These proteins have been proposed to be involved in the formation of a fibrillar piston-like structure, the pseudopilus (Figure 5**,** orange/red) (Campos *et al*., 2010; Douzi *et al*., 2009; Durand *et al*., 2003; Korotkov and Hol, 2008; Sauvonnet *et al*., 2000). The ATPase is located in the cytoplasm and provides the energy to power the system. GspE is associated with it through an interaction with the bitopic protein GspL (Arts *et al*., 2007; Bleves *et al*., 1996; Michel *et al*., 1998; Py *et al*., 2001). Whereas the proton motive force has been shown to be involved in the translocation of T2SS substrates and could drive the pseudopilus through the GspD channel, pushing out exoproteins to the external medium (Filloux, 2004; Hobbs and Mattick, 1993; Shevchik *et al*., 1997).

As its name implies, the T2SS pseudopilus is evolutionarily related and structurally similar to proteins that comprise type IV pili on bacterial cell surfaces, as well as some bacterial competence systems (Sauvonnet *et al*., 2000). Therefore, one

model for secretion through the T2SS channel proposes that these pseudopili polymerize in order to push the folded T2SS substrate through the outer membrane channel. In this "piston" model, "secretion-competent" proteins in the periplasm contact the periplasmic domain of the secretin. This interaction is believed to stimulate the cytoplasmic ATPase to drive polymerization of the T2SS pseudopili, which push proteins through the secretin channel (Hobbs and Mattick, 1993; Korotkov *et al*., 2012; Shevchik *et al*., 1997).

II.2.2.4 The *Dickeya dadantii* Stt T2SS

Sequencing of the *D. dadantii* genome led to the identification of genes that could encode a second T2SS called Stt. The Stt substrate, the protein PnlH, is not released in the outer medium but remains anchored to the outer face of the outer membrane. This anchoring occurs through an uncleaved N-terminal signal that also allows the translocation of the protein across the inner membrane via the Tat translocon. Thus, PnlH represents a new type of outer membrane protein (Ferrandez and Condemine, 2008). PnlH does not possess a cleavable signal sequence but is anchored in the outer membrane by an N-terminal targeting signal. Addition of the 41 N-terminal amino acids of PnlH is sufficient for anchoring various hybrid proteins in the outer membrane. This targeting signal presents some of the characteristics of a Tat (twin arginine translocation) signal sequence but without an obvious cleavage site.

It was found that the Tat translocation pathway is required for the targeting process. This mechanism of outer membrane protein targeting is probably widespread as PnlH was also addressed to the outer membrane when expressed in *Escherichia coli*. As PnlH was not detected as a substrate by Tat signal sequence prediction programs, this would suggest that there may be many other unknown Tat-dependent outer membrane proteins.

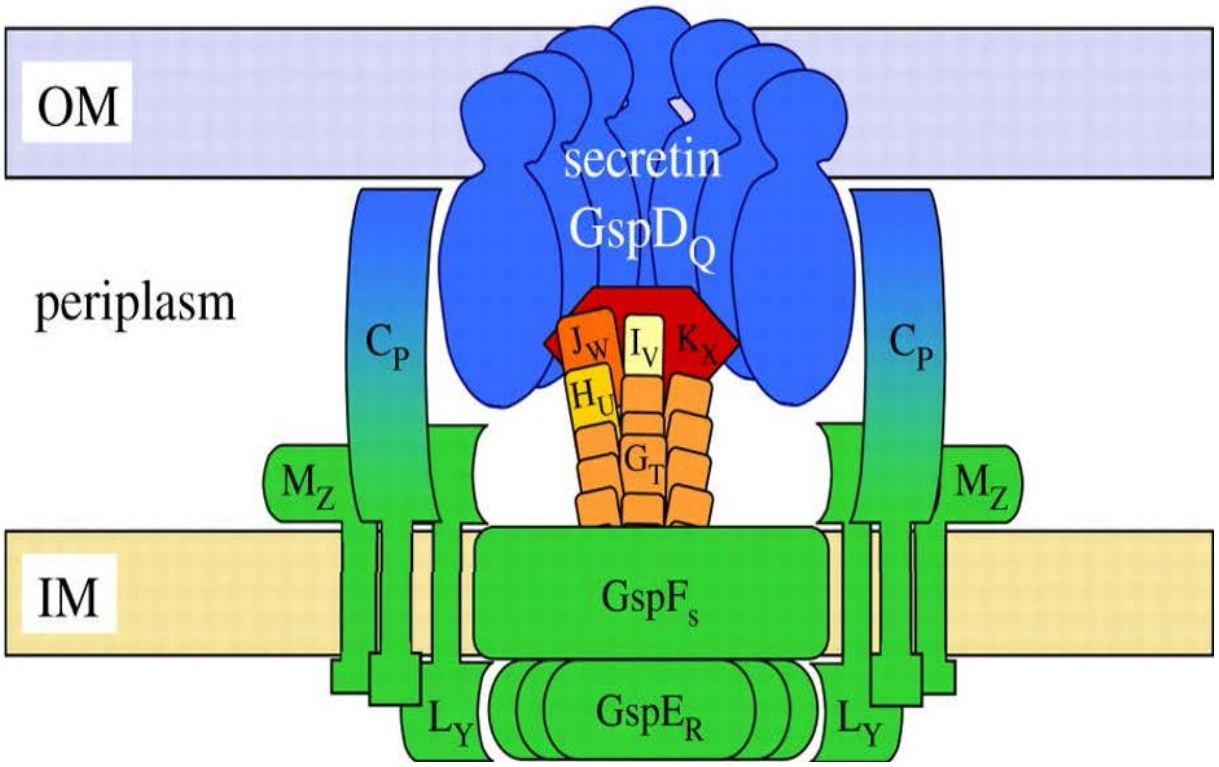

Figure 5 The model of the T2SS.

The secreton is divided into three sub complexes. Secretin GspD (blue) forms a dodecameric pore in the OM through its C-terminal domain whilst its N-terminal part protrudes in the periplasm. The IM surface, composed of T2SS proteins F, L and M, and the traffic ATPase GspE are coloured green. Secretin is connected to the IM surface through the transperiplasmic protein GspC(blue/green). The pseudopilus, mostly constituted by the GspG major pseudopilin and capped by the minor pseudopilins GspH, I, J and K quaternary complex, is shown in orange and red. Gsp proteins are indicated by their corresponding letter. (Douzi *et al*., 2012)

III Plant–pathogen interactions

III.1 Bacterial Resistance in Plants

Plants are constantly exposed to microbes. To be pathogenic, most microbes must access the plant interior, either by penetrating the leaf or root surface directly or by entering through wounds or natural openings such as stomata, pores in the underside of the leaf used for gas exchange. Once the plant interior has been breached, microbes are faced with another obstacle: the plant cell wall, a rigid, cellulose-based support surrounding every cell. Plants have evolved many immune responses (Figure 6) activated in different plant-pathogen interactions.

III.1.1 Elicitors in plant immune system

The presence of infectious agents is detected through the recognition of microbial signals. All signals that are perceived by plant cells and induce defense responses are considered as elicitors. Elicitors may be categorized in two classes: general (or non-specific) elicitors, which do not significantly differ in their effect on different cultivars within a plant species and may therefore be involved in general resistance, and specific elicitors, which are formed by specialized pathogen races or strains and function only in plant cultivars carrying the corresponding disease resistance gene (Montesano *et al*., 2003).

General elicitors are designated Pathogen-Associated Molecular Patterns (PAMPs) when isolated from infectious agents but they may also correspond to endogen plant host derived signals resulting from the action of the pathogen agent called DAMPs (Damage-Associated Molecular Patterns), to signals from non-pathogenic microorganisms referred here as MAMPs (Microbe-Associated Molecular Patterns) or to chemicals. The perception of general elicitors triggers a broad array of reactions,

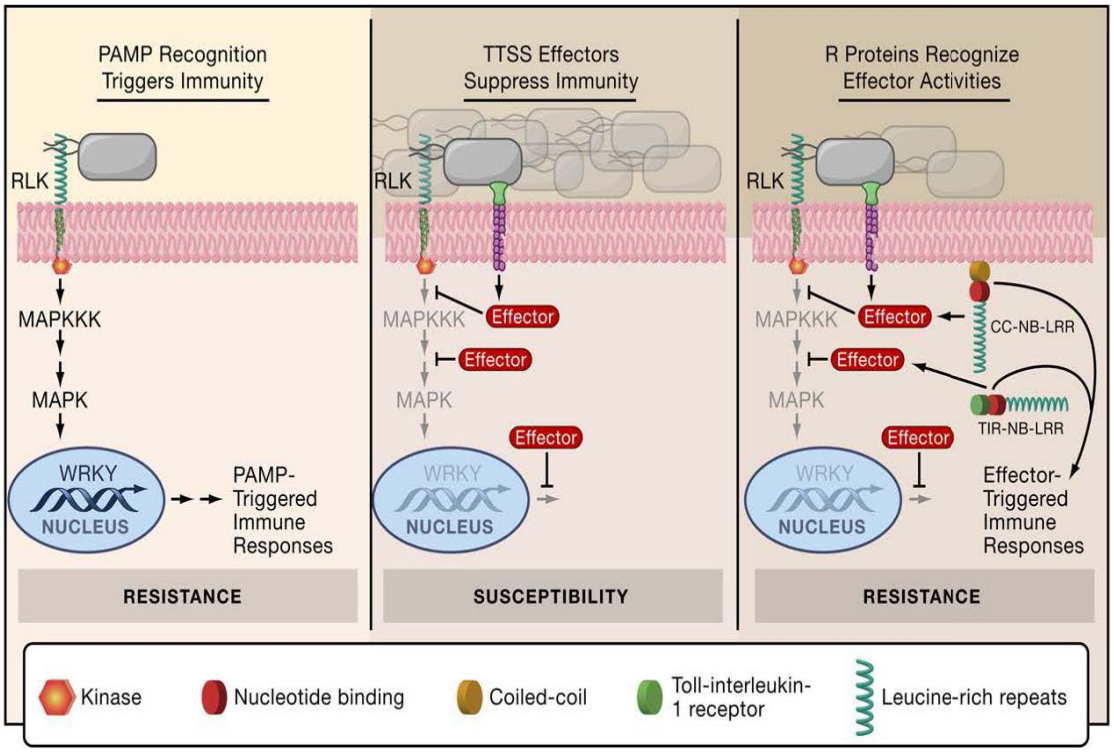

Figure 6 Model for the evolution of bacterial resistance in plants.

Left to right, recognition of pathogen-associated molecular patterns (such as bacterial flagellin) by extracellular receptor-like kinases (RLKs) promptly triggers basal immunity, which requires signaling through MAP kinase cascades and transcriptional reprogramming mediated by plant WRKY transcription factors. Pathogenic bacteria use the type III secretion system to deliver effector proteins that target multiple host proteins to suppress basal immune responses, allowing significant accumulation of bacteria in the plant apoplast. Plant resistance proteins (represented by CC-NB-LRR and TIR-NB-LRR) recognize effector activity and restore resistance through effector-triggered immune responses. Limited accumulation of bacteria occurs prior to effective initiation of effector-triggered immune responses. (Chisholm *et al*., 2006)

which culminate in the activation of the so-called basal resistance or PAMP-Triggered. Immunity (PTI) (Nicaise *et al*., 2009) (Figure 7**,** A). This defensive reaction may be strong enough to halt infection before the invader microbe becomes established. However, some successful pathogenic microorganisms may overcome basal resistance by delivering virulence effector proteins or DNA into host cells. These specific elicitors inhibit signalization pathways or the synthesis of defense compounds by the host plant and thus suppress this first type of immunity. Such signals are the specific elicitors and are likely the cause for susceptibility of many crops to virulent microbial pathogens. In response, plants have evolved a second line of defense through specific disease resistance (R) genes, the so-called effector-triggered-immunity (Henry *et al*., 2012; Jones and Dangl, 2006) (Figure 7**,** B). The recognized effector is termed an avirulence (Avr) protein. Because the effector-R protein relationship is highly specific, this R gene-mediated resistance appears to be similar to adaptative immunity in mammals. However, as R gene-mediated resistance is expressed through similar defense responses as those that are active in basal resistance, but on a much greater scale, ETI is considered as another form of plant innate immunity. Therefore, PTI and ETI are considered as primary and secondary innate immunity respectively.

III.1.2 Pattern Triggered Immunity (PTI)

In plant innate immunity, the first line of microbial recognition leading to active defence responses relies on the perception of pathogen-associated molecular patterns (PAMPs) by pattern-recognition receptors (PRRs). This recognition leads to PAMP-triggered immunity (PTI) (Zipfel, 2009).

PAMPs represent structures that are essential for microbial life and that are typically harbored by invading pathogens. These include cell surface constituents but may also be secreted enzymes or proteins normally located in the cytoplasm. A broad array of structurally diverse PAMPs has been described originating from fungal, oomycete and bacterial pathogens. Most of these PAMPs are oligosaccharides,

glycopeptides, and peptides. Some of these patterns such as Pep-13, xylanase and cold-shock protein are only perceived by a narrow range of plant species belonging to only one plant family (Felix and Boller, 2003; Marciniak *et al*., 2004). A representative example is EF-Tu in the family *Brassicaceae* (Kunze *et al*., 2004). By contrast, other PAMPs such as chitin, LPS and flagellin trigger defense responses in many host species even if there is some degree of specificity and perception efficacy for a plant family or species as in the case of flagellin (Zipfel *et al*., 2006).

PAMPs are perceived at the plant cell surface by high-affinity receptors typically consisting in an extracellular ligand-binding domain with leucine-rich repeats (LRR), a single transmembrane domain and an intracellular serine/threonine kinase-signaling domain. They are referred to as receptor-like kinases (RLK). Receptor-like proteins (RLPs) are similarly structured, but lack the cytoplasmic kinase domain. In *Arabidopsis*, 610 RLKs and 56 RLPs have been identified (Fritz-Laylin *et al*., 2005; Shiu and Bleecker, 2001). A large number of genes encoding RLKs and RLPs are transcriptionally induced upon PAMP treatment, illustrating the large diversity of such perception systems and suggesting their potential role in defense (Kunze *et al*., 2004; Zipfel *et al*., 2006).

III.1.3 Effector Triggered Immunity (ETI)

Effector triggered immunity (ETI) is triggered by recognition of pathogen effectors. ETI is an accelerated and amplified PTI response, resulting in disease resistance and, usually, a hypersensitive cell death response (HR) at the infection site (Jones and Dangl, 2006). HR typically does not extend beyond the infected cell: it may retard pathogen growth in some interactions, particularly those involving haustorial parasites, but is not always observed, nor required, for ETI. The recognized effector is termed an avirulence (Avr) protein.

Bacterial pathogens of animals are known to secrete only a limited number of effectors into host cells. However, plant pathogens such as *P. syringae* can secrete

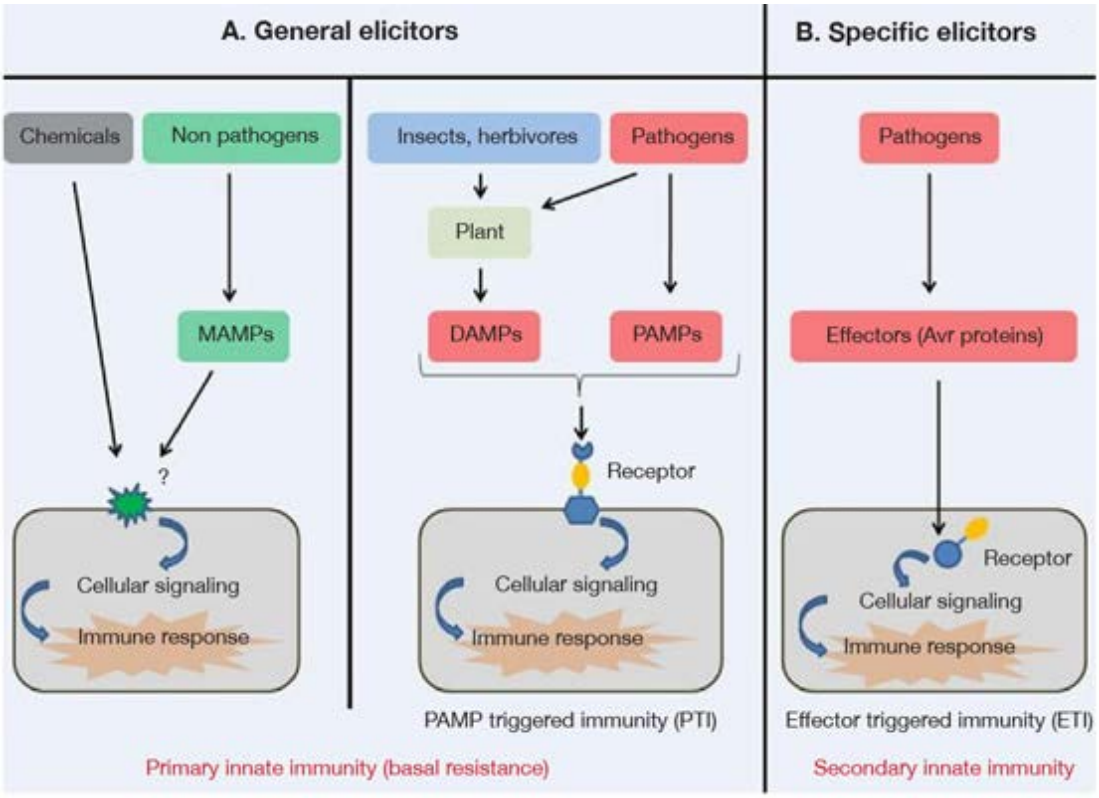

Figure 7 Elicitors in plant inmmune system.

A: General (or non-specific) elicitors do not significantly differ in their effect on different cultivars within a plant species and are involved in primary innate immunity. They include chemicals, Microbes-Associated Molecular Patterns (MAMPs) from non-pathogenic microorganisms, Damage-Associated Molecular Patterns (DAMPs) from plant surfaces resulting from the action of the invading agent and Pathogen-Associated Molecular Patterns (PAMPs) from pathogenic microorganisms. Even if perception of elicitors is often described as being receptor-mediated, only few binding sites have been characterized to date. B: Specific elicitors (or effectors) are formed by specialized pathogens and function only in plant cultivars carrying the corresponding disease resistance gene. Effectors typically lead to the secondary innate immunity after an intracellular receptor-mediated perception. (Henry *et al*., 2012)

approximately 20 to 30 effectors during infection (Chang *et al*., 2005). Effectors promote pathogenicity, and the T3SS is essential for the development of disease symptoms and bacterial multiplication (Staskawicz *et al*., 2001). By their collective action, effectors are hypothesized to alter plant physiology in susceptible hosts to sustain pathogen growth. Both fungal and bacterial effector proteins that are delivered to plants can possess enzyme activity (Table 3). These enzymes are responsible for modifying host proteins to enhance pathogen virulence and evade detection. Pathogens must protect themselves from these potentially detrimental effector enzymatic activities. Effectors may have prokaryotic chaperones keeping them unfolded prior to secretion, or effectors may possess eukaryotic activators. For instance, *P. syringae* AvrRpt2 is delivered to plant cells as an inactive enzyme, whereupon it is activated by eukaryotic cyclophilins such as *Arabidopsis* ROC1 (Coaker *et al*., 2005).

Bacterial effector proteins have also been implicated in activating plant transcription. Members of the *Xanthomonas* AvrBs3 effector family (e.g., AvrBs3, AvrXa10, and AvrXa7) contain a C-terminal nuclear localization signal (NLS) and an acidic transcriptional activation domain (AAD). These features imply that this family of effectors function in the plant nucleus to alter transcription during infection. In fact, the NLS of AvrBs3 is functional, and the AAD of AvrXa10 is capable of transcriptional activation of reporter genes in *Arabidopsis* and yeast (Zhu *et al*., 1998). The AvrBs3 effector family alters plant nuclear gene transcription during pathogen infection, likely as a means to downregulate host defenses.

Three plant signaling molecules regulate plant defense against microbial attack: salicylic acid (SA), jasmonic acid (JA), and ethylene (Thomma *et al*., 2001). Ethylene-dependent signaling is important for the plant's response to pathogens, mechanical wounding, and wounding induced by herbivores. SA-dependent signaling is critical in establishing local and systemic bacterial resistance, while JA-dependent signaling is induced in response to mechanical wounding and herbivore predation. The SA and JA defense pathways are mutually antagonistic, and bacterial pathogens have evolved to exploit this fact to overcome SA-mediated defense responses

Effector	Organism	Biochemical Function	Plant Target(s)	*R* Gene	Phenotype	Reference
AvrRpt2	*Pseudomonas syringae*	Protease[a]	RIN4	RPS2	Cleaves RIN4, Interferes with *R* gene-mediated defense, inhibits basal defense, and manipulates JA pathway	Reviewed by Mudgett (2005)
AvrB	*Pseudomonas syringae*		RIN4	RPM1	RIN4 phosphorylation, manipulates JA pathway	Reviewed by Mudgett (2005)
AvrRpm1	*Pseudomonas syringae*		RIN4	RPM1	RIN4 phosphorylation, inhibits basal defense.	Reviewed by Mudgett (2005)
HopPtoD2	*Pseudomonas syringae*	Protein phosphatase[a]			Suppresses programmed cell death and PR expression	Reviewed by Mudgett (2005)
AvrPphB	*Pseudomonas syringae*	Protease[a]	PBS1	RPS5	Cleaves PBS1, manipulates JA pathway	Reviewed by Mudgett (2005)
AvrPtoB	*Pseudomonas syringae*	E3 ligase,[a] ubiquitin-conjugating enzyme		Pto		Janjusevic et al., 2005
XopD	*Xanthomonas campestris*	Cysteine protease[a]	SUMO			Reviewed by Mudgett (2005)
AvrXv4	*Xanthomonas campestris*	Cysteine protease	SUMO	XV4		Reviewed by Mudgett (2005)
AvrBsT	*Xanthomonas campestris*	Cysteine protease	SUMO			Reviewed by Mudgett (2005)
Avr2	*Cladosporium fulvum*	Protease inhibitor	Rcr3	Cf-2	Inhibits RCR3 activity	Rooney et al., 2005
Avr4	*Cladosporium fulvum*	Chitin binding[a]	Chitinase	Cf-4		van den Burg et al., 2003
Avr-Pita	*Magnaporthe grisea*	Metalloprotease		Pi-ta		Jia et al., 2000
Pep-13	*Phytophthora sojae*	Calcium-dependent cell wall transglutaminase[a]		Elicitor	Activates plant defense responses	Brunner et al., 2002
EPI10	*Phytophthora infestans*	Kazal-like protease inhibitor[a]	Subtilisin A, P69B subtilase	Elicitor	Interacts and interferes with tomato PR-related protein P69B and subtilisin A	Tian et al., 2005
EPI1	*Phytophthora infestans*	Kazal-like protease inhibitor[a]	P69B subtilase	Elicitor	Interacts and interferes with tomato PR-related protein P69B	Tian et al., 2004

Table 3 Enzymatic activity of biochemically characterized effectors and selected elicitors.

Both fungal and bacterial effector proteins that are delivered to plants can possess enzyme activity. (Chisholm *et al*., 2006)

(Kunkel and Brooks, 2002). During infection, *Pseudomonas* bacteria produce coronatine, a JA mimic that contributes to virulence by suppressing SA-mediated host responses (He *et al*., 2004; Reymond and Farmer, 1998). Coronatine is not the only bacterial factor that interferes with SA-mediated defense responses. Multiple effector proteins have been shown to manipulate the JA pathway in concert, such as AvrB, AvrRpt2, AvrPphB, HopPtoK, and $AvrPphE_{pto}$ (He *et al*., 2004).

To cause disease, pathogens need to overcome multiple layers of defense responses. Cell wall fortification during infection, achieved by callose deposition in cell wall appositions (papillae), just below penetration sites, is a common defense response. Three *P. syringae* effectors prevent plant cells from establishing cell wall-based defenses (DebRoy *et al*., 2004; Hauck *et al*., 2003). AvrPto suppresses papillae formation, while AvrE and HopPtoM suppress callose deposition during infection (DebRoy *et al*., 2004; Hauck *et al*., 2003).

III.1.4 Hypersensitive response (HR)

ETI usually results in disease resistance at the infection site, a hypersensitive cell death response (HR). The HR is thought to deprive the pathogens of a supply of food and confine them to initial infection site. Necrotrophic pathogens, such as the fungi *B. cinerea* and *S. sclerotiorum*, however, can utilize dead tissue (Govrin and Levine, 2000). The hypersensitive response (HR) of plants resistant to microbial pathogens involves a complex form of programmed cell death (PCD) that differs from developmental PCD in its consistent association with the induction of local and systemic defence responses. Hypersensitive cell death is commonly controlled by direct or indirect interactions between pathogen avirulence gene products and those of plant resistance genes and it can be the result of multiple signalling pathways (Heath, 2000). Ion fluxes and the generation of reactive oxygen species commonly precede cell death, but a direct involvement of the latter seems to vary with the plant-pathogen combination. Protein synthesis, an intact actin cytoskeleton and salicylic acid also seem necessary for cell

death induction.

Several effector proteins from *P. syringae* pathovars are known to inhibit the HR (Nomura *et al*., 2005), though in most cases the molecular basis of this inhibition is as yet unclear. These effectors could also inhibit cell death triggered by the proapoptotic protein Bax in yeast as well as plants. This result suggests that certain bacterial effectors have evolved the ability to suppress programmed cell-death responses. Rather than actively suppress the HR, additional effectors seem to interfere with recognition events that trigger an HR. For instance, AvrRpt2 interferes with the HR triggered by AvrRpm1 (Ritter and Dangl, 1996), but AvrRpt2 is not known to suppress cell death in general.

III.1.5 Localized or systemic immunity in plant

When a resistance is established in the tissue surrounding the site of initial infection, it is called localized acquired resistance (Kombrink and Schmelzer, 2001) (Figure 8**,** A). However, via emission of molecular signals, defense mechanisms can also be induced in distal organs of a plant that is locally infected by a pathogen. Such systemic resistance reaction renders the host less susceptible to subsequent challenge by a pathogen or a parasite in distal tissues. This long-lasting phenomenon was termed systemic acquired resistance (SAR) (Henry *et al*., 2012; Iriti *et al*., 2010) (Figure 8, B). Methyl salicylate, jasmonates, azelaic acid and a diterpenoid have been proposed as mobile signals involved in the activation of SAR which confers enhanced resistance against a broad spectrum of pathogens (Shah and Zeier, 2013). Conceptually, SAR has been associated with the perception of elicitors from avirulent pathogens but a similar systemic defense may also be lighted on by DAMPs or by other compounds of biological but not microbial origins and by chemicals. Another induced resistance form is referred as induced systemic resistance which could be triggered by molecular patterns isolated from beneficial non-pathogenic microorganisms (MAMPs) (Mishra *et al*., 2009).

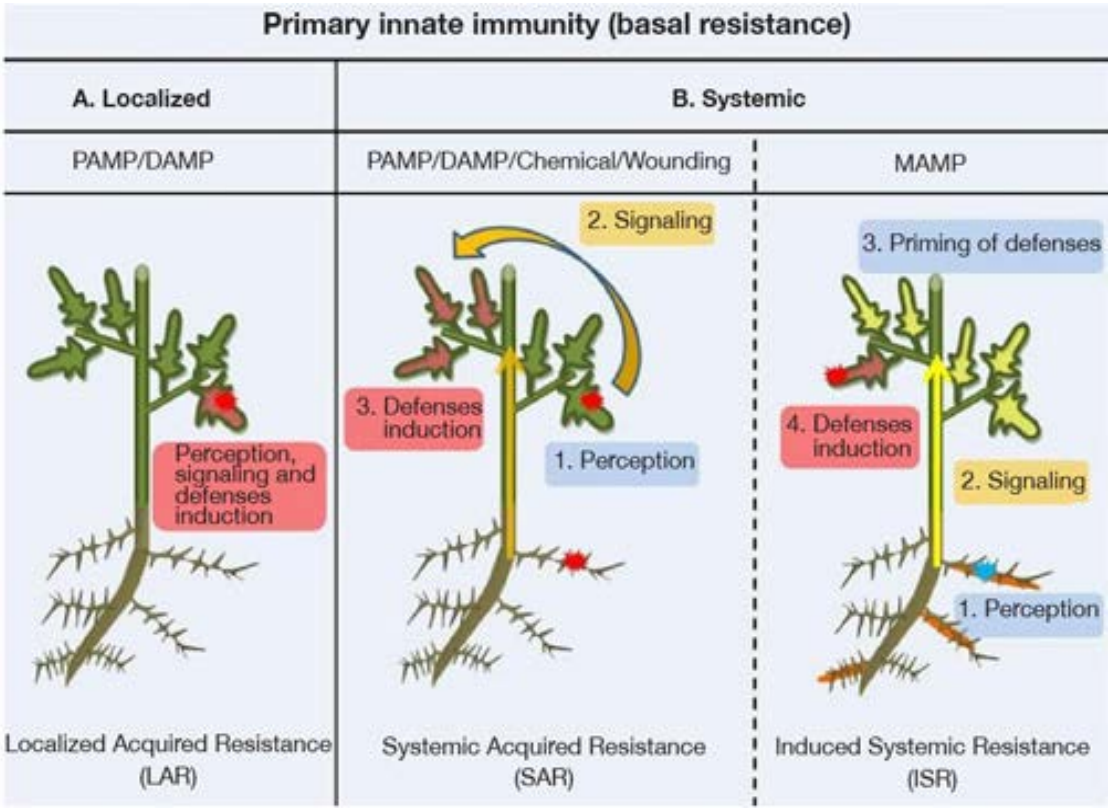

Figure 8 Localized (A) or systemic (B) immunity in plant.

Systemic aquired resistance corresponds to an enhanced state of defense responses after perception of pathogens or a range of compounds and is invariably associated with accumulation of salicylic acid and pathogenesis-related proteins in resistant tissues. Besides, induced systemic resistance is typically stimulated after perception of beneficial microorganisms but also leads to the establishment of an enhanced defense potential. This priming state allows faster defense responses induction upon subsequent pathogen attack. (Henry *et al*., 2012)

III.2 Defensive generation of reactive oxygen species (ROS)

As plants are confined to the place where they grow, they have to develop a broad range of defence responses to cope with pathogenic infections (Wojtaszek, 1997). Plant cells produce reactive oxygen species (ROS) including superoxide, hydrogen peroxide and hydroxyl radicals during the interaction with potential pathogens. The oxidative burst, a rapid production of reactive oxygen species released into the apoplast, is described as one of the earliest responses to pathogen infection and is generally associated with HR (Lamb and Dixon, 1997). Among the ROS produced during plant/pathogen interactions, the first detectable oxidants are superoxide anion ($O_2^{\bullet-}$) and hydrogen peroxide (H_2O_2), which is produced by spontaneous or enzymatic dismutation of superoxide. These compounds are moderately reactive, but they can be converted into more reactive species (especially the hydroxyl radical $OH^{\bullet}$). ROS have direct antimicrobial activities and can therefore reduce pathogen viability (Venisse *et al*., 2001). They have been also implicated in the destruction of the challenged plant cells, either through lipid peroxidation or through initiation of programmed cell death (Greenberg, 1997). H_2O_2 has been shown to play a central role in the expression of disease resistance in several plant/pathogen systems. It serves as substrate for oxidative cross-linking of various plant cell wall components leading to the reinforcement of cell walls and as a diffusible signal for the induction of defense-related genes in healthy adjacent tissues (Lamb and Dixon, 1997).

IV Importance of transition metals in plant-bacteria interactions

It is increasingly understood that the concentration of transition metals in the environment and the availability of essential metals to support pathogen growth can have a significant impact on the outcome of plant-pathogen interactions. Copper and

iron, along with other transition metals confer strong redox activity; in aqueous solution, their ions may also participate in reactions as Lewis acids. These properties make these metals able to catalyse biochemical reactions, giving them an essential role in metabolism (Nies and Brown, 1998). Iron has essential roles in oxygen metabolism, electron transport, lipid metabolism and the tricarboxylic acid cycle; in fact, there are known to be over 100 metabolic enzymes with iron-based cofactors (Massé and Arguin, 2005; Miethke and Marahiel, 2007). So fundamental are some of its uses that bacteria have been found to have controls both at the gene expression and post-transcriptional level to ensure that iron is directed to the most essential proteins when it is in limited supply (Massé and Arguin, 2005; Massé and Gottesman, 2002; Zaini *et al*., 2008).

Given the essential role of metals in living organisms, it is clear that either a lack, or an excess of essential metals may have a profound effect on a wide range of organisms, and by extension, their interactions. Zinc, for example, is present at varying concentrations in different soil types, including growth limiting concentrations in many agricultural soils and it becomes clear that the impact of these metals on plant-pathogen interactions must be taken into consideration in economically important agricultural settings.

IV.1 The availability and toxicity of transition metals

Plants generally have one main source of mineral nutrients: the soil, although foliar fertilisation is also used in some crop management systems. The availability of mineral nutrients in the soil may be further affected by mycorrhizal symbioses and rhizosphere bacteria. Although some opportunistic and soil-borne pathogens, such as *Ralstonia spp*., can obtain metals directly from the environment (Denny, 2006), pathogens that multiply inside the host are dependent on the host for their metal supply (Hancock and Huisman, 1981; Rico *et al*., 2011).

Necrotrophs, such as soft rot pathogens belonging to the genera *Dickeya* and *Pectobacterium*, have access to the full range of nutrients found within the colonised

tissue, as they break down cell walls and membranes and release metals and other compounds that are sequestered in the vacuole or bound within the cell wall (Hugouvieux-Cotte-Pattat *et al*., 1996). The tissue colonised may be of importance in determining metal availability, as certain metals may be retained within the roots of plants, particularly if toxic in excess (Lasat *et al*., 1996), or, if in short supply, will be translocated rapidly to sink tissues. Even within a tissue, there may be heterogeneity of availability as certain cell types may be used preferentially as stores of metals (Küpper *et al*., 2004, 1999) (Figure 9).

Many biotrophic and hemibiotrophic bacteria, such as *P. syringae*, colonise the apoplastic space between the cells of a plant leaves (Preston, 2000). As these pathogens have no or limited access to intracellular stores such as the vacuole, they face particular challenges in obtaining essential but redox active metals, which are often sequestered in the vacuole for the plant own protection (Küpper *et al*., 1999). For hemibiotrophic strains, these difficulties may be obviated at later stages of infection, but they may be considered to be of importance during biotrophic growth.

Given the importance of metals for life, it is unsurprising that organisms compete for them when they are in short supply, and that they have evolved specific systems that enable them to take up the metal ions that they require. This is of great importance in the case of iron, because, although an abundant metal, it exists most commonly as the insoluble and therefore nonbioavailable Fe^{3+} in aerobic environments (Miethke and Marahiel, 2007). For many plants and micro-organisms, the solution to this is to produce and secrete diffusible ligands, known as siderophores (Figure 9), which have high affinities for this otherwise unavailable ferric iron (Braud *et al*., 2009; Marschner *et al*., 1986), in conjunction with the synthesis of dedicated uptake proteins for the siderophore-Fe^{3+} complex, such as the TonB-dependent uptake system (Cornelis and Matthijs, 2002). Certain bacteria, including the opportunistic pathogen *Burkholderia cenocepacia*, can obtain iron directly from host iron-chelating proteins such as ferritin (Whitby *et al*., 2006).

Redox active metals are not simply required for life. A delicate balance must be

maintained, because these metals have the potential to become toxic at excess concentrations. Copper, for example, is able to displace other metals from complexes and to generate ROS. Similarly, iron is a potent generator of ROS (Miethke and Marahiel, 2007), which is the necessary corollary of the redox activity that makes it so fundamentally useful. ROS may cause oxidative stress and damage to cells (Fones and Preston, 2012). The observation that the toxic metal, cadmium, kills cells by creating waves of H_2O_2 and superoxide illustrates the damaging potential of ROS (Garnier *et al*., 2006). Additionally, excess metals may compete with required cofactors for binding sites in transport proteins and enzymes (Hanikenne, 2003; Stohs and Bagchi, 1995). This results in a need for stringently controlled metal ion homoeostasis, and mechanisms for tolerating elevated metal concentrations.

Metals are most toxic as free ions (Pollard *et al*., 2002), so an important facet of tolerance is chelation of metal ions into complexes to reduce their toxicity. Such complexes are often sequestered into specific subcellular compartments (Cosio *et al*., 2004; Krämer *et al*., 2000; Küpper *et al*., 1999). This strategy is common among plants; in barley, for example, metal toxicity is reduced by vacuolar and apoplastic sequestration (Brune *et al*., 1994). Chelating agents such as phytochelatins and metallothioneins are also known to be involved in metal tolerance in many plants; for example, phytochelatins are essential for tolerance to cadmium in *Arabidopsis thaliana* (Skelton *et al*., 1998), while metallothioneins have been shown to be upregulated in response to zinc stress in *Populus alba* (Castiglione *et al*., 2007).

IV.2 Competition for available metals between pathogens and hosts

The disruption of the pathogen's supply of metal is an obvious strategy for disease resistance, considering that microorganisms and host organisms are in competition for

metal ions (Bullen, 1981; Hammer and Skaar, 2012). Iron is one of the most abundant elements in the world (Expert *et al*., 1994), but in aerobic environments it mostly exists as the insoluble Fe^{3+} ion, so that its bioavailability is comparatively low (Touati, 2000). This makes iron one of the most intensely competed ions during host-pathogen interactions (Barrie Johnson and Hallberg, 2008; Nairz *et al*., 2010; Payne, 1993; Weinberg, 1993). The host strategy of withholding iron to limit pathogen growth has been particularly well documented in mammalian systems (Nairz *et al*., 2010). Vertebrates and invertebrates sequester iron by storage proteins such as transferrin and lactoferrin is common, and can be effective, as iron is needed for bacterial growth, pathogenicity and biofilm formation (Ong *et al*., 2006).

Evidence has been uncovered that indicates that plants also employ a strategy of pathogen iron-deprivation. In plants, a ferredoxin-like protein has been demonstrated to be involved in defence against *P. syringae* pv. tomato DC3000, *X. campestris* and *D. dadantii*, a pathogen known to depend on iron scavenged from host tissues during the progression of soft rot disease. The defensive function of this protein was found to rely on its ability to bind iron (Huang *et al*., 2006). There are also iron-binding proteins produced by pathogens, so that the final outcome depends on the interaction between host and pathogen iron-chelating agents (Boughammoura *et al*., 2007). *Arabidopsis* has been found to upregulate ferredoxin in response to the detection of iron-uptake siderophores from pathogens (Dellagi *et al*., 2005). Other chemicals that may be used to bind and withhold iron from pathogens include polyphenols, shown to be effective against *D. dadantii* mutants with reduced iron-uptake capacity (Estela Silva-Stenico *et al*., 2005), and to inhibit the growth of *P. syringae* pv. *syringae* B728a on leaf surfaces (Karamanoli *et al*., 2011).

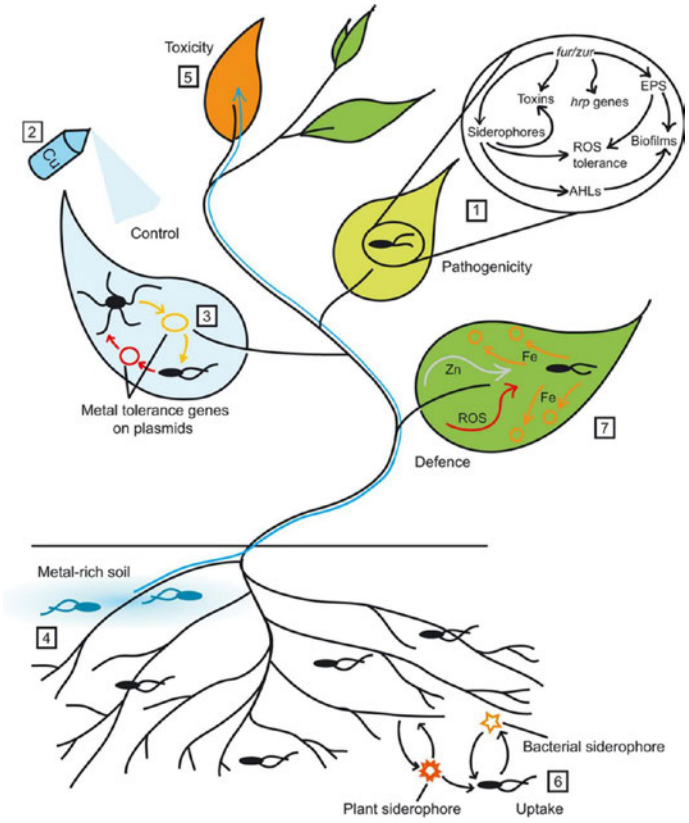

Figure 9 Metals in plant-microbe interactions.

Metals can influence the expression of various bacterial virulence factors, including toxins, EPS and hrp genes, most notably via signalling involving metal sensing systems including fur and zur, and metal uptake systems, particularly siderophores (1). Metals may also have roles in protecting the plant against infection and, especially in the case of copper, can be applied directly to crops as antimicrobials (2). This approach can lead to the development of metal resistant strains, accelerated by the horizontal transfer of resistance genes. Build-up of metals in the soil can affect microbial communities (4), with potential effects upon plant-microbe interactions, and can result in overexposure of the plant, causing toxicity symptoms such as russetting (5). Plants and microbes also compete for metals. Metal uptake often occurs via iron-chelating compounds such as siderophores, and soil-borne bacteria are frequently able to take up those produced by the plant, in addition to their own (6). Within the plant, competition for metals may also be important, with the withholding of metals, especially iron, being an important defence. Additionally, plants may use metals in defence, either as catalysts for ROS production, or more directly as antimicrobial toxins (7), as most clearly evident in the case of metal hyperaccumulating plants. (Fones and Preston, 2013)

IV.3 Mechanisms of plants to release essential metals to invading microbes

The plants' defence mechanism exposes the pathogen to an excess of a metal. An example is the bacterium *X. oryzae* pv. *oryzae*, which, when growing in the xylem of rice, can be limited by high concentrations of copper (Yuan *et al*., 2010). The importance of this for the outcome of this plant-pathogen interaction is illustrated by the evolution of a bacterial TAL effector protein that initiates transcription of *Xa13,* a rice gene encoding a transmembrane transporter that works in concert with two additional rice proteins to remove copper from the xylem (Yuan *et al*., 2011). Animals, too, are known to use copper as an antimicrobial (Samanovic *et al*., 2012). It has been suggested that a novel *Arabidopsis* MFS-family zinc transporter, an orthologue of which is induced by pathogen infection in maize (Simmons *et al*., 2003), may release zinc from the vacuole in infected tissues, thus playing a role in defence (Haydon and Cobbett, 2007). It has been suggested that zinc acts to limit bacterial growth by competing for manganese transporters (McDevitt *et al*., 2011).

IV.4 Mechanisms for bacteria to obtain metal from plants

IV.4.1 Iron in bacteria

All pathogenic bacteria require iron as a growth-essential nutrient. The process of multiplication requires acquisition of growth-essential nutrients, including iron, from the host. Although bacteria ensure a very important supply of iron for growth, excessive iron results in the Fenton reaction in the presence of H_2O_2 produced by metabolism to generate the highly reactive and extremely damaging hydroxyl radicals to bacteria (Figure 10). Therefore, the ability of pathogenic microorganisms to scavenge iron from their host environment and incorporate this element into proteins is a fundamental

requirement for the production of disease.

Iron reduction	$O_2^- + Fe^{3+} \rightarrow Fe^{2+} + O_2$
Fenton reaction	$Fe^{2+} + H_2O_2 \rightarrow Fe^{3+} + OH^- + \bullet HO$
Haber-Weiss reaction	$O_2^- + H_2O_2 \xrightarrow{\text{Fe catalysis}} \bullet HO + OH^- + O_2$

Figure 10 Oxygen free radicals formed by iron ion through Fenton reaction.

IV.4.2 Iron homeostasis in *Dickeya*

During the plant invasion process, *D. dadantii* encounter various environmental conditions, of which iron availability and production of ROS by the plant are two factors limiting their spread. Analysis of the role of iron in the pathogenicity of *D. dadantii* on Saintpaulia plants has shown that during infection, this bacterium requires two high-affinity-iron siderophores, chrysobactin and achromobactin (Franza *et al*., 2005). A first observation made by Neema *et al.* (Neema *et al*., 1993) indicated that iron incorporated into plant ferritins drastically decreased in soybean suspension cells challenged with *D. dadantii.* This effect was also observed during treatment of the cells with chrysobactin. The possibility of a competition for iron between the pathogen and the host was also illustrated by the observation that accumulation of polyphenols in plant tissues inhibits growth of mutants of *D. dadantii* affected in their siderophore-mediated iron transport pathway (Mila *et al*., 1996). Polyphenols have iron-chelating properties and could play the role fulfilled by iron-binding proteins, such as transferrin in animal immunity.

In order to identify plant genes that are regulated in response to infection by *D. dadantii*, Dellagi *et al*. differentially screened cDNA libraries from *Arabidopsis* (Dellagi *et al*., 2005) and showed that the gene encoding the ferritin AtFer1 is upregulated in infected plants. These authors established that accumulation of *AtFer1* transcripts and production of ferritins during infection is a defense reaction against proliferation of the pathogen. The siderophore chrysobactin, as well as desferrioxamine are elicitors of this response. As only the iron-free siderophores induce this reaction, it was suggested that these iron sequestering molecules could cause severe iron depletion in *Arabidopsis* leaf tissues, resulting in the redistribution of intracellular iron stores and/or the activation of iron acquisition systems of the cell. Intracellular redistribution could involve remobilization of vacuolar iron by the specific metal transporters Nramp3 and Nramp4 (Figure 11). Indeed, among the six NRAMP genes present in *Arabidopsis*, *AtNramp3* was found to be strongly upregulated in response to several biotic stresses.

IV.4.3 Production of multiple siderophores by *D. dadantii*

Siderophores are high affinity Fe(III)-scavenging/solubilizing molecules that, once loaded with iron, are specifically imported into the cell (Neilands, 1995). The production of siderophores by pathogenic bacteria can greatly contribute to their virulence, because these molecules can remove iron from a wide variety of organic substrates (Ratledge and Dover, 2000). In Gram-negative bacteria, production of a siderophore and proteins involved in uptake of its ferric complex is accurately controlled by the sensory and regulatory protein Fur. Fur protein acts as a dimer, each monomer containing a non-haem ferrous iron site (Hantke, 2001). If the cellular iron level becomes too low, the active Fur repressor losses Fe^{2+}, its co-repressor, and is no longer able to bind to its operator sites (de Peredo *et al*., 2001; Escolar *et al*., 1999).

D. dadantii produces two kinds of siderophore involved in high-affinity Fe uptake: achromobactin and chrysobactin. Both are needed for survival and full virulence in *planta* (Expert, 1999). The importance of these siderophores in mediating plant-

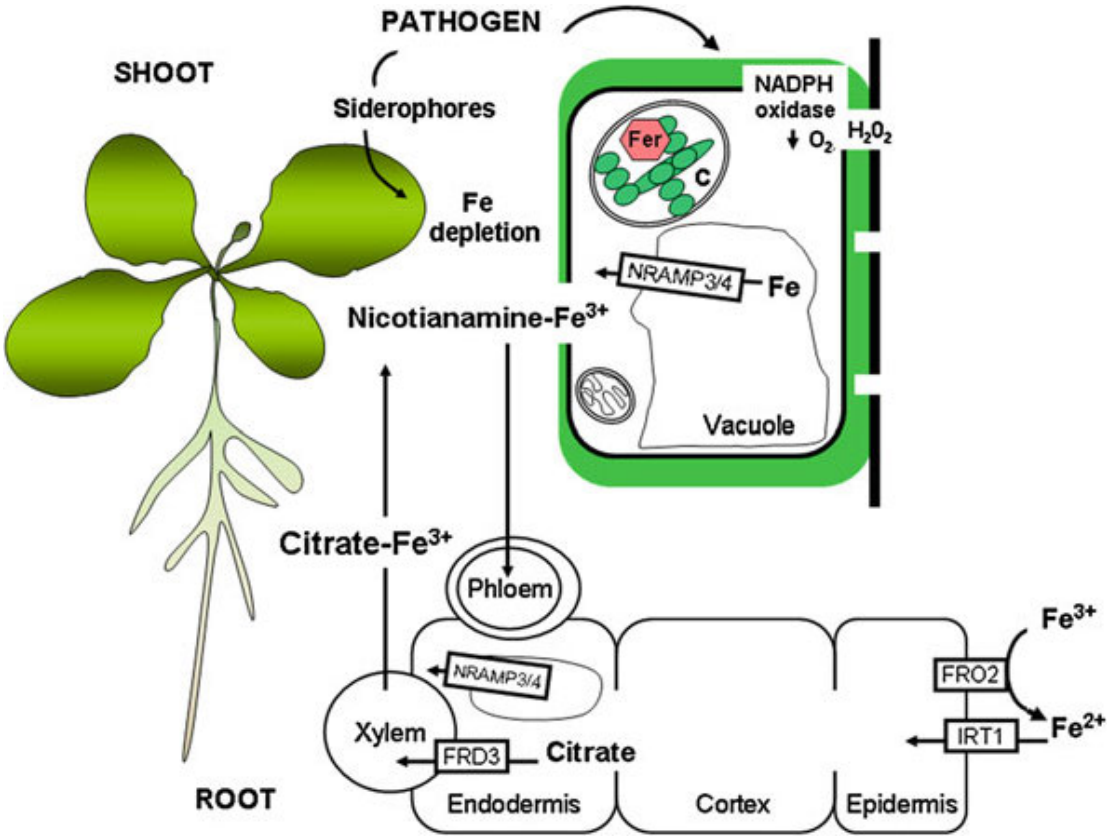

Figure 11 Schematic representation of plant iron acquisition and changes in iron trafficking during pathogenesis.

This model is based on the reactions triggered by *D. dadantii* during infection of *Arabidopsis*. Plants acquire iron from the soil. In dicots, Fe^{3+} is reduced to Fe^{2+} by the FRO2 ferric chelate reductase, and then transported through the plasma membrane by the iron-regulated transporter IRT1. Inside the plant, iron is transported essentially as ferric complexes of citrate in the xylem and of nicotianamine in the phloem. Storage and buffering occur in the apoplast and the organelles including vacuoles and plastids (C) that contain ferritins (Fer). Bacterial invasion triggers iron depletion in leaves, leading to a mobilization of vacuolar iron mediated by transporters AtNramp3 and AtNramp4. The reactive iron released in the cytosol contributes to amplify the production of reactive oxygen species and to induce ferritin synthesis in the chloroplast depriving the bacteria of iron. Infection also results in iron mobilization in the roots, from both the vacuole and the soil. (Expert *et al.*, 2012)

microbe competition for iron can be illustrated by the finding that chrysobactin production by *D. dadantii* leads to iron deficiency in the plant host, as measured by the amount of iron bound to plant ferritins (Neema *et al*., 1993).

The virulence of *D. dadantii* strain 3937 on African violets (*Saintpaulia ionantha*) depends on the production of chrysobactin (Enard *et al*., 1988; Masclaux and Expert, 1995; Neema *et al*., 1993). Chrysobactin is a bidentate ligand consisting of a monomer of 2,3-dihydroxybenzoyle-D-lysyl-L-serine (Persmark *et al*., 1989) (Figure 12) and thus is a less powerful ferric ion ligand than hexadentate siderophores like the tris-catecholate enterobactin. Chrysobactin is essential for *D. dadantii* cells to cause systemic infection (Rauscher *et al*., 2002).

Under iron-limited conditions, *D. dadantii* synthesizes a second siderophore called achromobactin belonging to the hydroxy/carboxylate class of siderophore (Franza *et al*., 2005) (Figure 13**)**. Achromobactin was uncovered on the basis of the phenotype of chrysobactin biosynthetic mutants, which are still able to form a halo of discoloration on Chrome Azurol S (CAS) agar medium, used to detect siderophore production.

Chrysobactin can compete efficiently with strong iron chelators (Persmark and Neilands, 1992), while achromobactin, which lacks catechol or hydroxamate, removes iron from mineral or weakly liganded forms, such as ferric citrate. *Dickeya* cells do not have the specific transport system for ferric citrate. A peculiarity of these two siderophores is that, although achromobactin and the transport of its ferric complex are highly induced by weak iron deficiency, achromobactin is produced at high basal levels in the presence of mineral iron. Under such conditions, chrysobactin-dependent iron uptake is completely repressed. Achromobactin thus resembles a preventative system that helps bacterial cells to cope transiently with a drastic loss of iron until chrysobactin is fully induced.

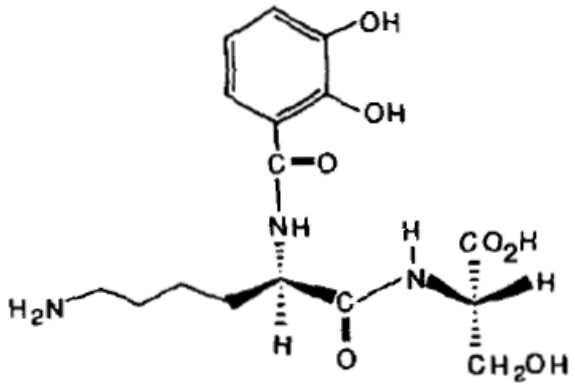

Figure 12 Structure of chrysobactin.

Chrysobactin is comprised of L-Serine, D -Lysine, and 2,3-dihydroxybenzoic acid (DHBA). (Persmark *et al*., 1989).

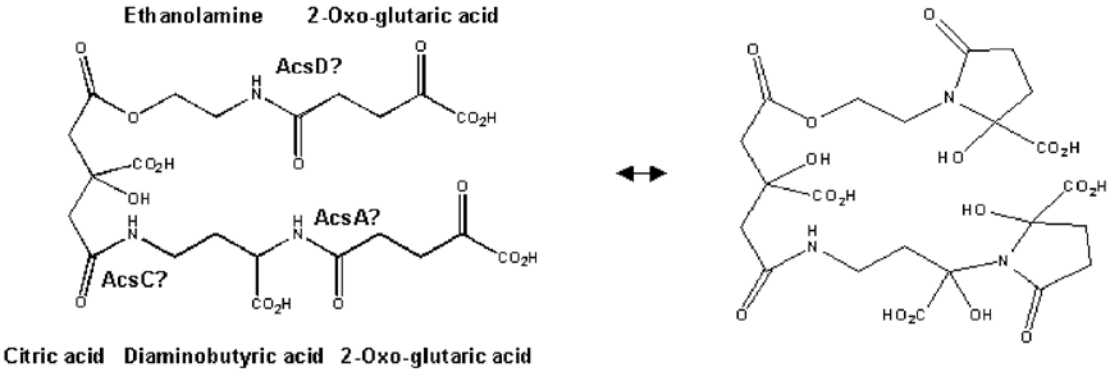

Figure 13 Structure of achromobactin and its cyclized form that prevails in neutral aqueous solution.

(Münzinger *et al*., 2014)

Proteins AcsD, AcsC and AcsA belong to a family of siderophore synthase components catalyzing amide bond formation reactions. (Martínez *et al*., 1994)

IV.4.4 Another iron acqusition system: the Fus system

A new mode of iron acquisition by bacteria has recently been described. Pectocin M1 and M2 are unusual bacteriocins produced by and able to kill *Pectobacterium* sp. They contain a M-class cytotoxic domain fused to a plant like ferredoxin domain (Grinter *et al*., 2014). *Pectobacterium* is able to use ferredoxin as an iron source in iron limiting medium. Moreover, addition of ferredoxin is able to reduce pectocin toxicity, indicating that both molecules compete for the same receptor on *Pectobacterium* surface. This receptor was identified by pull-down experiments using pectocin M1 as a bait. It is a TonB-dependent receptor which was named FusA. *fusA* is part of an operon form by *fusB*, *fusA*, *fusC* and *fusD*. This operon is also found in *Dickeya* species. FusB is a TonB-like protein, FusD is a fused ABC transporter and FusC has homology to M16 proteases. FusC has a high proteolytic activity against plant ferredoxin. In the absence of FusC iron loaded ferredoxin accumulates in the periplasm of *Pectobacterium*. Digestion of ferredoxin by FusC allows liberation of iron that can enter the cytoplasm through FusD (Figure 14). Thus, *Pectobacterium* and probably also *Dickeya* can acquire iron by importing in the periplasm an iron loaded protein.

IV.5 Copper in bacteria

While numerous studies have focused on the impact of iron availability during bacterial and fungal infections, increasing evidence suggests that copper is also involved in microbial pathogenesis. Copper (Cu) is a critical component of proteins involved in a variety of cellular processes. As a redox-active metal ion, Cu exists in the reduced [“Cu(I)” or ‘‘Cu^{+}’’] or oxidized state [‘‘Cu(II)’’ or ‘‘Cu^{2+}’’], thereby providing a rich chemical environment for diverse biological ligands that are partners for its many structural and catalytic roles. Enzymes and proteins such as Cu, Zn superoxide dismutase, cytochrome oxidase, methane mono-oxidase, dopamine ß-hydroxylase, and

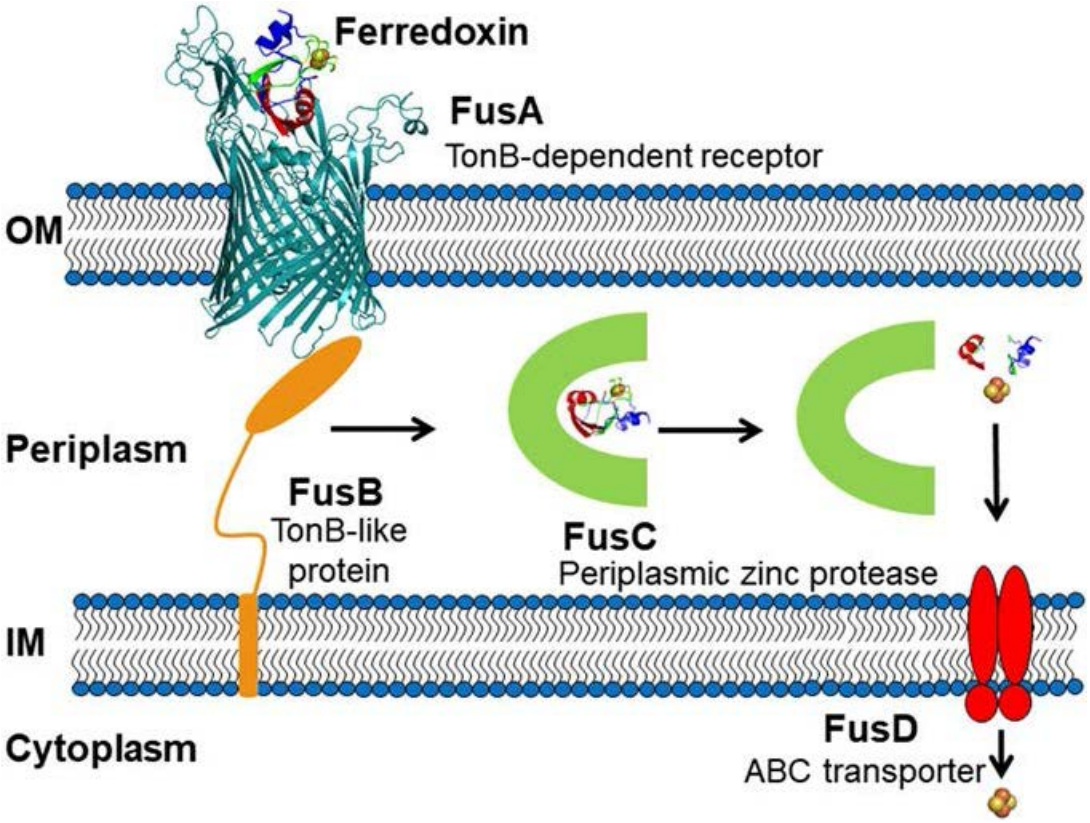

Figure 14 Iron released schematic model after ferredoxin import into *Pectobacterium*.

Ferredoxin is imported via the TBDR FusA presumably mediated by the TonB homolog FusB, which may play a conventional TonB-like role in removal of the plug domain from the lumen of FusA, or may directly contact the substrate. On transport to the periplasm, FusC cleaves ferredoxin to the release of the [2Fe-2S] cluster, which may be transported to the cytoplasm by the putative ABC transporter FusD. The exact form of iron present in the periplasm on release from ferredoxin remains to be determined, however. (Mosbahi *et al*., 2018)

the ethylene receptor all bind Cu as an essential ligand for their activity. Furthermore, analysis of 450 bacterial genomes found 72% encode at least one putative Cu-dependent protein (Ridge *et al*., 2008).

However, when unbound within a cell, redox cycling means copper is extremely toxic, largely due to its ability to catalyze Fenton chemistry (Table 4) causing the production of highly reactive hydroxyl radicals that damage biomolecules such as DNA, proteins, and lipids. The reduced form of the metal for this reaction can be generated by reaction with superoxide (or other cellular components such as low-molecular weight thiols), with the sum of these reactions, being referred to as the Haber–Weiss reaction (Liochev and Fridovich, 2002).

Bacteria tightly regulate cytoplasmic Cu concentrations in order to minimize toxicity while ensuring an adequate supply for cuproproteins. First, bacteria in general encode very few Cu dependent enzymes. Second, bacterial cuproproteins tend to be periplasmic or extracellular, rather than cytoplasmic. In the event Cu levels become too high, bacteria have also developed mechanisms to alleviate Cu-induced stress. CopA and CopB are P-type ATPases, similar to the ATP7A and ATP7B proteins in humans, which undergo conformational changes to drive Cu^{+} ion transport across membranes (Palmgren and Nissen, 2011) (Figure 15**)**.

$Cu^{+} + H_2O_2 \longrightarrow Cu^{2+} + OH^{-} + \bullet HO$
$Cu^{2+} + O_2^{-} \longrightarrow Cu^{+} + O_2$
$O_2^{-} + H_2O_2 \longrightarrow O_2 + OH^{-} + \bullet HO$

Table 4 Oxygen free radicals formed by copper ion through Fenton reaction.

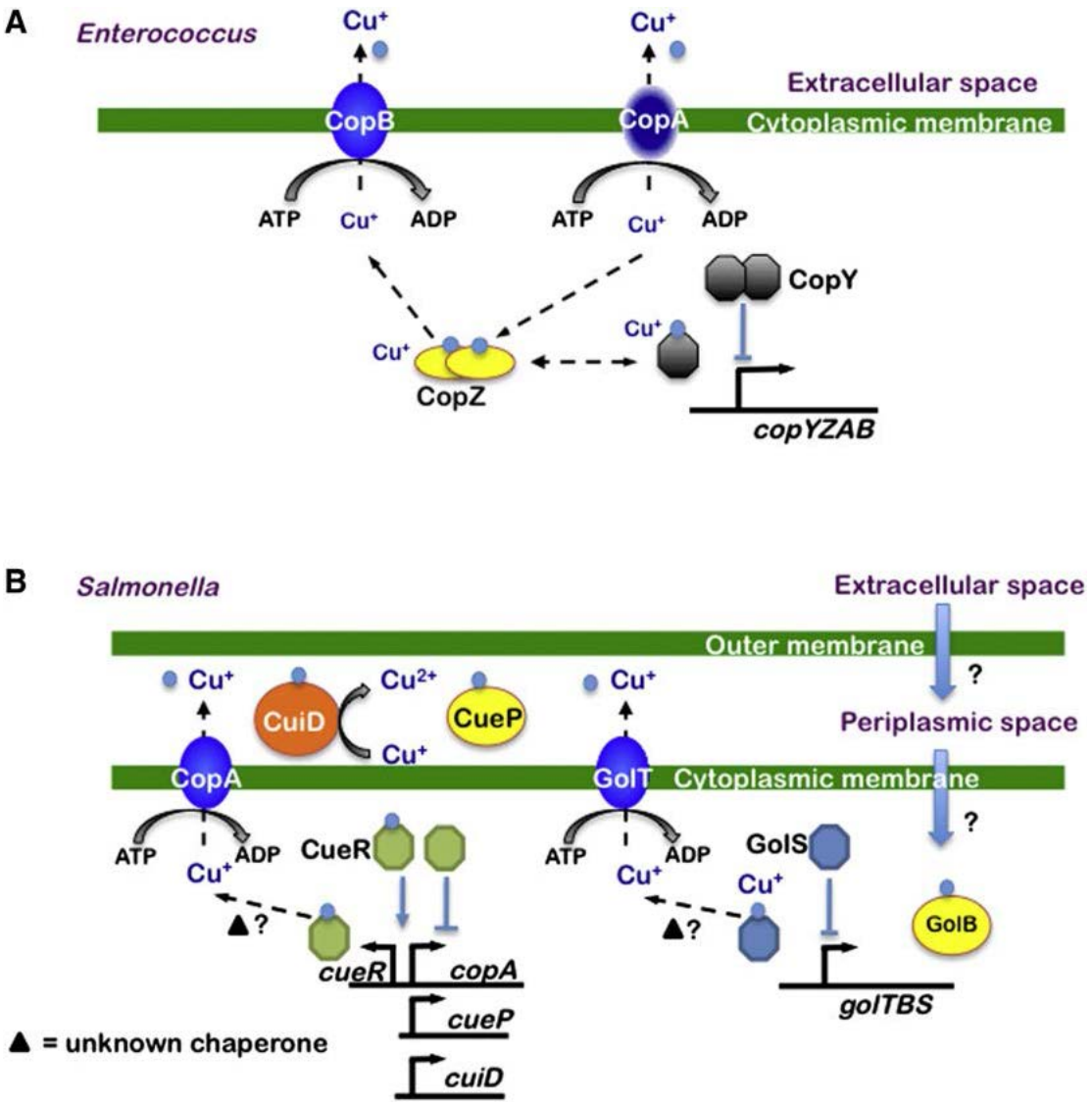

Figure 15 Cu homeostasis pathway models in Gram-positive and -negative bacterial pathogens. (A) Gram-positive bacteria, based on *E. hirae*. It is believed Cu (blue) enters the cell via CopA. CopZ, a Cu chaperone, forms dimers that bind two Cu^+ atoms and transfers them to CopY or other proteins. Consequently, a dimer of CopY bound to four Cu^+ detaches from the copA promoter and derepresses expression of copYZAB operon, allowing resistance to Cu toxicity. (B) Gram-negative bacteria, based on *Salmonella*. Left: Cue system. Cu enters the periplasmic space, most likely through porins in the outer membrane, and crosses the inner membrane into the cytoplasm by an unknown mechanism. Within the cytoplasm, the Cue system responds to Cu: CueR changes its conformation upon Cu^+ binding, resulting in the expression of cueP, copA, cuiD, and cueR. CopA

exports Cu^{+} to the periplasmic space and CuiD oxidizes Cu^{+} to Cu^{2+}. Maximum induction of copA and cueO genes upon Cu exposure is detected within 2–3 min (Thieme *et al*., 2008). CueR is extremely sensitive to Cu+ (10^{-21} M) (Changela *et al*., 2003) and therefore appears to be the primary Cu sensor in these bacteria. Right: Gol system. When Cu is in the inner space, GolS is thought to bind Cu+, resulting in derepression of the gol operon. GolT is proposed to export Cu+ to the perisplasm. CueP and GolB are proposed to be perisplasmic and cytoplasmic, respectively, Cu chaperones. (Samanovic *et al*., 2012)

V ABC transporters

Early biochemical studies on bacterial nutrient import systems revealed a class of multi-subunit transporters that all contained an essential cytoplasmic factor with ATP hydrolysis activity (Higgins, 1992). The primary structure of the ATP-binding domains of these transporters was highly conserved, including the presence of a phosphate-binding loop (P-loop or Walker A motif) and a short consensus sequence "LSGGQ". The family of transporters was subsequently termed ABC transporters in recognition of the "cassette-like" nature of the ATP-binding subunit (Higgins *et al*., 1986). Around the same time, biochemical studies on the mammalian multi-drug resistance (MDR) export pump P-glycoprotein revealed the presence of the very same motifs in its ATP-binding domain, demonstrating that the family of ABC transporters was represented not only in bacteria but also higher eukaryotes, including mammals. ABC transporters represent the largest protein family identified to date, highlighted by the fact that between 1 and 3% of bacterial and archaeal genomes encode for subunits of ABC transporters (Tomii and Kanehisa, 1998) from the current sequence information of microbial genomes.

Based on the direction of transport, ABC transporters can be classified as exporters or importers. Both consist of two nucleotide-binding domains (NBD) and two transmembrane domains (TMD) (Biemans-Oldehinkel *et al*., 2006; Higgins, 1992) (Figure 16). ATP hydrolysis on the NBD drives conformational changes in the TMD,

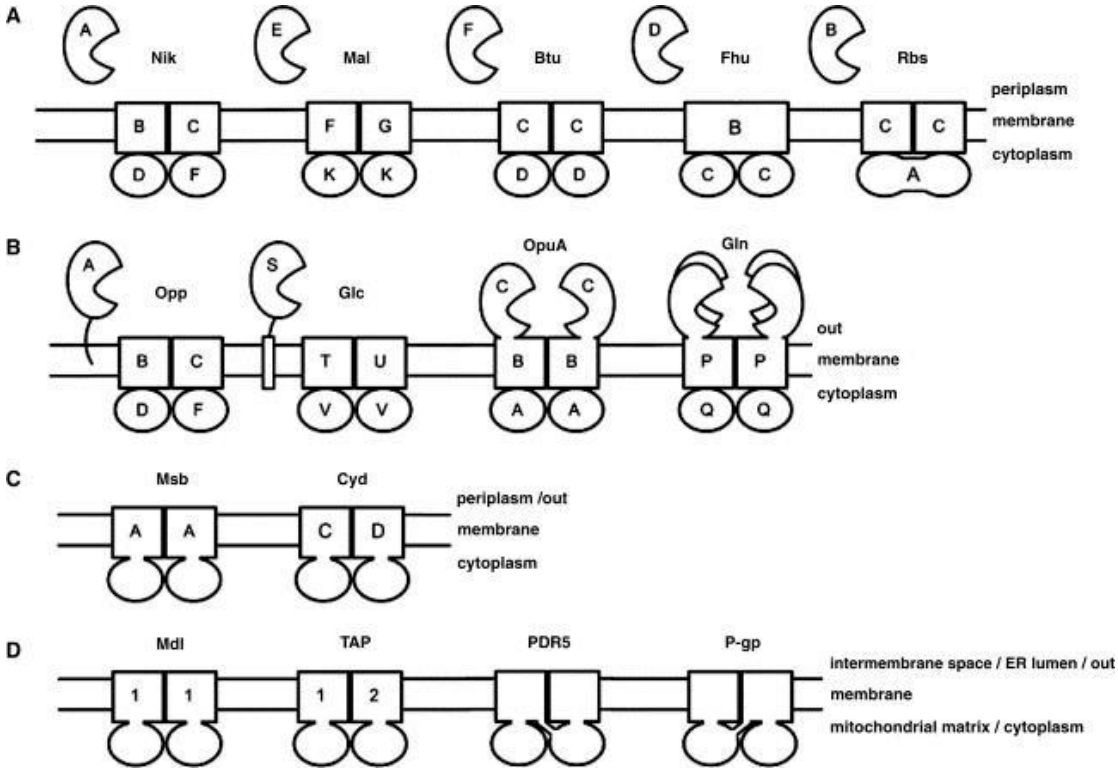

Figure 16 Domain architecture of ABC transporters.

Schematically indicated are: SBPs (pac-man shaped), TMDs (rectangles), and NBDs (ovals). (A) Gram-negative bacteria (all the examples are from *Escherichia coli*): Nik, nickel transporter; Mal, maltose/maltodextrin transporter; Btu, vitamin B12 transporter; Fhu, siderophore/haem/vitamin B12 transporter; Rbs, ribose transporter. (B) Gram-positive bacteria and Archaea: Opp, oligopeptide transporter from Lactococcus lactis; Glc, glucose transporter from *Sulfolobus solfataricus*; OpuA, glycine betaine transporter from Lactococcus lactis; Gln, glutamine/glutamic acid transporter from Lactococcus lactis. (C, D) Functional and structural homologues are present in all three kingdoms of life. (C) Msb, lipid flippase from *Escherichia coli*; Cyd, cysteine exporter from *Escherichia coli*. (D) Mdl, mitochondrial peptide transporter from *Saccharomyces cerevisiae*; TAP1/2 (ABCB2/3), human peptide transporter; PDR5, yeast pleiotropic drug resistance transporter; P-gp (MDR1/ABCB1), human multidrug transporter. (Biemans-Oldehinkel *et al*., 2006)

resulting in alternating access from inside and outside of the cell for unidirectional transport across the lipid bilayer. In the case of ABC importers, which are found in prokaryotes only, a fifth domain is part of the functional unit, the substrate binding domain, SBP. SBPs bind their ligands with high affinity and deliver them to the translocator (the TMDs), where the substrate is released into the translocation pore upon ATP binding and hydrolysis in the NBDs (Khare *et al*., 2009). Substrate-binding proteins (SBPs) are located in the periplasm of Gram-negative bacteria or lipid-anchored or fused to the TMD in the case of Gram-positive bacteria and Archaea (Heide and Poolman, 2002).

All ABC transporters are characterized by the possession of one or two copies of two basic structural features: a highly hydrophobic transmembrane domain, each containing 4 or 6 transmembrane spans, and a peripheral (cytosolic) ATP-binding domain or nucleoside-binding fold (Rea, 1999; Theodoulou, 2000). Most ABC proteins are primary pumps driven by ATP hydrolysis and transport a wide range of substrates including ions, sugars, lipids, peptides, pigments, xenobiotics, and antibiotics. To date, two major sub-classes of this superfamily have been identified in plants: these are the multidrug resistance-associated proteins (MRPs) and the multidrug resistance proteins (MDRs). Although the first ABC transporter to be cloned was an MDR-like gene from *Arabidopsis*, only certain MRPs in plants have been characterized functionally to date (Rea *et al*., 1998; Theodoulou, 2000). Both importing and exporting ABC transporters are found in bacteria, whereas the majority of eukaryotic family members function in the direction of export (Wilkens, 2015).

V.1 Mechanism of ABC transporters

Under physiological conditions, ABC transporters operate in a single direction (either import or export), although the drug efflux pump LmrA has been shown to be reversible under certain conditions (Wilkens, 2015), which means that the membrane domain must operate one or more “turnstile-like” gates that are tightly coupled to the

catalytic cycle on the NBDs. To satisfy this condition, the transmembrane domain alternates between outward- and inward-facing conformations. In the case of ABC transporters, conformational switching of the membrane domain for providing alternating access is driven by the binding of transport substrate and MgATP, followed by ATP hydrolysis and product release. Based on structural and biochemical data, several models of ABC transporter mechanisms have been proposed, most notably the "alternating site" (Senior *et al*., 1995), "switch" (Higgins and Linton, 2004), and "constant contact" (Sauna *et al*., 2007; Siarheyeva *et al*., 2010) models. While all these models share elementary steps, such as ATP-dependent NBD dimerization and the switching of the TMD between outward- and inward-facing conformations, the models diverge with respect to some of the details of the mechanism. Among the structurally and mechanistically best-characterized importers are the *E. coli* maltose (Chen, 2013; Orelle *et al*., 2010) (a type I) and vitamin B12 (Lewinson *et al*., 2010; Locher, 2016; Locher *et al*., 2002) (a type II) uptake systems. For the exporters, a large amount of biochemical and structural data are available for the multidrug resistance pumps from *Staphylococcus aureus* (Sav1866) (Dawson and Locher, 2006) and higher eukaryotes (P-glycoprotein, ABCB1) (Jin *et al*., 2012; Li *et al*., 2014; Loo and Clarke, 2005; Sharom, 2011), multidrug resistance-associated protein (MRP1, ABCC1) (Cole, 2014), the bacterial lipid flippase MsbA (Ward *et al*., 2007), and the transporter involved in antigen processing (TAP) (Oancea *et al*., 2009).

The basic catalytic cycle of ABC transporters includes the binding of SBPs (for importers) or the direct binding of a substrate (for exporters) to the TMDs, binding of two MgATP molecules to the NBDs, dimerization of the NBDs, switching of the TMDs between the in- and outward or out- and inward-facing conformations (depending on transporter type), ATP hydrolysis, phosphate, ADP and transport substrate release concomitant with NBD dissociation to reset the transporter to the ground state for the next cycle. The details and order of these steps depend, to some extent, on the transporter type, as illustrated in (Figure 17, A) for exporters, (Figure 17, B) for type I importers, and (Figure 17, C) for type II importers.

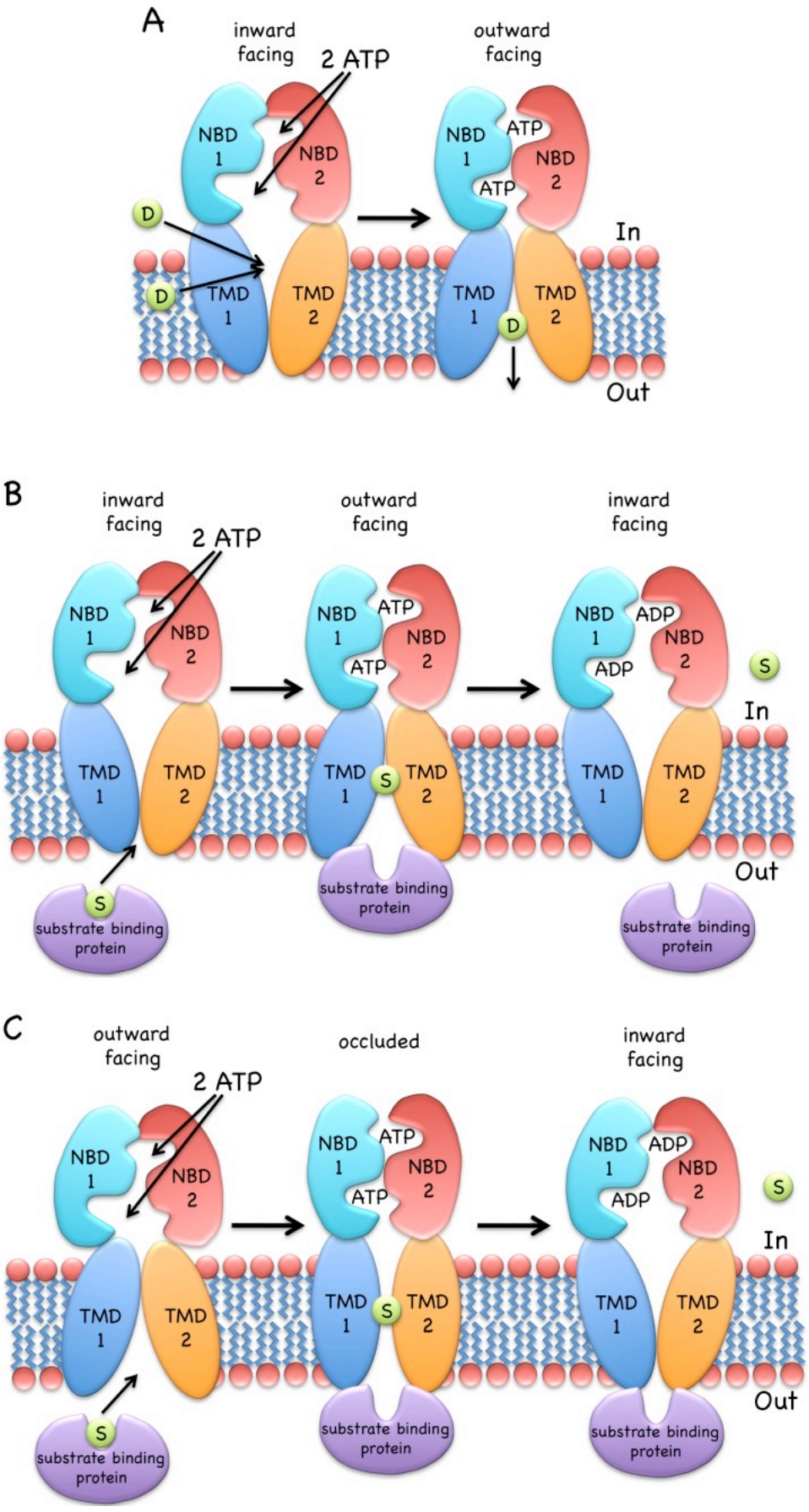

Figure 17 Schematic of the mechanism of ABC exporters and importers.

(A) The inward-facing exporter binds substrate "D" (drug) from the cytoplasm or the inner leaflet of the bilayer. After binding two molecules of MgATP, the nucleotide-binding domains (NBDs) dimerize and switch the transmembrane domain (TMDs) from the inward- to the outward-facing conformation, followed by the release of the drug to the extracellular milieu. ATP hydrolysis, ADP/Pi release and NBD dissociation resets the transporter to the inward-facing conformation. Note that there are likely intermediate conformations, some asymmetric, that have not yet been resolved by crystallography.

(B) The inward-facing type I transporter (e.g., MalFGK2) binds to the substrate containing periplasmic binding protein and two molecules of MgATP. NBDs dimerize and result in the outward-facing conformation. Substrate leaves the binding protein and binds to the TMDs mid-membrane. ATP is hydrolyzed and product release, together with NBD dissociation, resets the transporter to the inward-facing conformation.

(C) The outward facing type II importer (e.g., BtuCD) binds to substrate binding protein and two molecules of MgATP. Dimerization of the NBDs results in the occluded conformation with substrate confined to a sealed cavity mid-membrane. Subsequent ATP hydrolysis and NBD dissociation allows substrate to escape into the cytoplasm. A fourth, asymmetric, conformation as seen for BtuCDF is not shown. (Wilkens, 2015)

V.2 The substrate-binding protein family (SBPs)

Substrate-binding proteins (SBPs), and substrate-binding domains (SBDs), form a class of proteins (and protein domains) that are often associated with membrane protein complexes for transport or signal transduction. SBPs were originally found to be associated with prokaryotic ABC transporters (Berger, 1973; Quiocho and Ledvina, 1996; Tam and Saier, 1993). They use substrate-binding proteins (SBPs) or covalent-linked substrate-binding domains (SBDs) to capture the solute and deliver the molecule for translocation by the transmembrane domain of the ABC transporter (Fulyani *et al*., 2013). Recently, some SBDs have been shown to be part of other membrane protein complexes, such as prokaryotic tripartite ATP-independent periplasmic (TRAP)-transporters (Gonin *et al*., 2007; Mulligan *et al*., 2009), prokaryotic two-component regulatory systems [8], eukaryotic guanylate cyclase-atrial natriuretic peptide receptors (Felder *et al*., 1999; Misono, 2002), G-protein coupled receptors (GPCRs) and ligand-gated ion channels (Armstrong and Gouaux, 2000) (Figure 18).

V.3 Classification of SBPs

The first SBP crystal structure, the L-arabinose binding protein, was solved in 1974 (Berntsson, 2010). Many more have been elucidated since then. Overall the SBPs are built of two α / β domains, with a central β-sheet of five β-strands flanked by α-helices. The two domains are connected by a hinge-region, with the ligand binding site buried in between the two domains. In the absence of ligand, the protein is flexible with the two domains rotating around the hinge (Tang *et al*., 2007) and exists largely in the open conformation with both domains separated (Quiocho and Ledvina, 1996). Upon substrate binding, the closed conformation is stabilized, and the ligand is trapped at the interface between the domains. This process has been called the ‘‘Venus Fly-trap” mechanism (Mao *et al*., 1982).

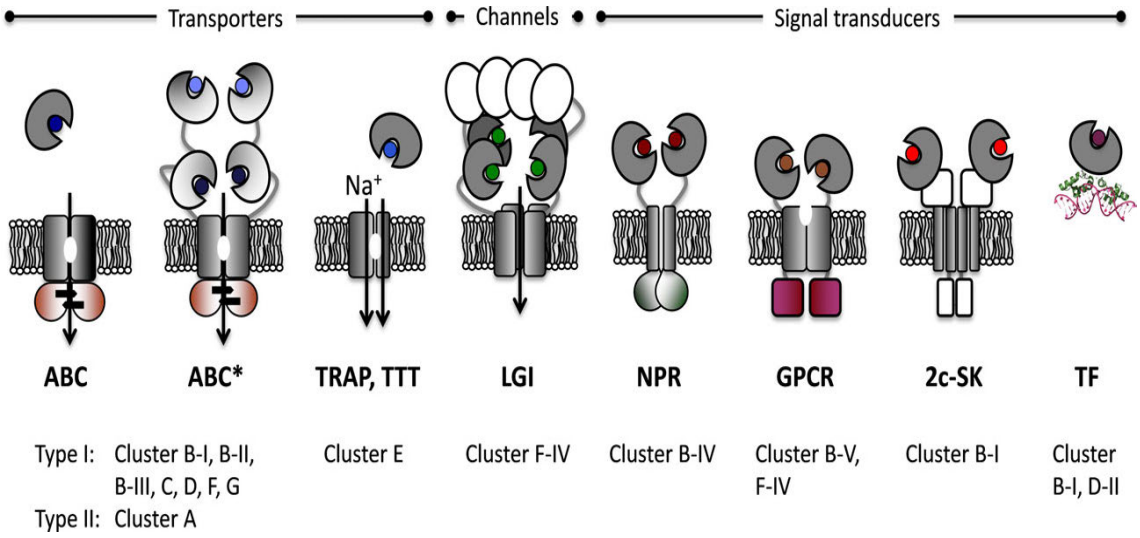

Figure 18 Schematic overview of SBP-dependent (membrane) proteins.

From left to right: ABC; an ABC importer with the SBP in the periplasm (in Gram-negative prokaryotes), ABC*; an ABC importer with two SBDs fused to the TMD, yielding four SBDs per transporter complex, TRAP/TTT; a tripartite ATP-independent periplasmic or tripartite tricarboxylate transporter with periplasmic SBP, LGI; a ligand-gated ion channel, based on the ionotropic glutamate receptors (tetrameric structures), with at the top the ATD domains involved in the oligomerization of the protein, NPR; a natriuretic peptide receptor with SBD, single transmembrane helix and an intracellular domain, GPCR; a G-protein-coupled receptor with a cytoplasmic domain, based on the metabotropic glutamate receptors, 2c-SK; a two-component sensor kinase and TF; a transcription factor with SBD and DNA-binding domain. In the cartoons, the SBPs or SBDs are indicated in gray and with a ligand bound (different colors). Below the cartoons, we indicate the clusters to which the SBP/SBD of the corresponding system belongs. Type I and Type II refers to different structural and functional classes of ABC transporters, and they clearly are also separate in the type SBP they interact with. (Scheepers *et al*., 2016)**.**

The SBPs grouped into six defined clusters (A–F) (Figure 19), three of which (clusters A, D and F) were further subdivided. Three proteins did not group with any of the six clusters. An overview of the characteristics of each (sub)cluster is shown (Table 5).

V.4 Cluster D of SBPs

The discernible feature of these proteins is that their hinge-region consists of two short strands, 4–5 amino acids long (Figure 19, D). This large group of SBPs binds a large variety of substrates; carbohydrates, putrescine, thiamine, tetrahedral oxyanion as well as ferric or ferrous iron. The subclusters found in this cluster correspond to thesubstrate specificity of the proteins. Likely, these subclusters are present due to the specific orientation and composition of the binding sites in these SBPs.

The first subcluster (D-I) contains a rather narrow substrate spectrum consisting of only carbohydrates such as maltose, glucose and galacturonide. Inspection of the structural distance tree reveals that these proteins have a larger similarity to the proteins in clusters C–F, than to the proteins in cluster B, although these proteins bind similar ligands. However, this subcluster has two additional distinguishing features when compared to the proteins of cluster B, namely size and domain organization. In subcluster D-I the SBPs are all slightly larger, with molecular weights above 40 kDa compared to 35 kDa of cluster B SBPs, and they all seem to have one small extra subdomain, as described for the maltose binding protein, which is the best characterized member of this subgroup (Spurlino *et al*., 1991).

A second, small, subcluster (D-II) contains polyamine-binding proteins, as well as the thiamine-binding protein TbpA. The third subcluster (D-III) is a very well-defined structural cluster, with proteins that bind tetrahedral oxyanions, and consists of molybdate-, sulfate-, and phosphate-binding proteins, like the molybdate binding protein ModA from *Archaeoglobus fulgidus* (Hollenstein *et al*., 2007).

The last subcluster (D-IV) contains only iron-binding proteins (FBPs). They all

bind either ferrous or ferric iron, usually via direct interactions with protein side-chains. A subset of the proteins (e.g. hFBP) also chelates the iron via a synergistic anion, whereas others do not require a bound anion (e.g. SfuA). The coordination of the iron ion, especially those that chelate the metal via a bound anion, is remarkably similar to mammalian transferrins, and these proteins have also been referred to as bacterial transferrins (Dhungana *et al*., 2003). However, the similarities in the metal coordination between the FBPs and the mammalian transferrins are believed to have arisen by convergent evolution (Bruns *et al*., 1997).

Cluster	Types of ligands	Classification by Fukami-Kobayashi et al. [37]	Additional information
A-I	Metal ions	Class III	Only associated with ABC-transporters
A-II	Siderophores	Class III	Only associated with ABC-transporters
B	Carbohydrates, Leu, Ile, Val, Autoinducer-2, Natriuretic peptide	Class I	Associated with ABC transporters, guanylate cyclase-atrial natriuretic peptide receptors and two-component sensor kinases. Homologous to *lac*-repressor type of transcription factors
C	Di- and oligopeptides, Arg, cellobiose, nickel	Class II	Only associated with ABC-transporters; extra large domain
D-I	Carbohydrates	Class II	Only associated with ABC-transporters; extra domain
D-II	Putrescine, thiamine	Class II	Only associated with ABC-transporters
D-III	Tetrahedral oxyanions	Class II	Only associated with ABC-transporters
D-IV	Iron ions	Class II	Only associated with ABC-transporters
E	Sialic acid, 2-keto acids, ectoine, pyroglutamic acid	Class II	Only associated with TRAP-transporters
F-I	Trigonal planar anions, unknown ligands	Class II	Only associated with ABC-transporters
F-II	Methionine	Class II	Only associated with ABC-transporters
F-III	Compatible solutes	Class II	Only associated with ABC-transporters
F-IV	Amino acids	Class II	Associated with ABC transporters, ligand-gated ion channels and GPCRs

Table 5 Overview of the determined clusters of SBPs.

Information of their ligand specificity, class and additional features.(Berntsson *et al*., 2010; Fukami-Kobayashi *et al*., 1999)

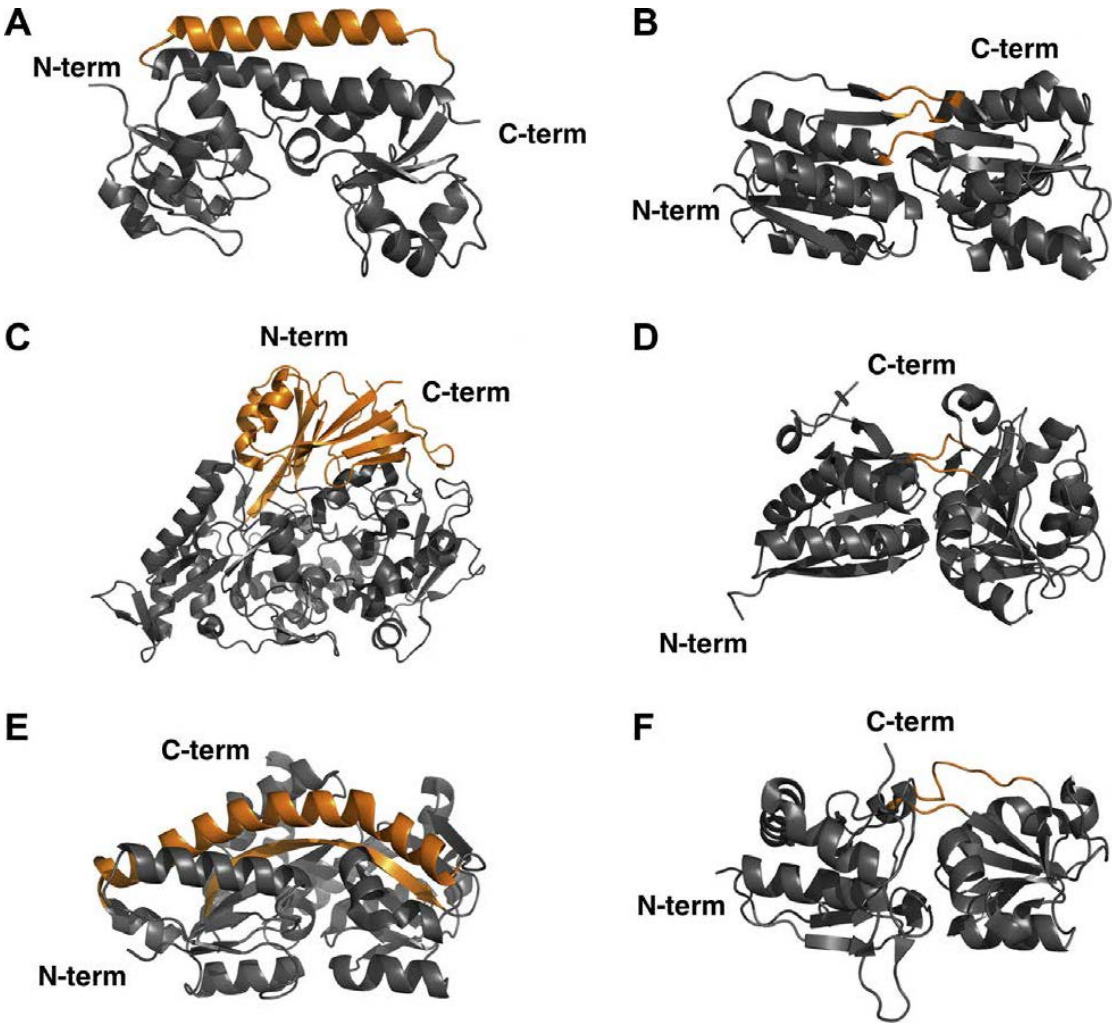

Figure 19 Six defined clusters of SBPs.

The different clusters of SBPs are shown with their distinct structural feature colored in orange. (A) Cluster A contains proteins having a single connection between the two domains in the form of a rigid helix. (B) Cluster B contains SBPs with three interconnecting segments between the two domains. (C) Cluster C contains SBPs that have an extra domain and are significantly larger in size when compared with the others. (D) Cluster D contains SBPs with two relative short hinges. (E) Cluster E contains SBPs associated with TRAP-transporters which all contain a large helix functioning as hinge region. (F) Cluster F contains SBPs with two hinges similar like cluster D, however, these hinges have almost double the length creating more flexibility inside the SBP. It should be noted that clusters A, D and F can be further subdivided based on the substrate of the SBP. (Berntsson *et al*., 2010)

Objectives of the study

D. dadantii is a plant pathogenic bacteria responsible of the soft rot disease of many plant of agronomic interest. Numerous studies have identified the Out T2SS and the proteins it secretes as important factors for the virulence of the bacteria. Secreted proteins are mainly CWDEs. Many of them are active on pectin. The pectin methylesterase PemA and the pectin acetylesterase PaeY demethylates and deacetylates, respectively, the homogalacturonate part of pectin in polygalacturonate which is cleaved by the pectate lyases PelA, PelB, PelC, PelD, PelE, PelI, PelL, PelN and PelZ in oligogalacturonate. RhiE is an endorhamnogalacturonate lyase that cleaves the rhamnogalacturonate I chain of pectin. In addition, the feruloylesterase FaeD cleaves side chains of pectin. The cellulase Cel5 cleaves the cellulose chains. Other proteins with no known enzymatic activity have been detected in the Out-dependent supernatant of *D. dadantii*: the necrosis inducing toxin NipE, and two proteins similar to avirulence proteins of *Xanthomonas*, AvrL and AvrM. Analysis of the Out-dependent secretome of another soft-rotting bacteria, *P. atrosepticum,* identified, in addition to these proteins, the protein ECA2134 of unknown function. This protein has two homologs in *D. dadantii*, that we named IbpS and IbpP. In this work, we determined the role of this family of proteins. We showed that Ibp proteins bind the redox active metals iron and copper and by this could prevent formation of ROS during plant infection. Ibp proteins are present not only in bacteria but also in fungi and oomycetes, mostly necrotrophic phytopathogens and in few animals (nematodes and Folsomia). Secretion of Ibp proteins could represent an antioxidant protection mechanism shared by necrotrophic phytopathogens required during infection.

Results

Chapter I: Article

Reactive oxygen species protection of necrotrophic phytopathogens by a conserved secreted metal binding protein

by Lulu Liu, Virginie Gueguen-Chaignon, Isabelle R Gonçalves, Christine Rascle, Martine Rigault, Alia Dellagi, Elise Loisel, Nathalie Poussereau, Agnès Rodrigue, Laurent Terradot, Guy Condemine

Submitted to Nature Communications

Reactive oxygen species protection of necrotrophic phytopathogens by a conserved secreted metal binding protein

Lulu Liu[1a], Virginie Gueguen-Chaignon[2a], Isabelle R Gonçalves[1a], Christine Rascle[1], Martine Rigault[3], Alia Dellagi[3], Elise Loisel[1], Nathalie Poussereau[1], Agnès Rodrigue[1], Laurent Terradot[4b], Guy Condemine[1b]

[1] Univ Lyon, Université Lyon 1, INSA de Lyon, CNRS UMR 5240 Microbiologie Adaptation et Pathogénie, F-69622 Villeurbanne, France.

[2] Protein Science Facility, SFR BioSciences, UMS3444/US8, Lyon, France

[3] Institut Jean-Pierre Bourgin, UMR1318 INRA-AgroParisTech, 78026 Versailles Cedex France

[4] UMR 5086 Molecular Microbiology and Structural Biochemistry, Institut de Biologie et Chimie des Protéines, CNRS-Université de Lyon, France.

[a] These three authors contributed equally to the work

[b] Corresponding authors

Summary

Few secreted proteins involved in plant infection common to necrotrophic bacteria, fungi and oomycetes have been identified except for plant cell wall-degrading enzymes. Herein, we have identified and characterized the properties of the Iron binding protein S (IbpS), a protein secreted by the plant pathogenic bacterial necrotroph *Dickeya dadantii*. Homologs of this protein are present not only in Gram+ bacteria but also in fungi, oomycetes, most phytopathogens, and some animals. The gene originating from bacteria was transferred once in oomycetes and most likely several times in fungi. The 1.7 Å crystal structure of IbpS reveals a classical Venus Fly trap fold that forms dimers in solution and in the crystal. IbpS is capable of binding the redox-active metals iron and copper. The protein is involved in the infection process of the bacterial pathogen *D. dadantii* and of the fungal necrotroph *Botrytis cinerea.* We propose that secreted IbpS binds exogenous iron, copper and possibly other metals, thereby preventing their intracellular accumulation and ROS formation in the microorganisms. Secretion of this metal-binding protein appears to be a common antioxidant protection mechanism shared by necrotrophic phytopathogens and required during infection.

Plants are regularly exposed to biotic stresses causing important economic losses. Major diseases are caused by phytopathogenic bacteria, viruses, fungi or oomycetes due to infectious strategies developed by the parasites that enable them to feed and grow on their hosts. To undergo their infectious cycle, plant pathogens adopt diverse parasitic lifestyles. For example biotrophs develop and feed on living tissues by maintaining a tightly regulated interaction in which the microbe does not kill its host [1]. Necrotrophs feed on dead tissues after inducing their necrosis or collapse [2] and hemibiotrophs evolve as biotrophs during the early stages of infection and then shift to a necrotrophic phase [3]. The secretion of host-selective or host-nonselective toxins and of plant cell wall-degrading enzymes are among the common strategies deployed by necrotrophic and

hemibiotrophic phytopathogens [4, 5] that contribute to the depolymerization of the structural plant cell wall polysaccharide components. Among all characterized proteins secreted by phytopathogenic microbes, only Nep1-like proteins (NLP) have been detected in fungi, oomycetes and bacteria [6]. These proteins trigger leaf necrosis and plant immunity-associated defences in dicotyledonous plants [7]. The widespread occurrence of this protein family in phytopathogenic microbes highlights their importance for the pathogens and a clear virulence role for this family has been observed in the bacterium *Pectobacterium carotovorum* and the fungus *Verticillium dalhiae* [8].

Upon infection, plants can activate a large array of defense responses regardless of the infectious parasites [9]. Effective defenses involve the production of reactive oxygen species (ROS), cell wall strengthening, and the production of phytoalexins and pathogenesis-related (PR) proteins. Plants are equipped with a basal immune system called Pattern Triggered Immunity (PTI) that is based on the recognition of conserved motifs, called microbe-associated molecular patterns (MAMPs) followed by activation of the abovementioned defenses [10]. Some pathogens can secrete effector proteins to suppress PTI. Plants have evolved resistance proteins capable of detecting such effectors thereby triggering strong defenses that culminate in a controlled, localized cell death called hypersensitive response. This strong immune response is termed effector triggered immunity (ETI).

ROS production comprises a general response occurring during either PTI or ETI. During infection, the superoxide anion produced by a plasma membrane anchored NADPH oxidase is the first ROS source, followed by a rapid dismutation of the superoxide anion into hydrogen peroxide [11]. In the presence of the redox-active metals Fe^{2+} and Cu^{2+}, hydrogen peroxide catalyses the Fenton reaction to produce the highly toxic hydroxyl radical which can severely damage macromolecules such as proteins, DNA and lipids. Although copper and iron can catalyse the formation of highly toxic ROS, these transition metals are essential for most living organisms since they function as cofactors of enzymes involved in key redox reactions. Because of this dual property,

Cu^{2+} and Fe^{2+} homeostasis is tightly regulated in all organisms to ensure their physiological needs and avoid toxicity. During a host-pathogen interaction, the management of these metals by both partners is complicated [12, 13, 14] and the oxidative stress generated may have deleterious effects on both the host and the pathogen. Thus, antioxidant systems are activated during infection both in the host and the microbe to control metal toxicity. The importance of copper in bacterial plant infections has not been investigated while the role of iron in the interactions of both animals and plants with their pathogens has been studied extensively. Iron is present in low amounts in plants, found mostly in the cell walls, vacuoles, plastids and the nucleus [15] [16]. In the plastids, iron is stored into proteins called ferritins which play major roles as antioxidant [17]. The fight for iron between plants and bacteria has been thoroughly studied using the soft rot-causing bacterial pathogens *Dickeya* and *Pectobacterium*. The limited availability of iron in the plant apoplast leads to the *D. dadantii* production of two siderophores to scavenge iron, achromobactin [18] and chrysobactin [19]. Both are required for the systemic progression of maceration symptoms in the host [20] [21]. Lowering free iron levels by injection of the siderophores chrysobactin or deferrioxamine activates plant immunity in *Arabidopsis thaliana* [22, 23]. In *A. thaliana* leaves, the accumulation of the AtFer1 ferritin around invading bacteria in response to *D. dadantii* infection is thought to avoid oxidative stress by scavenging iron and to deprive the bacteria from iron [12]. Iron is also a cofactor necessary for the activity of PelN, a pectate lyase secreted by *D. dadantii* required for full virulence on chicory leaves [24]. Interestingly, *A. thaliana* defensins AtPDF1.1 are antimicrobial peptides able to bind iron. Infection of leaves with *P. carotovorum* subsp. *carotovorum* induces the *AtPDF1.1* gene expression and an iron deficiency response in the plant [25]. Thus iron plays multiple roles during plant bacterial infection and both partners try to control the metal availability.

In this study we showed that IbpS, a protein secreted by *D. dadantii*, can bind Fe^{3+} and Cu^{2+}. We demonstrated that by binding these metals, IbpS reduces the toxicity of H_2O_2, probably by preventing the Fenton reaction. Injection of this protein into *A. thaliana* leaves triggers an iron deficiency response. This protein has homologs in

fungi and oomycetes, most likely due to the result of horizontal transfer of a coding gene from bacterial origin. The reduced pathogenicities of *D. dadantii ibpS* and *Botrytis cinerea ibp* mutants reveal the importance of this conserved protein in the infectious process deployed by necrotrophic microbes probably because of their impaired capacity to detoxify ROS produced during infection. Our data suggest that Ibp proteins could represent a novel antioxidant protection mechanism common to necrotrophic phytopathogens.

Results

IbpS is a type II secretion system substrate. The secretion of proteins by the type II secretion system (T2SS) is essential for the virulence of the soft rot bacteria *Pectobacterium atrosepticum* and *D. dadantii* [26]. Analysis of the *P. atrosepticum* SCRI1043 secretome identified several proteins secreted by the Out T2SS [27]: plant cell wall degrading enzymes, the virulence factor Nep (NLP) and three proteins of unknown function, ECA2134, ECA3580 and ECA3946. We investigated whether homologs of these three proteins of unknown function exist and are secreted by *D. dadantii* 3937. A BLAST search [28] identified two proteins similar to ECA2134 in the *D. dadantii* genome: ABF-18996 (88% identity) and ABF-14625 (69% identity) (named hereafter as IbpS and IbpP, respectively, see below). These proteins possess a predicted signal sequence necessary for secretion by a T2SS and are annotated as periplasmic components of ABC transport systems. ABC transport systems are generally composed of one or two nucleotide binding proteins, one or two transmembrane proteins and a high-affinity periplasmic substrate binding protein (SBP)[29]. While genes coding for these proteins are usually organised in operon in bacterial genomes, it is not the case for the genes encoding IbpS and IbpP. The *ibpS* gene is located in a cluster of genes encoding type three secretion system substrates (HrpK, HrpW and DspE) and the contact-dependent growth inhibition protein CdiA1 (Supplementary Fig. 1). IbpP is

positioned next to genes coding for the secreted proteases PrtA, PrtB and PrtC and for their secretion

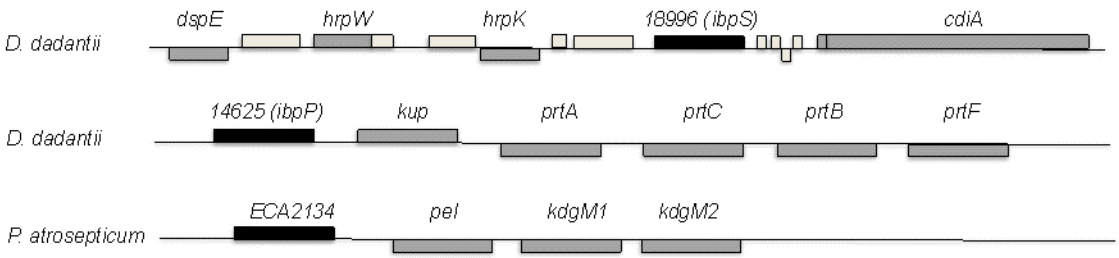

Supplementary Fig. 1 Genetic environment of *D. dadantii ibpS*, *ibpP* and *P. atrosepticum* ECA2134. The genes *ibpS*, *ibpP* and *ECA2134* are shown as black boxes. Genes with known functions are shown in dark grey, and those with unknown function are shown in light grey. *D. dadantii* 3937 GenBank accession no. CP002038.1, *P. atrosepticum* GenBank accession no. BX950851.1.

system PrtF. In *P. atrosepticum* ECA2134 is adjacent to the genes encoding the pectate lyase Pel, and KdgM1 and KdgM2, the two pectin degradation product outer membrane channels (Supplementary Fig. 1). The absence of genes encoding ABC transport components in the vicinity of these genes and the presence of virulence factor genes in both bacteria support a role for these proteins in virulence rather than in transport. This hypothesis was also supported by transcriptomic analyses. In *A. thaliana* infection experiments by *D. dadantii*, *ibpS* was identified as one of most expressed genes at early stages [30, 31]. We thus tested whether the presence of plant tissues could induce *ibpS* expression. When *D. dadantii* cells were cultured in the presence of chicory leaves (fresh or autoclaved), *ibpS* expression was increased by six-fold compared to the control (Supplementary Fig. 2). In contrast, pectin degradation products polygalacturonate and galacturonate, known to induce most *D. dadantii* virulence genes [32] had no effect on *ibpS* expression (Supplementary Fig. 2). The basal level of *ibpP* expression was very low and none of the tested conditions induced expression of this gene whose expression was undetectable in *D. dadantii* 3937.

We tested IbpS secretion in a "chicory-induced" *D. dadantii* culture using IbpS antibody. The protein could be detected in the extracellular medium of a wild-type *D. dadantii* strain culture but remained inside the cells in an *outD* mutant (Supplementary Fig. 3). IbpS is thus a T2SS substrate like ECA2134 in *P. atrosepticum*.

***ibpS* has homologs in eukaryotes.** Proteins from the Ibp family were searched in the NCBI non redundant database using the PSI-BLAST program and 897 proteins from 383 species/strains (222 bacteria and 161 eukaryotes; Supplementary Table 1) were retrieved. Ibp proteins are thus not only encoded by genes present in some Gram- and Gram+ bacteria, but also by genes in oomycetes, fungi and in two metazoa, the springtail *Folsomia candida* and the cereal cyst nematode *Heterodera avenae*. Interestingly, most of the organisms possessing at least one *ibp* gene are

phytopathogens that have an hemibiotrophic or necrotrophic lifestyle (Supplementary Table 1). The genome of the hemibiotroph oomycete *Phytophthora sojae* harbors the

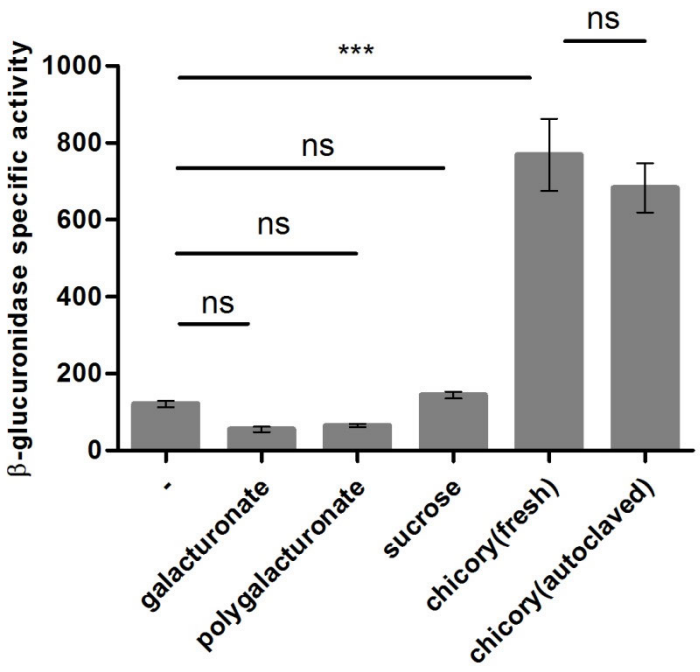

Supplementary Fig. 2 Expression of *D. dadantii ibpS* in various growth conditions. *D. dadantii* strain A5488 containing the *ibpS-uidA* fusion was grown in M63 + glycerol medium in the presence of the indicated compounds. ß-glucuronidase activity was measured with *p*-nitrophenyl-ß-D-glucuronate. Activities are expressed in µmoles of *p*-nitrophenol produced per minute and per milligram of bacterial dry weight ± standard deviation. Data are expressed as the mean (n = 4) from four independent experiments. *** $p < 0.0001$.

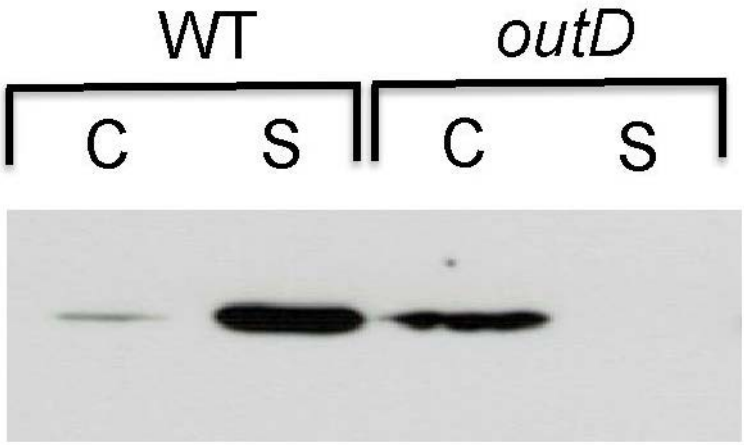

Supplementary Fig. 3 *D. dadantii* IbpS is secreted by the Out secretion system. Wild-type and *outD* mutant strains were grown overnight in M63 + glycerol medium containing a slice of chicory. The supernatant (S) and cellular (C) fractions were separated by SDS-PAGE. After blotting, IbpS was immunodetected.

most *ibp* genes (10) while BlastP searches on the EnsemblProtist website [33] showed that two others *Phytophthora* species (*P. parasitica* and *P. nicotianae*) and two necrotrophy species (*Pythium ultimum* and *P. aphanidermatum*) also have at least 6 *ibp* genes (Supplementary Fig. 4). Putative signal sequences were predicted in Ibp proteins by the SignalP server [34] and also by the TatP 1.0 server [35] in the case of bacterial Ibp. Overall, putative signal sequences were predicted in 241 Ibp proteins from eukaryotes (over 301, 80%), 153 proteins from Gram+ bacteria (over 191, 80%) and 171 proteins from Gram- bacteria (over 405, 42%). The latter percentage is biased by an over-representation of *Pseudomonas* proteins in the NCBI non-redundant database. When the 231 proteins of *Pseudomonas* were excluded from the analysis, signal sequences were predicted in 143 Ibp proteins (over 174, 82%) from Gram- bacteria. Numerous Ibp proteins are thus potentially secreted.

To avoid species representation bias, 70 species were selected to study the evolution of their proteins belonging to the Ibp family (Supplementary Table 2). Eukaryotic Ibp proteins do not form a monophyletic group (Fig. 1), which, together with their patchy taxonomic distribution, suggests that they originate from distinct horizontal gene transfers (HGTs) from bacteria. The Ibp proteins of oomycetes and metazoa formed well-supported groups with bacterial proteins, among which *D. dadantii* IbpS and IbpP were found, in the trees constructed using two phylogenetic approaches (maximum likelihood (ML) and Bayesian). The fungal proteins of the Ibp family mainly form two well-supported classes that group together. Class I members were found in Basidiomycota species and some Ascomycota species, including *Botrytis cinerea* while class II members were found in only Ascomycota species. In these two classes, the genes had intronic regions but introns from the class I genes had no homology with those of the class II genes (Supplementary Fig. 5), which was the outcome expected if two independent HGTs led to these two classes. Other fungal proteins from the Zoopagomycota were grouped by only species. Overall, the evolutionary relationships of fungal proteins with the rest of the Ibp protein family were

not clearly resolved in the phylogenetic topologies, providing no clue to the bacteria at the origin of the transfers to fungi. Finally, the different bacteria did not form monophyletic groups per taxonomic class. Instead, several well-supported nodes grouped proteins from different bacterial groups together suggesting that HGTs also occurred between bacteria.

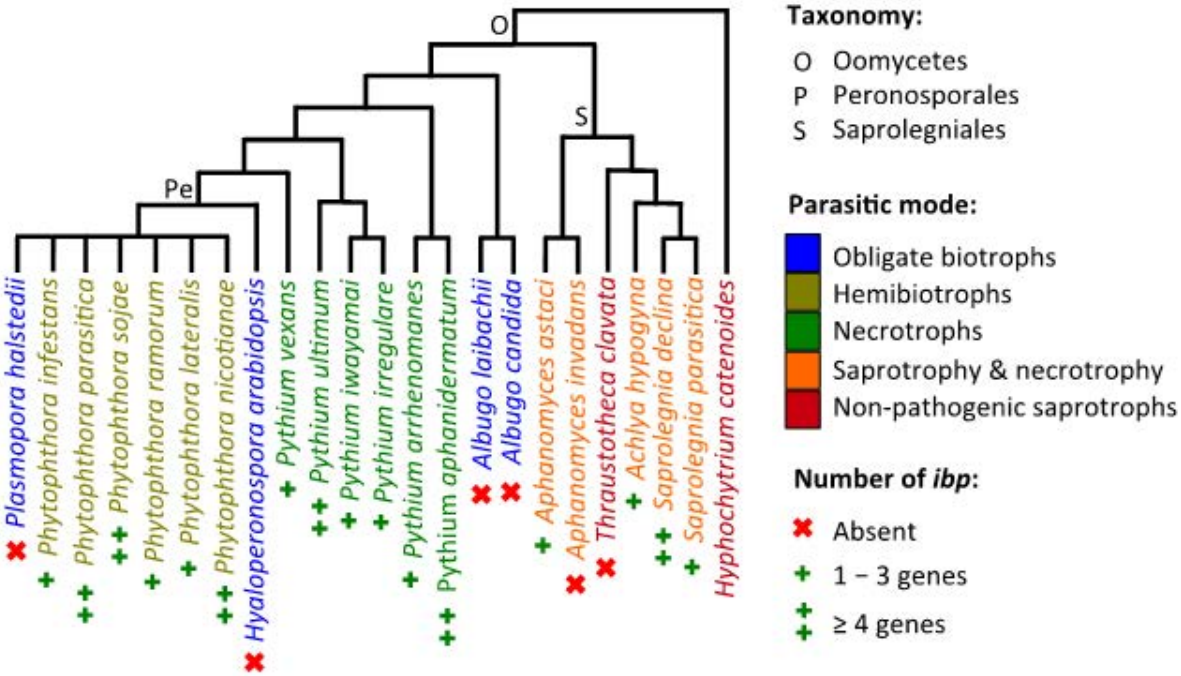

Supplementary Fig. 4 The number of *ibp* genes is associated with the parasitic mode in oomycetes. The schematic representation of the phylogeny of the oomycetes with *Hyphochytrium catenoides* as an outgroup is adapted from [1]. *ibp* gene numbers results from the PSI-BLAST search with the NCBI nr database (see Methods) and additional BLASTP searches on the EnsemblProtist website.

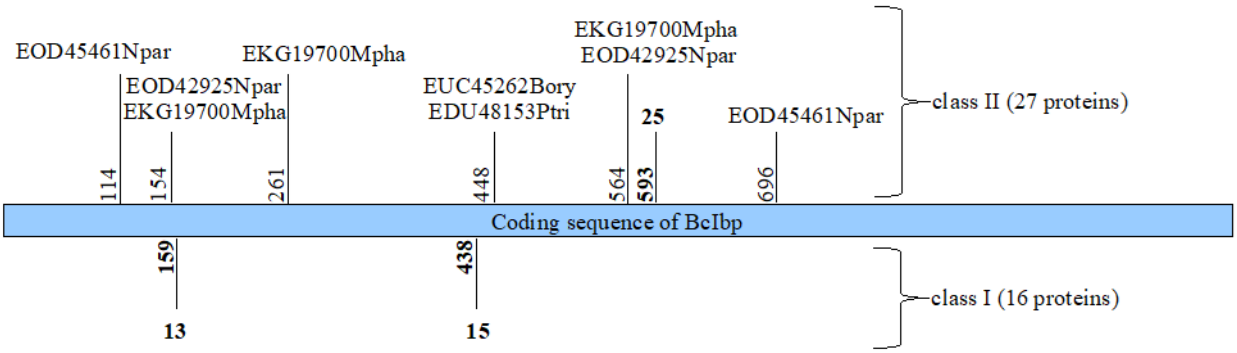

Supplementary Fig. 5 Fungal class I and II Ibp-encoding genes have no common introns. The intron positions were mapped on the coding sequence (CDS) of the *Botrytis cinerea ibp* gene, after alignment of the *ibp* CDSs of the two classes from the corresponding multiple protein alignment (http://wwwabi.snv.jussieu.fr/public/Clustal2Dna/). Each vertical line represents an observed intron position, written on the side of these lines. At their top (class II) or bottom (class I) tip, the number of protein sequences having the corresponding intron is marked or replaced with the name of the corresponding sequences if few sequences were available. For the list of genes belonging to classes I and class II, see supplementary Table 2.

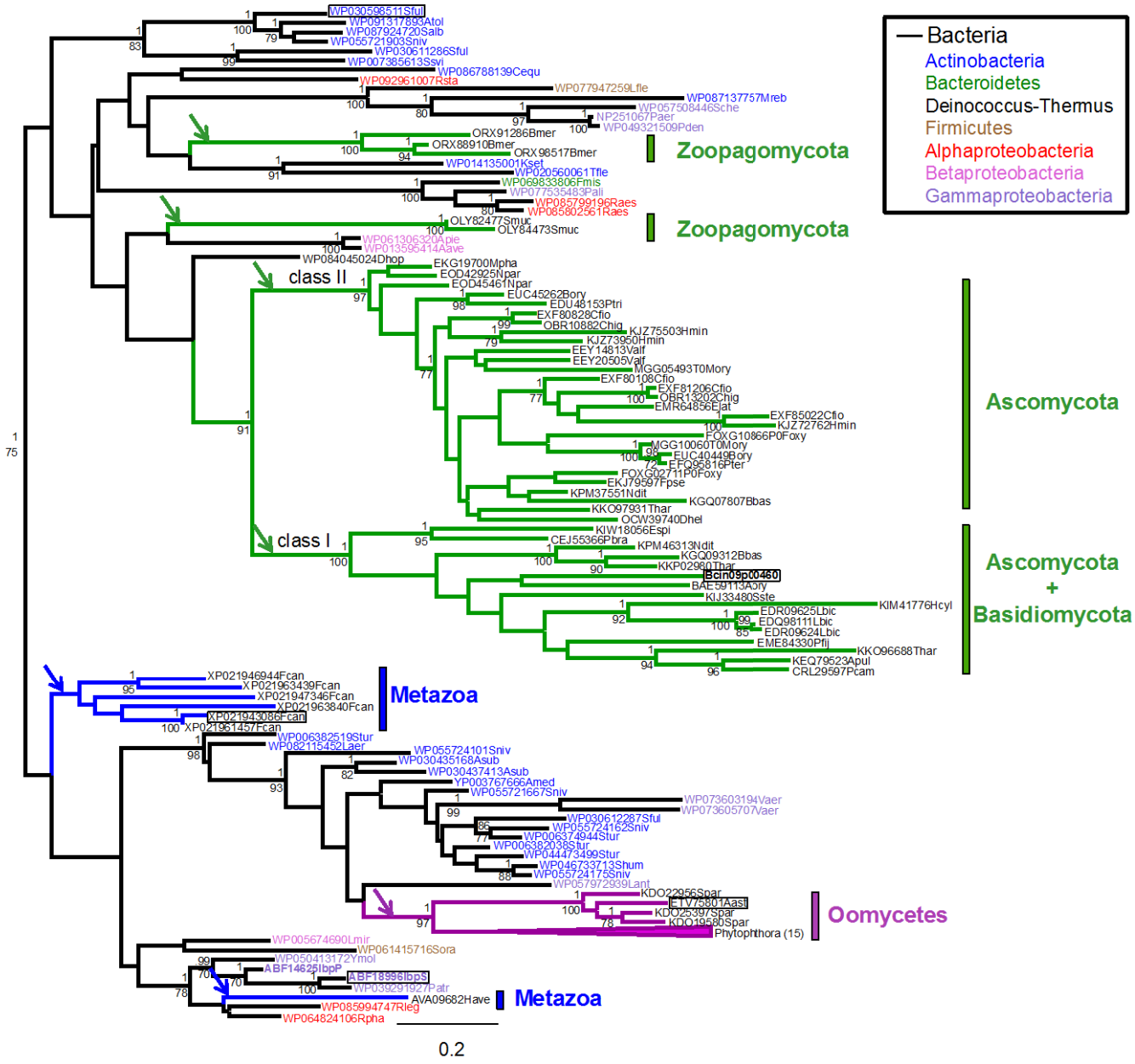

Fig. 1. Phylogeny of IbpS and homologs. An alignment of 198 amino acids from 122 sequences was used to construct the phylogenies. The maximum likelihood tree was used as a reference topology. Bootstraps of interest ≥70 are shown below the branches and the corresponding posterior probabilities in the Bayesian topology are reported above. Arrows represent probable transfer events from bacteria to eukaryotes. The names of the proteins analysed in this study are indicated in bold. The structure-based sequence alignment of the proteins with a boxed name is shown in Supplementary Fig. 8. The branches leading to fungal proteins are coloured green, those leading to oomycete proteins are coloured in red and those leading to metazoan proteins are coloured in blue. The bacterial protein names are coloured as described in the box. The corresponding species and sequence accession numbers are available in Supplementary Table 2.

Ibp family members are metal binding proteins. To determine whether the functionalities of the proteins were conserved despite the genetic transfers and the phylogenetic distances, we investigated the properties and roles of the bacterial IbpS and IbpP proteins as well as those of the distant fungal *B. cinerea* BcIbp protein. Given that IbpS and IbpP in *D. dadantii* showed homology to SfuA, the ferric iron binding protein of the SfuABC transporter, we speculated that Ibp proteins could also bind iron. When purified IbpS was incubated with Ni-NTA, Cu-NTA, Zn-NTA and Fe-NTA resins, IbpS interacted with Fe-NTA and Cu-NTA matrixes but did not with Ni-NTA and Zn-NTA matrixes (Fig. 2a). Similarly, IbpP and BcIbp also bound the Fe-NTA and Cu-NTA resins (Supplementary Fig. 6).

To gain insight into the metal-binding property of the protein, metallation of IbpS by Fe^{3+} was monitored by UV-visible spectrometry by following the spectral changes between 230 and 800 nm. The addition of increasing amounts of $FeCl_3$ led to the appearance of 2 absorption bands at 250 nm and 320 nm (Fig. 2b). The signal increased linearly up to 15 equivalents of Fe^{3+} and no saturation was observed (Supplementary Fig. 7a). Because IbpS was not saturated with Fe^{3+}, the extinction coefficient could not be deduced from the spectra. The metallation was not due to non-specific binding as the signals at 250 nm and 320 nm were still recorded after buffer exchange using gel-exclusion columns (Fig. 2b and inset). The metallation of IbpS was carried out in the presence of the Fe^{3+} donor, Fe-NTA, which is a strong affinity Fe^{3+} chelator, or Fe-citrate, which is a weaker affinity chelator and detected by UV-visible spectroscopy. In both cases, IbpS was able to compete with these anions, leading to absorption spectra identical to those obtained when using $FeCl_3$ as the Fe^{3+} donor. Finally, IbpS was mixed with Fe^{3+}-CAS (Chrome Azurol S) and the binding of Fe^{3+} to CAS yielded an absorption band at 650 nm [36] (Fig. 2c). When IbpS was added in increasing amounts to the Fe^{3+}-CAS solution, the absorption at 650 nm decreased indicating that IbpS sequestered Fe^{3+} from Fe^{3+}-CAS (Fig. 2c).

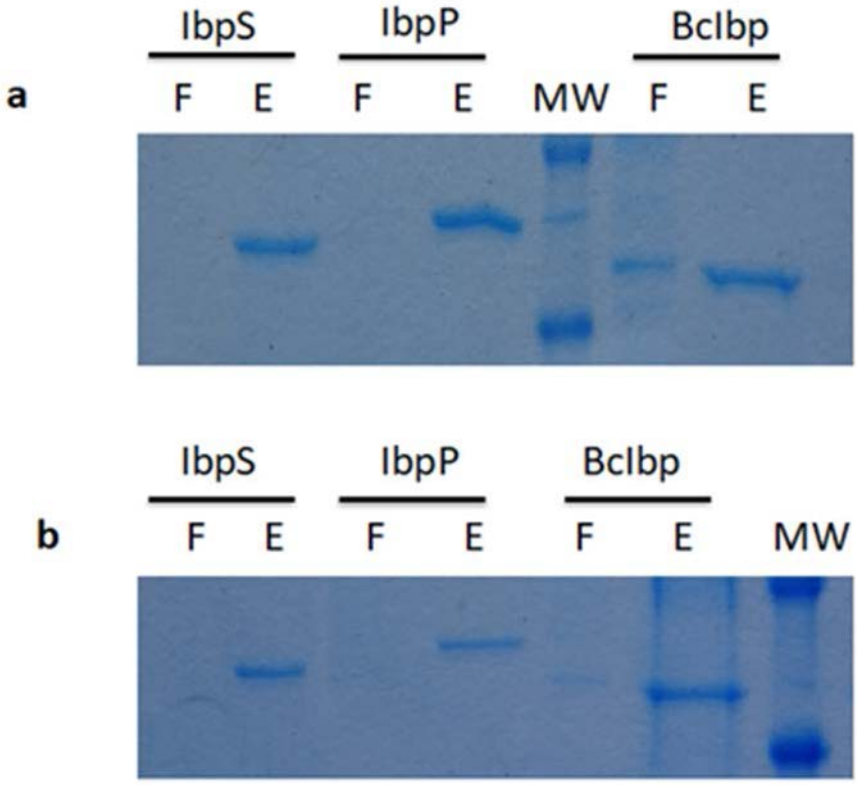

Supplementary Fig 6 IbpS, IbpP and BcIbp bind iron and copper. **a-b** IbpS, IbpP or BcIbp (10 µg) in 100 µl of A buffer was incubated with 100 µl of the (**a**) Cu-NTA or (**b**) Fe-NTA resins for 15 min. After centrifugation the supernatants (flowthroughs) were removed and the resins were washed three times with 1 ml of buffer A. Protein was eluted with 100 µl of 50 mM EDTA and 10 µl of the flowthrough (F) or eluate (E) was loaded onto a SDS-PAGE gel.

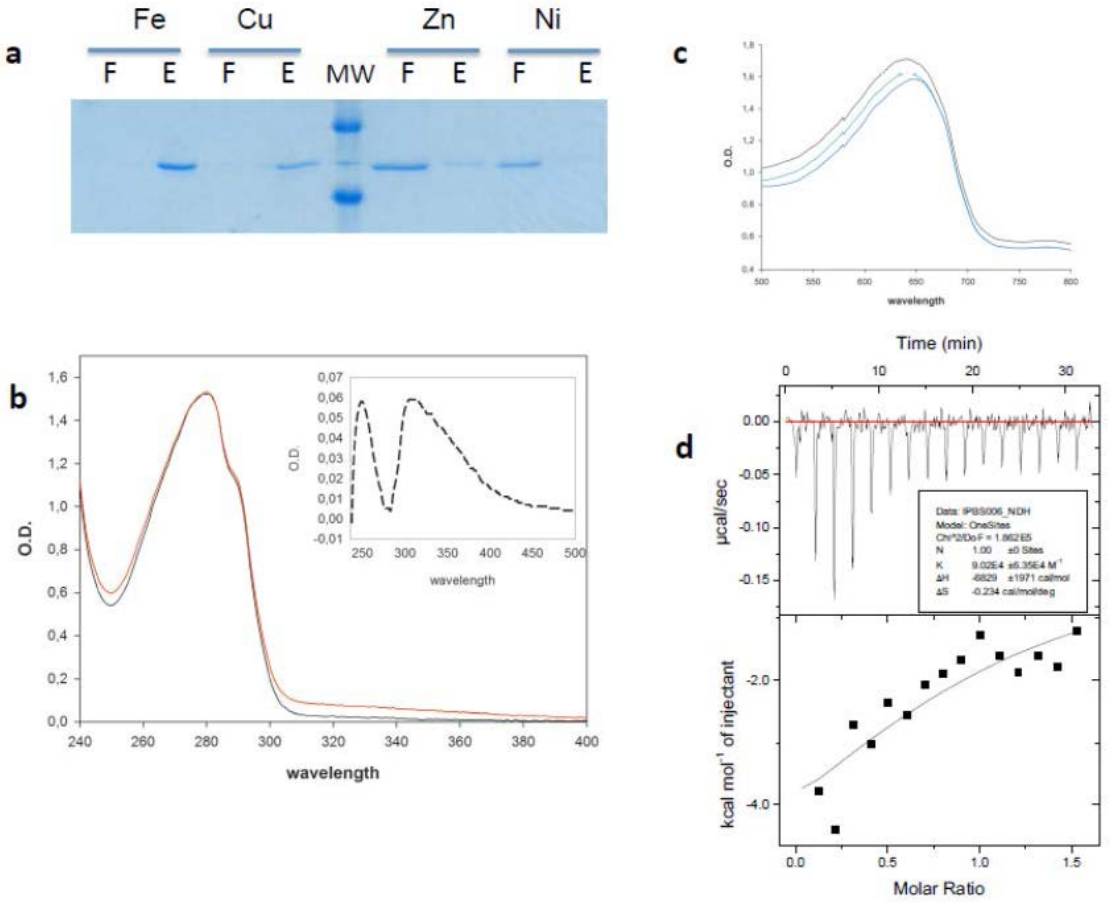

Fig. 2. IbpS is a metal binding protein. **a** IbpS (10 µg) in 100 µl of A buffer was incubated with 100 µl of Fe-NTA, Cu-NTA, Ni-NTA or Zn-NTA resins for 15 min. After centrifugation the supernatants (flowthroughs) were removed and the resins were washed three times with 1 ml of buffer A. The protein was eluted with 100 µl of 50 mM EDTA and 10 µl of flowthrough (F) or eluate (E) was loaded onto an SDS-PAGE gel. **b** UV-visible Fe titration of 70 µM apo-IbpS. The protein was incubated with up to 10 equivalents of $FeCl_3$ added sequentially, and then buffer-exchanged to remove any unbound metal. Black: apo-protein, red: metal-loaded protein. Inset: The differential spectrum corresponding to the subtraction of the apo protein spectrum is shown. **c** UV-visible CAS titration of apo-IbpS. IbpS at 50 and 100 µM was incubated with 0.06% CAS. The spectra were recorded after overnight incubation at 4°C. Black: CAS, green: CAS + 50 µM IbpS, blue: CAS + 100 µM IbpS. **d** Isothermal titration calorimetry of IbpS. $Cu(II)Cl_2$ (1 mM) titrated into apo-IbpS (120 µM) in 10 mM Tris-HCl buffer (pH 7.0) at 30 °C. A blank run consisting of $CuCl_2$ dilution in the experimental buffer was performed and values subtracted from the assay. Top, raw data. Bottom, plot of integrated heats versus the Cu/IbpS ratio. The solid line represents the best fit for a one-site binding model.

IbpS possesses 11 tryptophan residues in its mature form and can generate a strong fluorescence emission signal at an excitation wavelength λ= 280 nm. This signal was not altered upon the addition of up to 20 metal equivalents of divalent cations such as Zn^{2+}, Ni^{2+}, Co^{2+} and Cd^{2+} (data not shown). In contrast, the addition of increasing amounts of Fe3+ ions gradually quenched this signal demonstrating that this metal altered the environment of at least one tryptophan residue (Supplementary Fig. 7b). The binding curve was biphasic. A saturation was observed for 1 equivalent of Fe (Supplementary Fig. 7c). Then the addition of increasing amounts of FeCl3 did not lead to the saturation of the spectra (Supplementary Fig. 7d). These results indicate that IbpS binds one Fe, and then that non-specific binding also occurs. In these conditions it was not possible to determine an affinity constant from the spectra for the first site. Thus, an alternative approach, isothermal titration calorimetry (ITC) was utilised. However, the quality of the binding isotherm did not allow the determination of a K_D neither, certainly in reason of the non-specific binding of Fe.

IbpS was retained on the Cu-NTA resin indicating that this protein can bind Cu^{2+} ions. However, fluorescence spectroscopy showed altered IbpS spectra in the presence of Cu^{2+}. Saturation of the titration was obtained for one equivalent of Cu (Supplementary Fig. 7d). In order to determine an affinity constant ITC experiments were performed. The titration of Cu^{2+} into a solution of purified IbpS in 10 mM Tris-HCl buffer pH 7.0 induced significant enthalpy changes. A one-site binding model with stoichiometry of 1 was used to fit the data, yielding a Kd of 10 μM (± 15) (Fig. 2d). These results show that IbpS binds one Cu^{2+} with a micromolar affinity.

Taken together these results clearly indicated that IbpS and IbpP bound Fe^{3+} and Cu^{2+} which is the reason why ABF-18996 was named IbpS (for iron binding protein secreted) and ABF-14625 IbpP, respectively.

IbpS is prototypal of a novel class of substrate binding proteins. The crystal structure of the translocated region of *D. dadantii* IbpS (residues 28 to 372) was solved

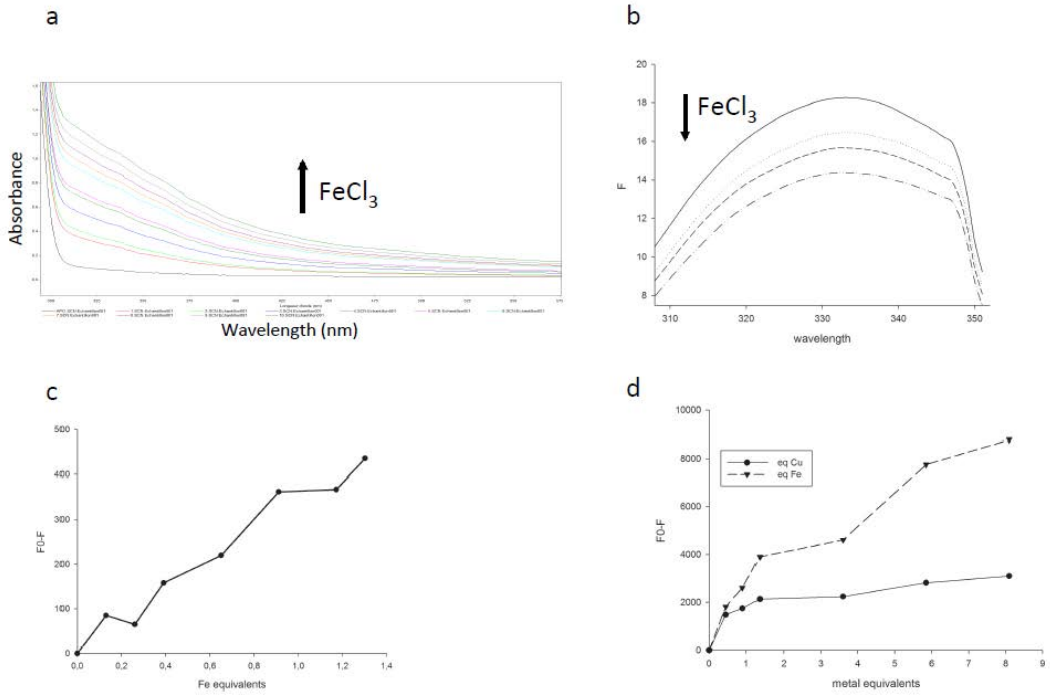

Supplementary Fig. 7 a UV-visible Fe titration of 70 µM apo-IbpS. The protein was incubated with up to 10 equivalents of $FeCl_3$ added sequentially. **b** Fluorescence spectra of 70 µM IbpS titrated with up to 10 equivalents of $FeCl_3$ added sequentially. **c** Fluorescence spectra of 38 µM IpbS titrated with the indicated equivalents of $FeCl_3$. The F0-F values are plotted. **d** Fluorescence spectra of 40 µM IbpS titrated with the indicated equivalents of $FeCl_3$ (dashed line) or $CuCl_2$ (solid line). The F0-F values are plotted. The experiments were performed four times. A typical experiment is shown.

Table 1: Data collection and refinement statistics

	IbpS	IbpS-Iron	IbpS-SeMet
Wavelength	0.9730	1.5895	0.9788
PDB Entry	6FJL	6HHB	
Resolution range	47.55 - 1.7 (1.761 - 1.7)	47.99 - 1.8 (1.86 - 1.80)	47.72 - 1.80 (1.89 - 1.80)
Space group	P 1 21 1	P1	P 1 21 1
Unit cell	77.45 112.31 78.72 90 95.53 90	58.89 78.89 83.91 73.25 74.74 84.92	76.88 112.26 79 90 94.8 90
Total reflections	502926 (70465)	442176 (42714)	1738809 (218801)
Unique reflections	146429 (21285)	111674 (10701)	122446 (16267)
Multiplicity	3.4 (3.3)	4.0 (4.0)	14.2 (13.5)
Completeness (%)	99.7 (99.4)	86.3 (82.8)	98.40 (89.9)
Mean I/sigma(I)	8.6 (1.3)	14.9 (2.5)	16.3 (5.3)
Wilson B-factor	25	22.12	15.9
R-merge	0.06 (0.6)	0.06 (0.5)	0.09 (0.4)
R-meas	0.07 (0.7)	0.07 (0.6)	0.10 (0.46)
R-pim	0.04 (0.39)	0.03 (0.28)	0.04 (0.17)
CC1/2	0.99 (0.85)	0.99 (0.85)	0.99 (0.95)
CC*	0.99 (0.95)	1 (0.96)	1 (0.98)
Reflections used in refinement	146072 (11977)	111650 (10703)	
Reflections used for R-free	7358 (235)	5524 (510)	
R-work	0.174 (0.314)	0.155 (0.219)	

R-free	0.206 (0.345)	0.191 (0.262)	
CC(work)	0.97 (0.87)	0.97 (0.86)	
CC(free)	0.96 (0.80)	0.96 (0.76)	
Macromolecules	10990	11010	
Ligands	18	16	
Solvent	1132	1129	
Protein residues	1380	1380	
RMS(bonds)	0.007	0.008	
RMS(angles)	1.03	1.11	
Ramachandran favored (%)	98	98	
Ramachandran allowed (%)	2	2	
Ramachandran outliers (%)	0	0	
Rotamer outliers (%)	0.2	0.3	
Clashscore	2.99	2.02	
Average B-factor	37	26.9	
Macromolecules	36.30	26.0	
Ligands	49.4	55.0	
Solvent	43.2	34.8	

Statistics for the highest-resolution shell are shown in parentheses.

at a resolution of 1.7 Å using the single anomalous dispersion method (Table 1). The asymmetric unit of the crystal contains four chains A, B, C and D that are nearly identical (rmsd <0.4 Å). The structure of the IbpS monomer displays a typical SBP fold with two α/β lobes connected by a central hinge region consisting of an extended two-strand β-sheet (Fig. 3a and Supplementary Fig. 8). The SBP fold is associated with ligand binding to a pocket located between the two lobes via the so-called "Venus's flytrap" [37]. In absence of ligand the two lobes are in flexible open conformation and close upon substrate binding. An structural homology search using DALI server [38] showed that IbpS is most similar of the SBP class II/cluster D [29] (Z score >20), a subgroup that encompasses proteins interacting with a large variety of substrates such as carbohydrates, polyamine, tetrahedral oxyanions or ferrous or ferric iron [29, 39]. However, the structure of IbpS exhibits some unique features. The protein displays an additional α-helix at its N-terminus and an extended C-terminal tail (residues 352-372) that, to our knowledge, are not observed in the other members of the class II/cluster D family. The C-terminal tail connects the two lobes on the edge of the substrate-binding pocket (Fig. 3a) and appears to stabilize the protein in a conformation similar to a closed state, even in the absence of ligand. Furthermore, the central α-helix in the substrate binding pocket, which is involved in iron or ligand binding in several classII/cluster D members such as AfuA [40] or FutA [41] is absent in *D. dadantii* IbpS structure and replaced by an extended loop (Fig. 3b). Consequently, the *D. dadantii* IbpS ligand-binding pocket is significantly different from that of other classII/clusterD family members and IbpS does not have the residues involved in iron supplementary Fig. 8). Moreover, the ligand-binding pocket is partly occluded by the C-terminal tail and the N-terminal part of α2. Instead, IbpS structure reveals a tunnel that runs perpendicular to the hinge β-strands and is open at both sides of the protein surface (Supplementary Fig. 9)

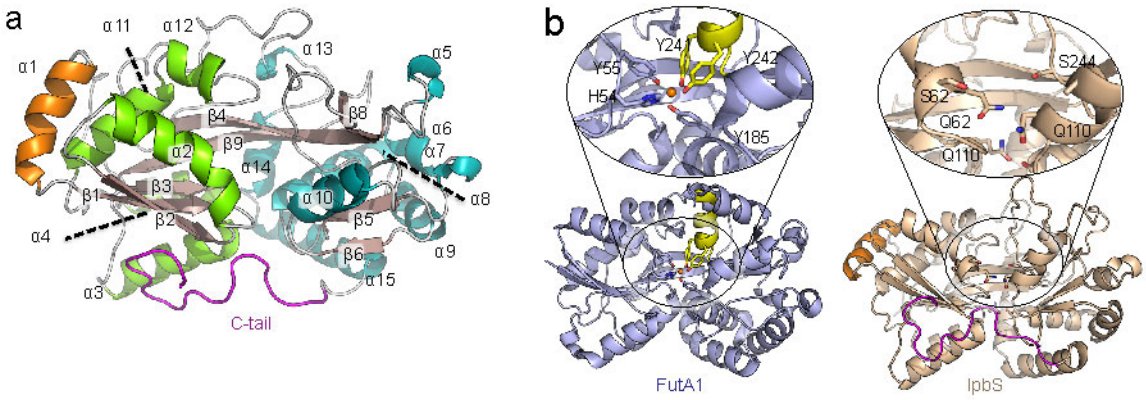

Fig. 3. Structure of IbpS. **a** Ribbon representation of the crystal structure of IbpS (chain A). β-strands are coloured in brown, α-helices are coloured in green (N-lobe) or blue (C-lobe) except for α1 helix coloured in orange. The C-terminal tail is coloured in magenta. **b** Comparison of the iron-binding site of FutA1 (PDB code 3F11) with the corresponding residues in IbpS after superimposing the two structures. The iron atom is depicted as an orange sphere in FutA1. Residues Y241, Y242, Y55, Y185 and H54 coordinating iron in FutA1 are not conserved in IbpS. In particular the Y241/Y242-containing helix of FutA1 is replaced by a loop in IbpS, that has only a serine (S244) pointing towards the substrate binding pocket.

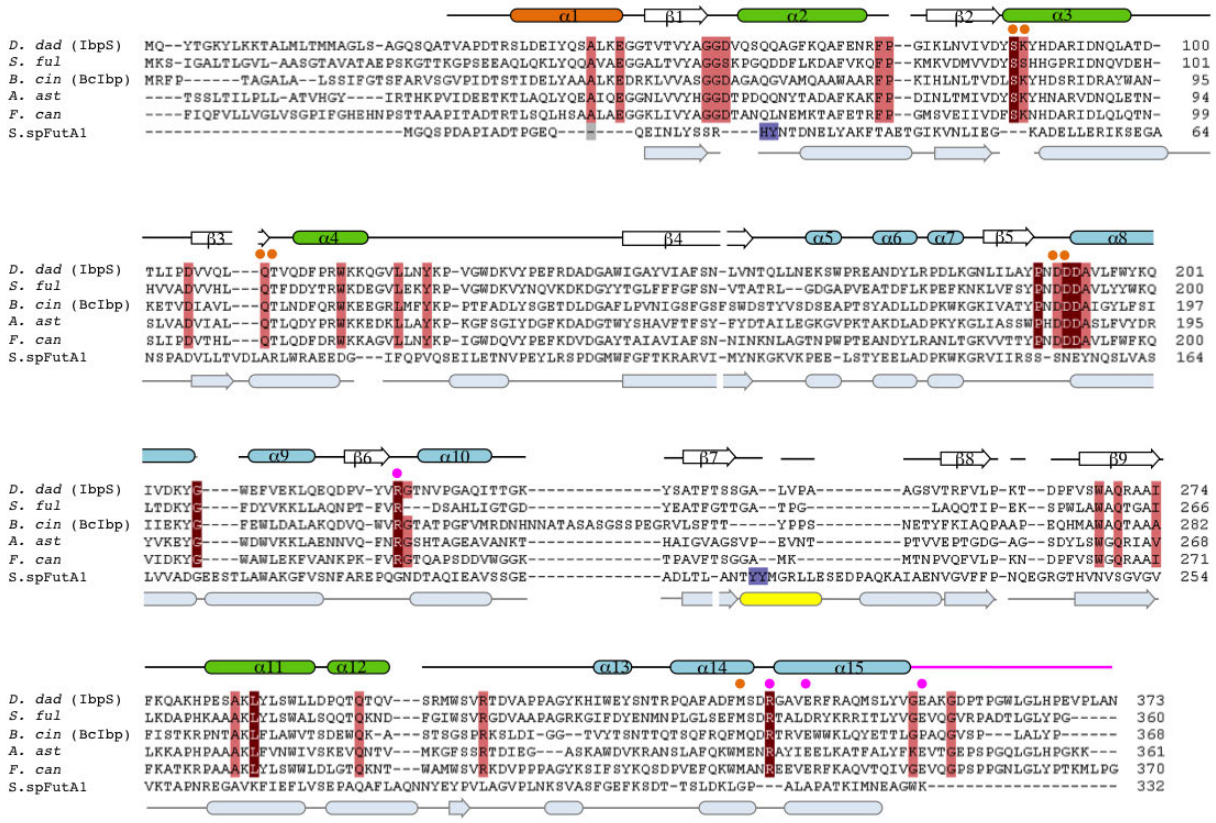

Supplementary Figure 8. Structure-based sequence alignment of IbpS with homologs. Sequences corresponding to Ibp proteins from *Dickeya dadantii* (IbpS, ABF18996), *Streptomyces fulvoviolaceus* (WP030598511), *Botrytis cinerea* (BcIbp, 09p00460), *Aphanomyces astaci* (ETV75801), *Folsomia candida* (XP029143086) were aligned with Clustal O. The corresponding species are also indicated in the phylogenetic tree (Fig. 1). The sequence of FutA1 from *Synechocystis sp.* corresponding to the crystal structure (pdb 3F11) was aligned by structural superimposition using DALI. Residues coordinating iron in FutA1 are shaded in blue. Secondary structures of IbpS and of FutA1 are indicated above and below the sequences, respectively and coloured according to Fig. 3a. Strictly conserved residues are coloured in firebrick and strongly conserved (95%) residues are coloured in salmon. Orange dots indicate residues participating to the iron-binding pocket in IbpS. Magenta dots indicate residues involved in the dimerisation interface.

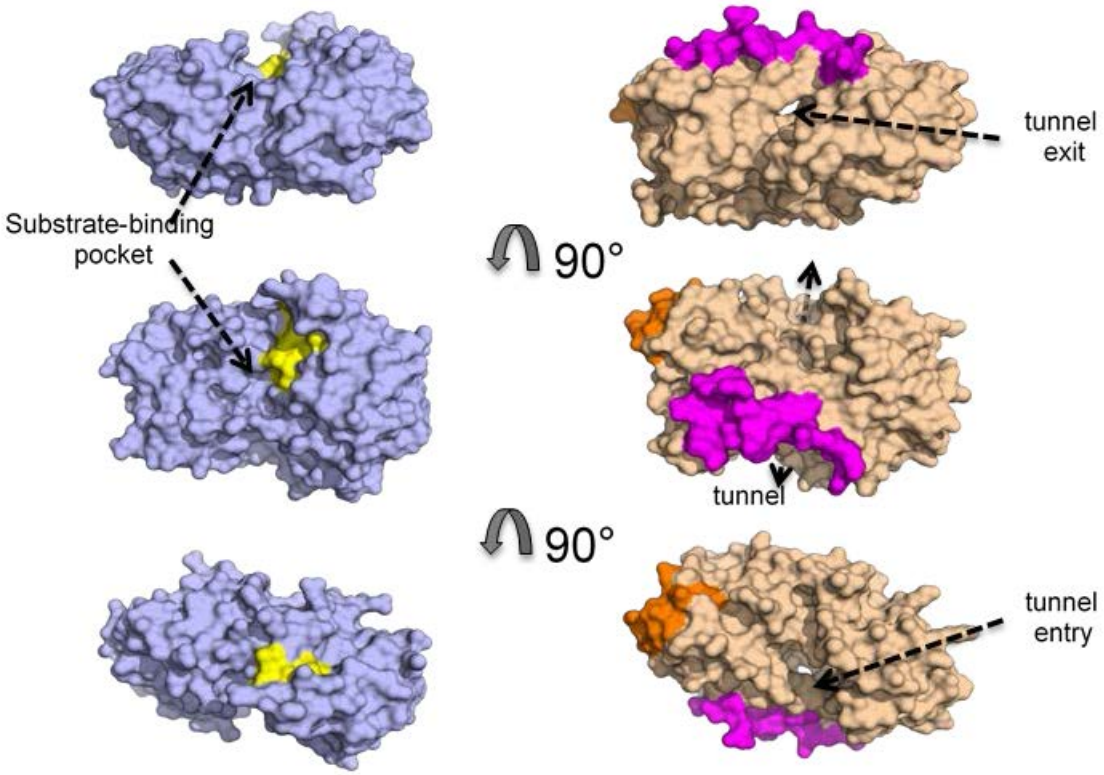

Supplementary Figure 9. Structural comparison of the accessible surfaces of FutA1 (pdb code 3F11) and IbpS structure. The structures are coloured in blue (FutA1) with the helix involved in iron binding coloured in yellow as in Fig 3a). IbpS is coloured in wheat, except for the additional N-terminal helix (orange) and C-terminal tail (magenta). The figure illustrates the structural difference of the canonical substrate-binding pocket and the presence of a tunnel in IbpS structure.

IbpS forms dimers. We observed two dimers in the crystal formed by A and D' (symmetry-related of chain D) and B and C' (symmetry-related of chain C) that were original and not found in other SBP structures to our knowledge (Fig. 4a). The interface buries 1230 $Å^2$ and is made of electrostatic interactions between α3 from chain A and α15 from chain D' and vice versa and between the two α15 helices. There, R337 and R344 make hydrogen bonds with the adjacent α15 E341. The interface also involves hydrophobic interactions between the two C-terminal tails that extensively interact with α15 and with each other. Notably, E353 inserts into the adjacent subunit to form a salt bridge with the buried R223 from the β6-α10 loops (Fig. 4b). Several residues involved in the dimerization, including R223 and R337 are strongly conserved (Supplementary Fig. 8) suggesting that dimerization might be a general feature of the Ibp protein family. To determine whether IbpS forms dimers in solution we performed size exclusion chromatography coupled with multi-angle laser light scattering (SEC-MALS) measurements. As seen in Fig. 4c, the protein eluted as a single peak with a calculated mass of 79 kDa, thus in agreement with a dimeric form (theoretical mass of 79 kDa). Because no other significant interface was found in the crystal, the A/D' dimer very likely exists in solution.

A low-affinity metal binding site is present in IbpS. Given that IbpS bound iron and copper in our metallation experiments, we tried to co-crystallize the protein in the presence of various metals. While crystals could be obtained in the presence of Zn, Mn, Cu, none of the crystal structures solved showed any evidence of metal binding. In the case of iron, the protein was co-crystallized with $FeCl_3$ and the structure of iron bound IbpS was solved at a resolution of 1.8 Å (Table 1). The protein crystalized in a different crystal form with the P1 space group and four molecules per asymmetric unit. All four molecules were bound to a single iron atom at the same binding site (Fig.5a-c). The structures of IbpS and Fe-IbpS were nearly identical and no important structural modification was observed. As suspected from our previous analysis, the metal did not bind at the canonical SBP cluster D protein substrate-binding pocket. Instead, the iron

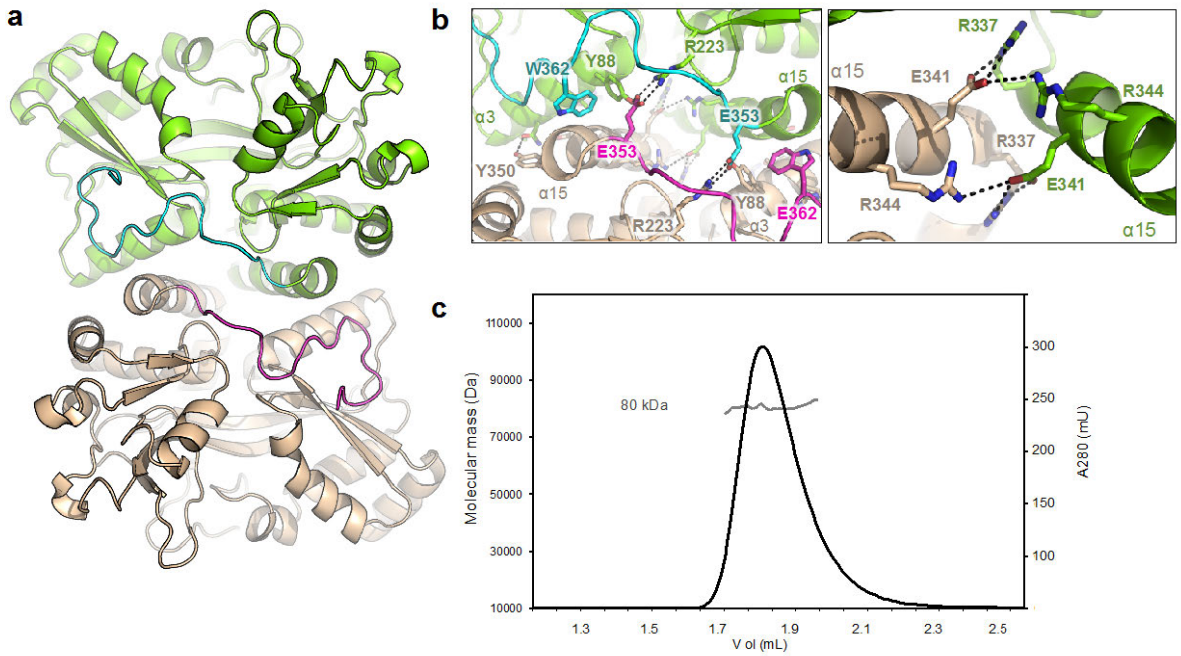

Fig. 4. IbpS is a dimer. **a** Cartoon representation of the IbpS dimer between chains A (green) and D' (wheat). The C-terminal tails of chains A and D' are coloured blue and magenta, respectively. **b** Close-up views of the dimer interface. The residues involved are indicated, and the side chains are shown as ball-and-sticks and coloured like that in **a**. **c** SEC_MALS analysis of the IbpS dimer.

atom was located near the dimer interface (Fig 5a), at the entry of tunnel identified previously (Supplementary Fig. 9). The metal sits in a cavity formed by residues S86, K87, Q110, T111, M334 and a triple aspartate motif of the α5 - β8 loop (D191, D192, D193, Fig. 5c) and containing a dense network of water molecules. In this negatively charged cavity the iron is poorly coordinated (only a water molecule according to the "Check my metal" server - https://csgid.org/csgid/metal_sites [42]) (Fig 5c). This poor coordination might explain the weak binding affinity of IbpS observed in our metallation assays and suggests that metal binding is reversible. Strikingly, when residues conservation based on the alignment of 122 sequences of IbpS homologs was mapped on the IbpS structure, most of the conserved residues (100% and 95% sequence identity) cluster at the iron-binding site, suggesting that this feature is critical for the protein function and conserved across the Ibp family (Fig. 6).

Intracellular metal concentration modification by extracellular IbpS. Metal binding by a secreted protein could decrease the metal available in the external medium thereby decreasing the intracellular bacterial metal level. To test this hypothesis, we used the *acsA* gene expression as a sensor of intracellular Fe^{2+} level. *acsA* encodes a protein involved in achromobactin synthesis and its expression is under the control of the transcription factor Fur in response to Fe^{2+} concentrations [21]. When bacteria were grown in an iron-depleted medium, *acsA* was expressed at a high level and the addition of 2 µM of Fe^{3+} to the medium repressed its expression by 1.5-fold (Fig. 7a). Addition of Fe^{3+} and 2 µM ethylene-N, N'-bis (2-hydroxyphenyl-acetic acid (EDDHA) to the medium prevented repression since EDDHA chelates iron. The addition of 20 µM IbpS to the growth medium led to results similar to those obtained with EDDHA, suggesting that IbpS in the external medium reduced the intracellular iron concentration (Fig. 7a).

The intracellular Cu^{2+} concentration was then monitored in *E. coli* using the *luxCDABE* reporter gene fused to the autoregulated copper binding response regulator *czcR3* as a biosensor of intracellular Cu^{2+} levels. The activity of the reporter increased

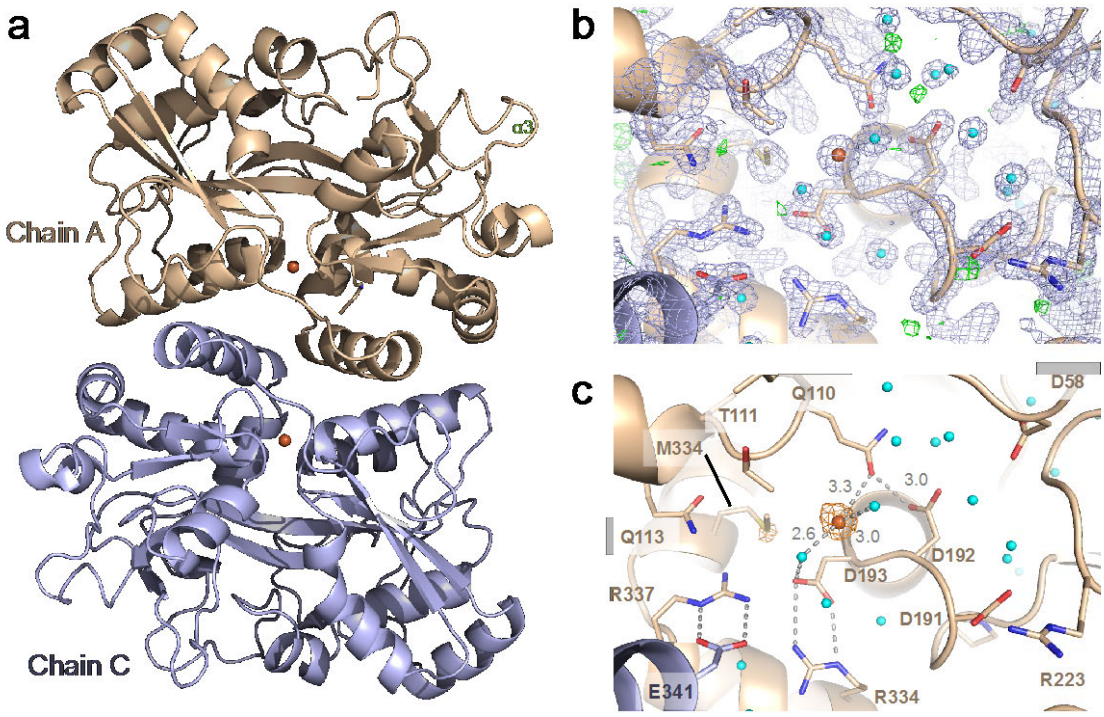

Fig. 5. Structure of Fe-IbpS. **a** Cartoon representation of Fe-IbpS dimer with iron atom (orange sphere) bound to chain A (wheat) and C (light blue). **b** Close-up view of the iron-binding site in chain A. The structure is depicted in ball-and-stick with water molecules and iron atom represented as spheres coloured in cyan and orange with an overlay of $2F_o$-F_c electron density (blue mesh, contoured at 2.0 σ) and F_o-F_c map (green mesh, contoured at 3σ). **c** Same view as **b** with an overlay of the anomalous electron density map contoured at 4σ (orange mesh). Interactions at the iron binding sites are shown as grey dashed lines and distances are indicated in Å.

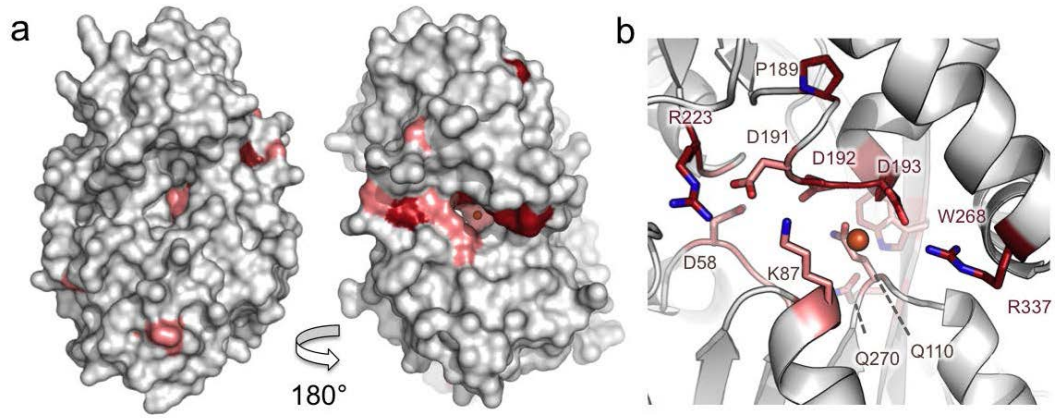

Fig. 6. IbpS unusual iron-binding site involves conserved residues. **a** Two different orientations of a surface representation of the iron-binding site of IbpS. Strictly conserved residues are coloured in firebrick and strongly conserved (95%) residues are coloured in salmon (see also Supplementary Fig. 8). Sequence conservation was obtained from the alignment of 122 sequences used to generate the phylogenic tree (Fig.1). **b** Detailed view of the metal binding site with side chains shown as ball-and-stick. Iron atom is depicted as an orange sphere.

as a function of external Cu^{2+} concentration (Fig. 7b). When IbpS was added exogenously together with Cu^{2+}, the activity of the fusion dropped to a level comparable to that in the condition in which no Cu^{2+} was added (Fig. 7b). These results show that IbpS is capable of reducing the intracellular Cu^{2+} concentration by chelating it in the external medium.

To determine whether IbpS can affect the iron status *in planta*, leaves of *A. thaliana* seedlings were infiltrated with purified IbpS at a concentration of 6 µM. The expression levels of two plant genes known to respond to iron concentration were monitored. Expression of the gene encoding the plant transcription factor bHLH38 is upregulated under iron deficiency [43] while the ferritin-encoding gene, *AtFER1* is upregulated under iron excess and repressed under iron deficiency [44]. Twenty-four hours after IbpS treatment, *bhlh38* expression was upregulated and *AtFER1* expression was decreased (Fig. 7c). These data indicate that the plant experienced iron deficiency stress upon IbpS treatment, which is consistent with the capacity of the protein to bind iron.

Protective effect of Ibp proteins on bacterial cells exposed to hydrogen peroxide. Plant defense reactions involve the production of H_2O_2 which generates highly reactive ROS, such as OH°, that kill the pathogens in the presence of iron or copper. We hypothesized that IbpS secretion would reduce the concentrations of free iron and copper in the plant apoplasm, consequentially also reducing the production of ROS. In *Erwinia amylovora*, production of the siderophore desferrioxamine which binds iron protects the bacteria from H_2O_2-induced death [45]. When *D. dadantii* cells were exposed to 10 mM H_2O_2 a strong decrease in viability was observed (Fig. 8a). When IbpS or IbpP (50 µM) was added to the medium 5 min prior to the addition of bacteria, a protective ability against H_2O_2-induced death was observed. The same level of protection was obtained by adding the iron chelator EDDHA at 50 µM and a similar protection effect was observed in *E. coli* cells exposed to 30 mM H_2O_2 (Fig. 8b). Thus,

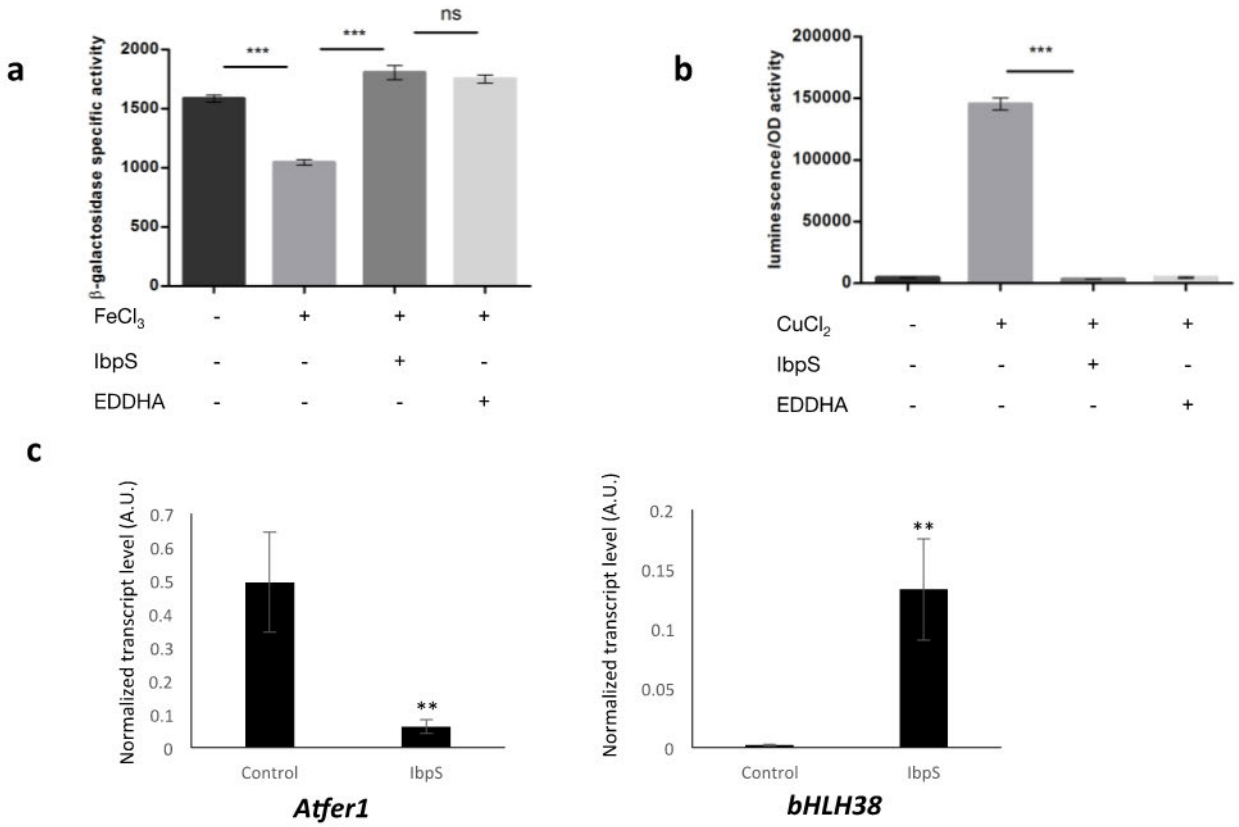

Fig. 7 Modification of the intracellular metal concentration by extracellularly added IbpS. **a** *D. dadantii* strain A6050 containing the *acsA-lacZ* fusion was grown overnight in low phosphate + glycerol medium either supplemented or not with 2 µM $FeCl_3$, 20 µM IbpS or 2 µM EDDHA. ß-galactosidase activity was measured with *o*-nitrophenyl-ß-D-galactose. The activities are presented as the mean value from at least four separate experiments and expressed in µmoles of *o*-nitrophenol produced per minute and per milligram of bacterial dry weight ± standard deviation. Data are expressed as the mean ($n = 6$) from four independent experiments. *** $p < 0.0001$. **b** *E. coli* strain W3110 containing the plasmidic *czcR3-luxCDABE* fusion was grown in low phosphate + glycerol medium either supplemented or not with 2 µM $CuCl_2$, 20 µM IbpS or 2 µM EDDHA. Luminescence was recorded during 8 h; the value of the maximum activity recorded during the kinetics is plotted on the graph (luminescence (A.U.)/OD 600 nm). Data are expressed as the mean ($n = 3$) from three independent experiments. *** $p< 0.0001$. **c** Expression of the *A. thaliana Atfer1* and *bHLH38* genes. *A. thaliana* leaves were infiltrated with Buffer A or 6 µM IbpS in buffer A. After 24 h, RNA was extracted, reverse transcribed and subjected to real time qPCR using gene-specific primers. Gene expression is indicated in arbitrary units and was normalized against synthetic constitutive gene *clathrin* and *actin* transcript levels. Experiments were performed two times with similar results. Representative data are shown. Bars, SD of the normalized ratio. For each point, six plants were used, and three leaves per plant were infiltrated. Significant differences between control and IbpS treaments is indicated by **: t-test $p < 0.05$.

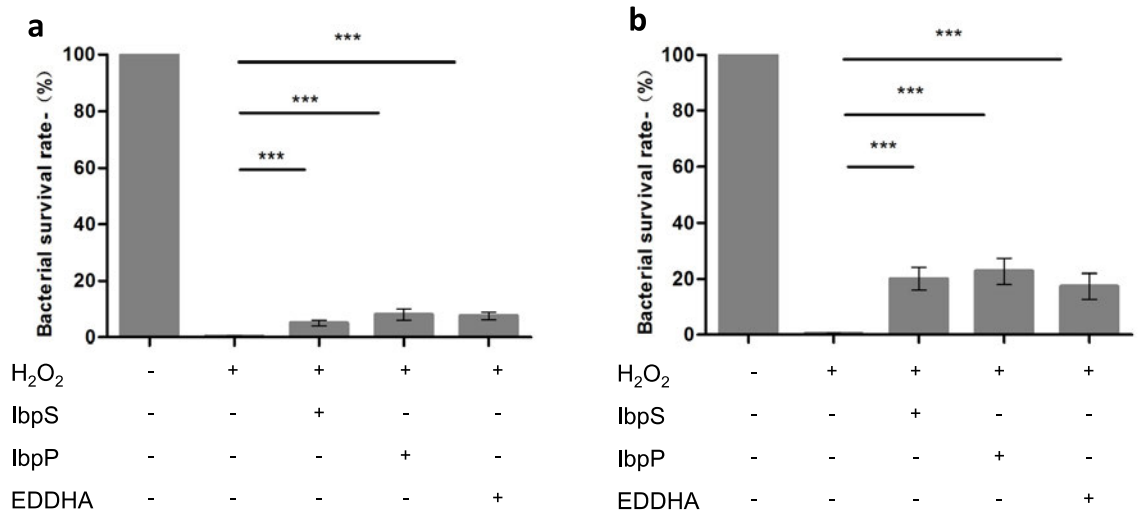

Fig. 8 IbpS protects bacteria exposed to hydrogen peroxide.

a *D. dadantii* A4922 or **b** *E. coli* NM522 cells were resuspended in water either supplemented or not with 50 µM IbpS, 50 µM IbpP or 50 µM EDDHA. After 5 min, 10 mM (**a)** or 30 mM (**b)** H_2O_2 was added. After 30 min, the number of viable bacteria was determined by plating serial dilutions on LB agar plates. Data are expressed as the mean from five independent experiments. *** $p < 0.0001$.

the binding of trace amounts of metal present in the medium by IbpS prevents H_2O_2-induced bacterial death.

Ibp proteins are involved in the infectious process of the necrotrophic microbes *D. dadantii* and *B. cinerea.* In a large-scale transcriptome analysis of *B. cinerea* during cucumber infection, at 96 h postinfection, the *Bcibp* gene (genome annotation: Bcin09g004) was upregulated 3.6-fold [46]. We analyzed *Bcibp* gene expression during bean leaf infection: leaves were inoculated with a suspension of spores and *Bcibp* expression was detected as early as 16 h postinfection (hpi) before emergence of symptoms. An increase in *Bcibp* expression was observed throughout the colonization and maceration of plant tissues (Supplementary Fig. 10). Thus *Bcibp* is expressed in *B. cinerea* and its expression is induced during plant infection.

D. dadantii ibpS and *B. cinerea ibp* mutants were created and tested on various plants to estimate the role of the protein in virulence. A clear diminution of symptoms was visible on *A. thaliana* leaves infected with the *D. dadantii ibpS* mutant compared to that in plants infected with the wild-type strain (Fig. 9a, b). The development of symptoms often stopped at stage 2 (part of the infected leaf maceration) and fewer completely macerated leaves and less generalization to the entire plant were observed. This phenotype could be complemented by introduction of a plasmid bearing *ibpS* in the *D. dadantii* mutant (Supplementary Fig. 11). To test whether the production of IbpS protects bacteria from ROS produced by the plant, we performed infection tests with the *atrbohD-atrbohF A. thaliana* mutant, which is unable to produce H_2O_2 after a *D. dadantii* infection. No differences in the time of appearance or extension of symptoms were observed between the plants infected with the wild type strain and the *D. dadantii ibpS* mutant (Fig. 9c, d). Thus, an IbpS-nonproducing strain is no longer disadvantaged when infecting a plant that does not produce H_2O_2. Although the *Arabidopsis* mutants

may also be altered in other aspects of their immune responses, this result suggests a protecting role of IbpS against these defences during infection.

The infection of cucumbers and beans with the *B. cinerea Bcibp* mutant also revealed a defect in virulence (Fig. 9e, f). Six days after contamination with the mutant, 55% of the the cucumber cotyledons and 43% of primary bean leaves exhibited no symptoms in contrast to the leaves infected with the wild-type strain which were totally macerated. In some cases (8% of cucumbers and 33% of beans) primary lesions were observed but did not progress (Fig. 9e, f). Thus absence of Ibp protein production led to the reduced virulence of both a bacterium and a fungus.

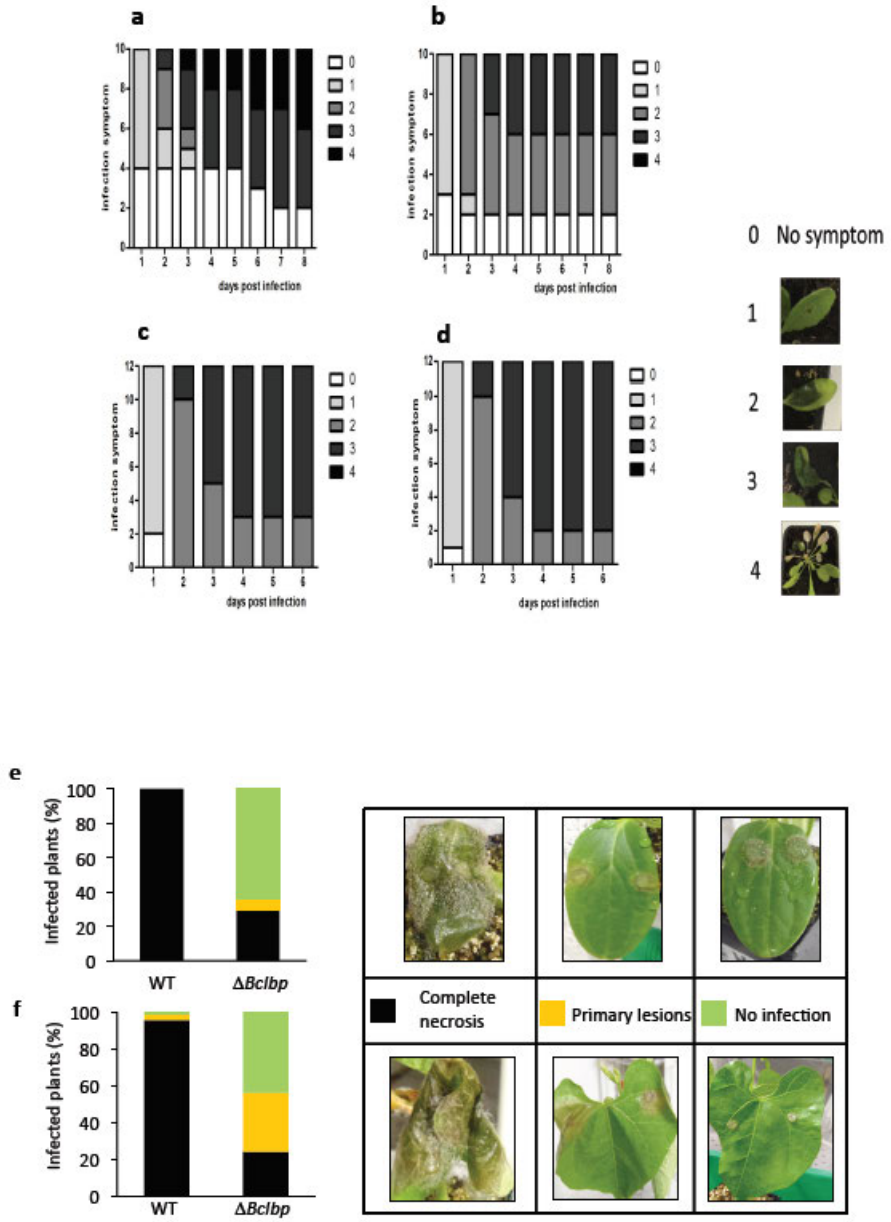

Fig. 9 Reduced virulence of *D. dadantii* and *B. cinerea ibp* mutants. **a-d** Evolution of the symptoms on *A. thaliana* Col0 (**a** and **b)** and *atrbohD-atrbohF* (**c** and **d**) after inoculation with the wild-type strain (**a** and **c**) or the *ibpS* mutant (**b** and **d**). Infection was performed on a single leaf by the deposition of a drop containing approximately 50 bacteria on a wound made by a needle. Symptoms were classified in five stages as shown on the right. stage 0: no symptoms; stage 1, symptoms around the spot of

infection: stage 2: maceration of the leaf limb; stage 3: maceration of the whole leaf, including the petiole; stage 4: generalization to the whole plant. * indicates a statistical difference ($p< 0.05$) between results of the wild type and the mutant strain at a given day. ns: not significant. No difference in class distribution was observed for the *atrbohD-atrbohF* mutant infection. One representative experiment out of four (for the Col0 infection) and out of three (for the *atrbohD-atrbohF* mutant infection) is represented. **e-f** Pathogenicity assays of the *B. cinerea* WT and Δ*Bcibp* strains on cucumber cotyledons (**e**) and French bean leaves (**f**). Seven-day-old plants were infected with 3-day-old mycelial plugs. Disease symptoms were scored 6 days after infection. The disease categories and symptom developments on both plant hosts are indicated on the right. All tests were performed in three independent experiments with at least fifteen leaves or cotyledons per strain for each test and two points of infection per leaf or cotyledon.

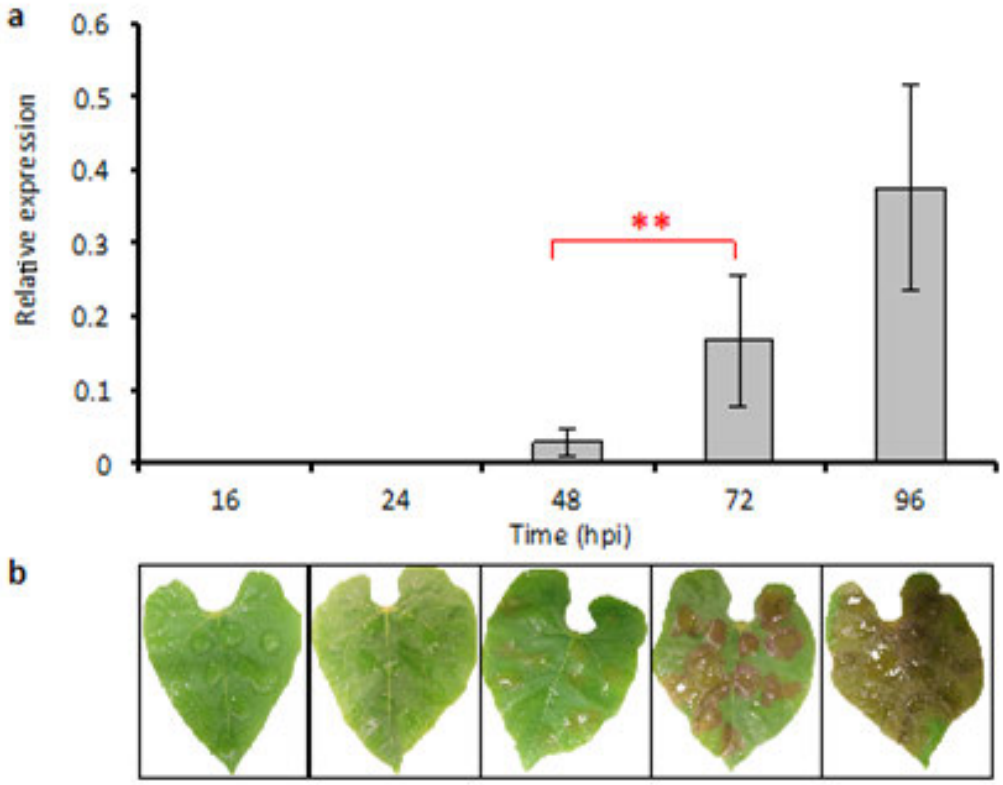

Supplementary Fig. 10 The *Bcibp* gene is expressed by *B. cinerea* during infection. **a** Expression levels of the *BcIbp* gene during the kinetics of French bean leaf infection by *B. cinerea*. The actin-encoding gene, the *bcef1α* gene (Bcin09g05760) and the *bcpda1* gene (Bcin07g01890) were used as a reference. Three independent biological replicates were assessed for each experiment. Standard deviations are indicated, and the asterisks indicate a significant difference (Student's *t* test, ** *p*-value <0.005) in gene expression compared with that at a previous time point. **b** The stages of infection are shown for each time point.

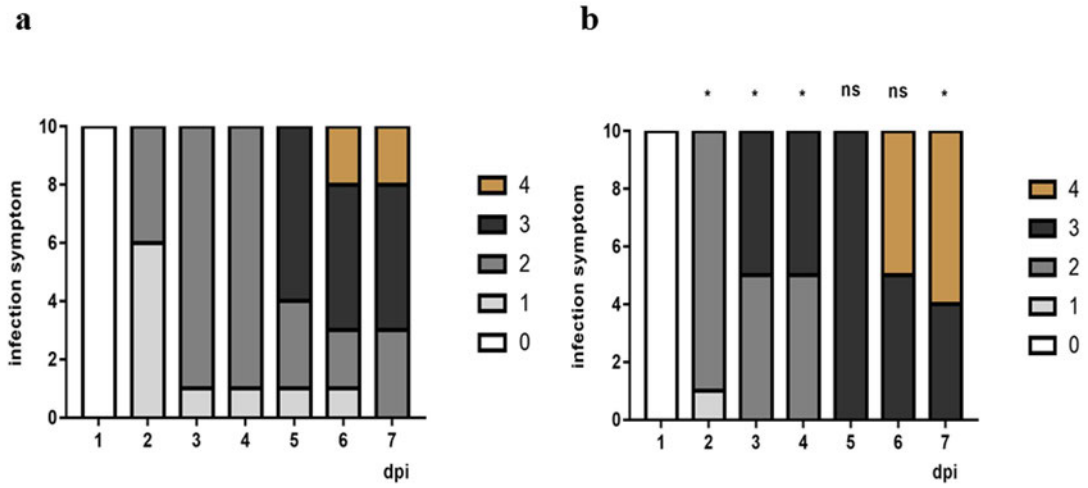

Supplementary Fig. 11 Complementation of the *ibpS* mutation. Evolution of the symptoms on *A. thaliana* Col0 inoculated by **a** the mutant strain A4988/pMMB-mcs5 and **b** the complemented strain A4988/pMMB-*ibpS*, Infection was performed on a single leaf by the deposition of a drop containing approximately 50 bacteria on a wound made by a needle. Symptoms were classified in five stages as shown on the right. stage 0: no symptoms; stage 1, symptoms around the spot of infection: stage 2: maceration of the leaf limb; stage 3: maceration of the whole leaf, including the petiole; stage 4: generalization to the whole plant. * indicates a statistical difference ($p< 0.05$) between results of the A4988/pMMB-mcs5 and A4988/pMMB-ibpS strains at a given day. ns: not significant.

Discussion

In this study, we have identified and characterized a novel family of proteins secreted by several plant pathogenic microorganisms. Our work establishes that members of the Ibp family exhibit the same fold as SBP proteins albeit with significant modifications making of IbpS structure a prototype for this novel family [29, 39]. We found that IbpS is secreted in the outer medium by *D. dadantii* (Supplementary Fig 3). Given that its homolog in *Streptomyces scabies* is also secreted [47] and that many of the homologs identified herein have a signal sequence, these data collectively suggest that most Ibp are secreted proteins.

Ibp-encoding genes appear to have been transferred many times not only from prokaryotes to prokaryotes but also from prokaryotes to eukaryotes. These bacteria-to-eukaryote transfers, the most common inter-kingdom HGT event [48] are classified as 'maintenance transfers' when they originate from endosymbiotic organelles and as 'innovation transfers" when they provide the recipient with a new functionality. Herein, we report a new example, of an 'innovation transfer', with several independent transfers of bacterial Ibp-encoding genes to oomycetes, animals and fungi. The antioxidant property displayed by this secreted metal scavenging protein might provide protection to the recipients. In oomycetes, the transfer occurred prior to the radiation of the different lineages, as Peronopsorales and Saprolegniales species possess monophyletic homologs. Several duplications resulted in a multigenic family, especially abundant in *Phytophthora* and *Pythium* spp., corresponding to hemibiotrophic and necrotrophic plant pathogen species, respectively. In contrast, the obligate biotrophs, *Hyaloperonospora arabidopsis* and *Albugo* spp, and the nonpathogenic saprotroph *Thraustotheca clavata*, have secondarily and independently lost the *ibp* gene (Supplementary Fig. 4). Thus, the secreted Ibp protein could be of particular importance for pathogenicity, predominantly plant pathogenicity. Many other HGTs detected thus far in oomycetes have putative functions associated with plant pathogenicity [49]. Two bacteria-to-animal HGTs of the *ibp* gene have also occurred. First, in the cereal cyst nematode *Heterodera avenae*, the *ibp* gene was shown to encode

a putative effector [50, 51]. HGTs of bacterial origins in plant parasitic nematodes have participated in the evolution of their capacity to parasitize plants [52] which might be an ongoing process as the *H. avenae* Ibp protein is very similar to that of *Rhizobium* spp., suggesting a recent transfer in this nematode. Second, in the parthenogenetic springtail arthropod *F. candida*, several duplications followed the transfer of the *ibp* gene, which now exists in six copies. These genes constitute some of the 809 'foreign' genes in the *F. candida* genome, of which 40% have a bacterial origin [53]. This widespread soil arthropod interacts and feeds on various plant pathogens [54]. Finally, *ibp* genes might have been transferred to fungi via multiple events as fungal Ibp proteins do not form a monophyletic group, and the two classes observed in *Dikarya* genomes do not share introns (Fig. 1 and Supplementary Fig. 5). Given the patchy distribution of species for these two classes, secondarily losses and fungus-to-fungus transfers most likely occurred. Many Pezizomycotina species harboring *ibp* genes, such as *B. cinerea* or *Magnaporthe oryzae*, are necrotroph or hemibiotroph phytopathogens. However, the correlation between the number of *ibp* genes and lifestyle is less clear than that observed for oomycetes. The maximum number of *ibp* genes observed in a fungal genome was four, observed in *Colletotrichum fioriniae* responsible for anthracnose in a wide range of crops and wild plants worldwide. However, the endoparasitic nematode *Hirsutella minnesotensis* and the plant symbiotic *Laccaria bicolor* also possess three genes each.

Controlling intracellular metal concentration reduces toxicity and ROS production. In bacteria, this can be achieved by not only reducing metal uptake but also by effluxing or sequestering the metal [55]. For example, overproduction of the FetA FetB iron exporter in *E. coli* increased its resistance to oxidative stress [56]. Iron can also be buffered in the cytoplasm via storage proteins, such as the ferritin FntA in *E. coli*. Sequestration in the periplasm is another way to control the metal concentration. The *Salmonella enterica* CueP protein reduces Cu^{2+} to Cu^{0} in the periplasm which lowers its cytoplasmic concentration [57]. Controlling the intracellular metal concentration via sequestration outside the bacteria has been documented much less often. The copper binding protein CopM and the iron binding protein FutA2 of *Synechocystis* PCC6803

have been found outside the cell, a location suggested to contribute to intracellular metal homeostasis [58 59].

During early steps of *A. thaliana* infection by *D. dadantii*, *ibpS* expression is strongly induced [30], while the chrysobactin and achromobactin siderophores are not yet synthesized, indicating that iron concentration is not limiting for bacterial growth at this stage of infection. Iron is strongly associated with cell walls in *A. thaliana* leaves and part of it is stored in plant ferritins [15]. Maceration of the tissues by pectinases contributes to liberate iron. Our work suggests that, given its rather low affinity for metal, IbpS might buffer iron concentration in the macerated tissue by transiently incorporating it to prevent its entry into the bacterial cell. The low affinity might enable the use of iron later in the infection process, for instance by siderophores which have a much higher affinity for iron and are produced later by the bacterium. It is also possible that IbpS binds to a different ligand *in vivo* and has a much higher affinity for metal-complexes or requires structural re-arrangements that have not observed in our study. Nevertheless, the conservation of the residues involved in iron binding in IbpS strongly suggests that the novel binding site identified here accomplishes a common, essential function in all members of this family. While Ibp proteins are mostly found in necrotrophic phytopathogenic microorganisms, some are also produced by nonpathogenic or nonplant-associated microorganisms. Therefore the proteins in these organisms may play a more general role in metal homeostasis or stress resistance.

Methods

Bacterial strains and media. *D. dadantii* and *E. coli* strains used in this study are described in Supplementary Table 3. *D. dadantii* and *E. coli* cells were grown at 30 and 37°C respectively in LB medium or M63 minimal medium supplemented with a carbon source (2 g/l). When required antibiotics were added at the following

concentration: ampicillin, 100 µg/l, kanamycin and chloramphenicol, 25 µg/l and 2 g of chicory leaf tissue were added in 5 ml of M63 medium. Media were solidified with 1.5 g/l agar.

Fungal strains, growth conditions and phytopathogenicity assays. *Botrytis cinerea* (teleomorph *Botryotinia fuckeliana* (de Bary) Whetzel) strain B05.10 was maintained on solid sporulation medium, as previously described [60], and was used as a recipient strain for genetic modifications. For DNA preparations, the mycelium was grown on solid sporulation medium for 3 days on the surface of cellophane membranes inoculated with 4-mm mycelial plugs. Infected plant tissues were collected after inoculation of one-week-old French bean (*Phaseolus vulgaris var Saxa*) leaves using conidia collected from 10-day-old sporulation medium cultures. Ten 50µl-droplets of a conidial suspension (10^3 conidia/ml in sporulation medium) were deposited on the surface of each leaf. Ten leaves were inoculated for each experimental condition. The infected plants were incubated at 21°C under 100% relative humidity and dark (10 h)-daylight (14 h) conditions. At different stages of symptom development, leaves were harvested and frozen at -80°C. Infection assays were also performed with cucumber (*Cucumis sativus*) cotyledons using 4 mm plugs collected from 3-day-old mycelium sporulation medium.

Construction of *D. dadantii* and *B. cinerea* mutants. *D. dadantii ibpS* mutant. A DNA fragment containing the *ibpS* gene was amplified with the primers 18996L+ and 18996L- and ligated into plasmid pGEM-T (Promega). A *uidA*-kan cassette was inserted into the unique Kpn2I site to create a *ibpS-uidA* transcriptional fusion. The construction was introduced into *D. dadantii* by electroporation After several cultures in low phosphate medium [61] in the presence of kanamycin, bacteria were plated on GL + kanamycin. Recombination and loss of the plasmid were checked by replica plating on GL + ampicillin. Correct recombination was checked by PCR using oligonucleotides flanking *ibpS. B. cinerea Bcibp* mutant. Knockout mutants were constructed using a gene replacement strategy (Supplementary Fig. 12), and the deletion DNA cassette was

generated by double-joint PCR. The 5'(1080 bp) - and 3'(522 bp)-flanking regions of *Bcibp* were amplified from *B. cinerea* genomic DNA (100 ng) using the primer pairs For-5'-ibp/Rev-5'-ibp and For-3'-ibp/Rev-3'-ibp, respectively. Rev-5'-ibp and For-3'-ibp also contained sequences homologous to the hygromycin resistance cassette containing the *hph* gene under control of the *trpC* promoter of *A. nidulans* and previously amplified from pFV8 [62] using the primers For-Hygro and Rev-Hygro. Purified amplicons were combined and amplified together using the nested primers PCR3-FOR and PCR3-REV, which bind within the 5' upstream and the 3' downstream fragments of the target gene, respectively. The gene replacement cassette was verified by DNA sequencing. *B. cinerea* transformation was carried out using protoplasts as previously described [63], except that the protoplasts were transformed with 1.5 µg of DNA and plated on medium supplemented with 70 µg/ml hygromycin (Invivogen, France) containing 200 g/l sucrose and 2 g/l $NaNO_3$. Diagnostic PCR was performed to detect homologous recombination in the selected hygromycin-resistant transformants using the primer pairs P1/P2 and P3/P4.

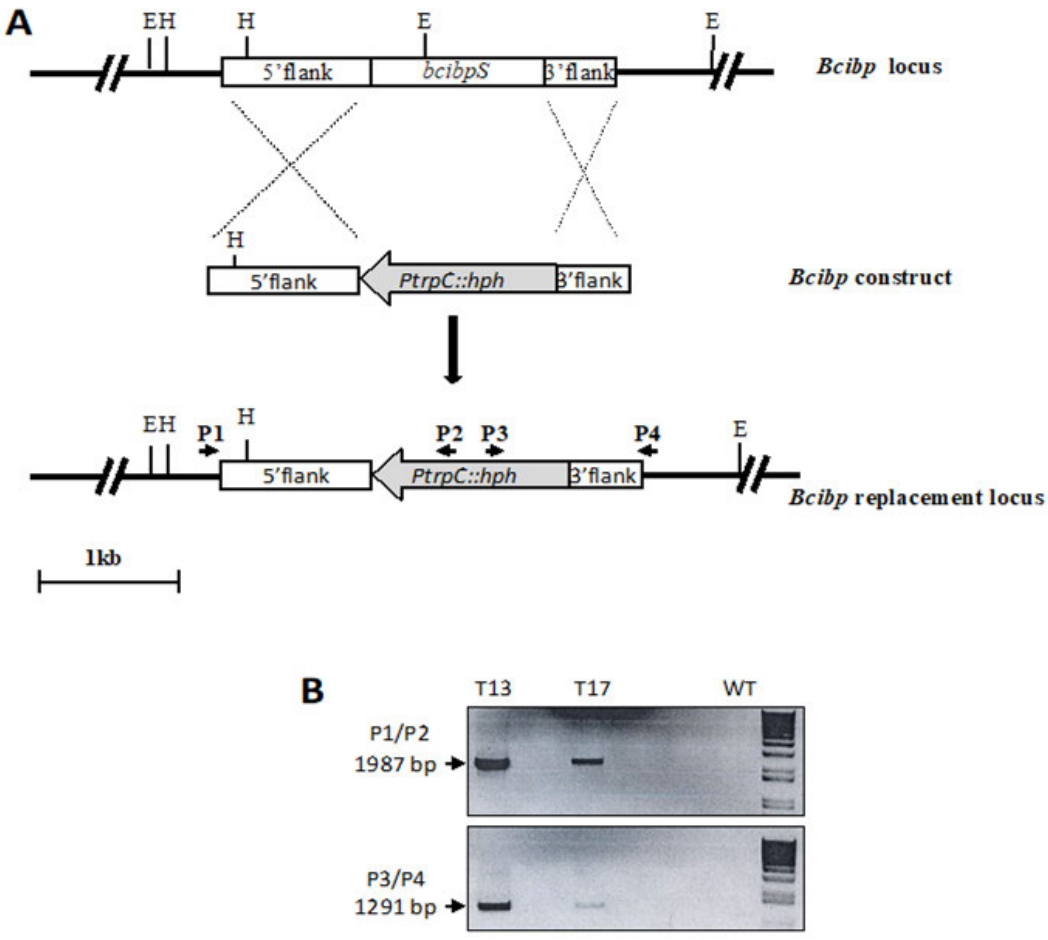

Supplementary Fig. 12 Construction and verification of *B. cinerea Bcibp*-null mutants. **a** Schematic representation of replacement of the *Bcibp* gene with the hygromycin resistance gene (*hph*) flanked by 1.080 kp of 5' sequence and 0.522 kb of 3' sequence from the *Bcibp* locus. The primers (black arrows) used for PCR analysis are indicated. **b** Diagnostic PCR was performed to identify the deletion mutants. The primers pairs are indicated.

Protein purification, antibody production and Western blotting. The coding sequences of *ibpS*, *ibpP* and *Bcibp* without signal sequence were amplified with the primers 18996GEX+ and 18996GEX-, 14625GEX+ and 14625GEX-, and Bc96GEX+ and Bc96GEX-, respectively. The amplified DNAs were digested with BamHI and XhoI and ligated into pGEX-6p3 plasmid (GE Healthcare) digested with the same enzymes. The pGEX derivatives producing the fusion proteins were introduced into *E. coli* NM522 strain. Cells were grown in LB medium to OD_{600} 0.8 and protein production was induced with 1 mM isopropylthiogalactoside (IPTG) for 3h. Cells were collected by centrifugation, resuspended in buffer A (50 mM Tris pH 7.0, 100 mM NaCl) and broken in a French cell press. Unbroken cells were eliminated by centrifugation. The fusion proteins were bound on Protino Glutathione Agarose 4B (Macherey-Nagel) equilibrated with buffer A, washed several times with the same buffer and the proteins were liberated by addition of Prescission® protease (GE Healthcare) according to the manufacturer's protocol. The protein was incubated with 1 mM EDTA to remove any trace metal. EDTA was eliminated using PD-10 buffer exchange columns (GE Healthcare). The purified protein was injected to a rabbit for antibody production (Covalab, Villeurbanne, France). For Western blot, proteins were separated by SDS-PAGE and transferred onto a PVDF membrane (Millipore). Anti-IbpS antibodies were used at a dilution 1/10 000.

For crystallogenesis experiments, the protein was loaded on a Superdex 75 column equilibrated in 50 mM Tris-Cl pH 7.0, 100 mM NaCl. IbpS eluted as a single peak and fractions were pooled and concentrated to 10 mg/ml. Protein concentration was determined using a Nanodrop spectrophotometer (Thermo Scientific). Labelling of IbpS with selenomethionine was performed by growing *E. coli* NM522/pGEX-IbpS in M63 + glucose medium. When OD_{600} reached 0.5, selenomethionine (40 µg/ml), 1 mM IPTG and all amino acids except methionine and cysteine were added at a concentration of 0.01%. Cells were grown overnight and treated as described for wild-type IbpS. Pure SeMet-IbpS was concentrated to 6.6 mg/ml. The presence of three seleno-methionines was confirmed by mass-spectrometry using a Voyager-DE Pro MALDI-TOF mass

spectrometer (Sciex) equipped with a nitrogen UV laser (λ=337 nm, 3 ns pulse). The instrument was operated in the positive-linear mode (mass accuracy: 0.05%) with an accelerating potential of 20 kV. Typically, mass spectra were obtained by accumulation of 600 laser shots and processed using Data Explorer 4.0 software (Sciex). Samples were mixed with sinapinic acid (saturated solution in 30% acetonitrile and 0.3% trifluoroacetic acid), deposited on the MALDI target and air-dried before analysis. Spectra obtained for WT-IbpS and for SeMet-IbpS show respectively MH+ at m/z 39493.3 and 39638.7 corresponding to the expected increment in mass when replacing the three Met by three Se-Met.

Crystallization, data collection, structure determination, model building and refinement. Crystallization conditions were screened at 19°C by the sitting-drop vapor-diffusion method and commercial kits from Hampton Research, Molecular Dimensions Limited and Qiagen in 96-well plates (TTPLabtech iQ plates and Molecular Dimensions Limited MRC plates) with a TTP Labtech Mosquito nanodispenser. Initial crystals were obtained with IbpS at 10 mg/ml with a reservoir solution containing 30% PEG 4000, 80 mM magnesium acetate, 50 mM sodium cacodylate pH6.5 (condition C1 of Natrix crystallization screen, Hampton Research) and 30% PEG 1500 (condition D7 of Crystal Screen crystallization screen, Hampton Research). Optimized crystals of IbpS grew in 24% PEG 4000, 80 mM magnesium acetate, 50 mM sodium cacodylate pH 6. IbpS-SeMet crystals were obtained in 28% PEG 4000, 80 mM magnesium acetate, Tris-HCl 100 mM pH 7.4. Crystals were cryoprotected with the crystallization condition supplemented by 15% ethylene glycol and 10% glycerol for native crystals and SeMet crystals, respectively and flash cooled in liquid nitrogen. To obtain the Fe-bound IbpS structure, concentrated protein was incubated with increasing concentrations of $FeCl_3$ to a final concentration of 1.8 mM. The solution was then filtrated on a Zeba column (Thermofisher) and drops were immediately set up. Best crystals were obtained in 20% PEG 3350, 0.1M BisTrisPropane pH 8.5, 0.2M $NaNO_3$ (condition H5 of PACT1er crystallization screen Molecular Dimensions). X-ray

diffraction data from native and selenomethionine derivative crystals were collected at 100K at the European Synchrotron Radiation Facility (in Grenoble, France) beamline ID23EH1 for both data. Crystals of native and SeMet IbpS diffracted to a resolution of 1.7 Å and 18 Å, respectively. They belonged to the space group $P2_1$ and contained four molecules per asymmetric unit (Table 1). Crystals of Fe-bound IbpS diffracted to 1.8 Å and belonged to the space group P1 with four molecules per asymmetric unit. Diffraction data were indexed and integrated using XDS [64] and scaled with SCALA from the CCP4 program suite [65]. Data collection statistics are given in Supplementary Table 4. The structure was solved by the single wavelength anomalous dispersion method with Se-Met crystals data using the Autosol program of the PHENIX suite [66]. Phasing statistics are given in Table S4. The experimental map was of excellent quality and approximately 80% of the model could be built automatically with the Autobuild program and completed by manual building using COOT [67]. The model was used as a template for molecular replacement in the native dataset. The atomic positions and TLS parameters were refined using PHENIX [66] (Table 1) Structure refinement was performed using the Phenix program Refine [68] to a Rfree/Rwork of 0.17/0.20. The structure of Fe-IbpS was solved by molecular replacement and refined to a Rfree/Rwork of 0.15/0.19. Atomic coordinates and structure factors have been deposited in the Protein Data Bank with accession code 6FJL for native IbpS and 6HHB for Fe-IbpS.

Analysis of gene expression *in planta*. Five week-old seedlings of *Arabidopsis thaliana* Col0 were grown under short days (8-h light/16-h dark) with 21°C temperature and 70% relative humidity. Leaves were infiltrated with the indicated treatments using a syringe without a needle, then harvested 24h after treatment followed by freezing in liquid nitrogen. Total RNAs were purified with TRIzol reagent (Thermo Fisher Scientific) according to the manufacturer's instructions. Total RNA concentration was determined using a NanoDrop ND-1000. RNA samples were treated with DNaseI-RNase free (Thermo Fisher Scientific) to remove any DNA contamination. A total of 1 µg of DNase treated RNA was reverse transcribed using the RevertAid (Thermo Fisher

Scientific) and 0.5 µg of oligodT primers following the supplier's instructions. One µl of the 1:10 diluted cDNA was subjected to real time qPCR using SYBR Green PCR Mastermix (Takyon, Eurogentec) and gene specific primers (*bHLH38* Forward, *bHLH38* Reverse; *AtFER1* Forward, *AtFER1* Reverse; *Clathrin* Forward, *Clathrin* Reverse; PP2a3-F, PP2a3-R). The reference gene *clathrin* and PP2a were used to normalize gene expression profiles.

Analysis of gene expression in *B. cinerea.* Experiments were performed as described [69]. DNA-free total RNA was extracted from infected bean leaves and 2.5 µg were used for the synthesis of cDNA using the Thermoscript^{TM} RT-PCR system kit (Invitrogen, USA) according to the manufacturer's recommendations. Real-time quantitative PCR (qRT-PCR) experiments were performed in 96-well plates using ABI-7900 Applied Biosystems (Applied Biosystems, USA). Primer pairs were designed using Primer Express (Applied Biosystems, USA). The amplification reactions were carried out using SYBR Green PCR Master Mix (Applied Biosystems, USA) with the following protocol: 95°C for 10 min and 40 cycles of 95°C for 30 s and 60°C for 1 min. Relative quantification was based on the $2^{-\Delta Ct}$ method using the actin-encoding gene (Bcin16g02020), the *bcef1α* gene (Bcin09g05760) and the *bcpda1* gene (Bcin07g01890) as normalization internal controls. Three independent biological replicates were analysed.

Virulence tests on plants. Infection of 6-week-old *A. thaliana* Col-0 and the *atrbohD-atrbohF* mutant [70] by *D. dadantii* was performed according to Lebeau *et al*. [71]. One leaf per plant was wounded with a needle and inoculated by depositing a 5 µl droplet of a bacterial suspension at 10^4 bacteria/ml in water. Plants were kept at 22°C at high humidity. The virulence was estimated daily by visual examination of leaf damage with the following scale: 0 = no symptoms, 1 = symptoms around the spot of infection, 2 = maceration of the leaf limb, 3 = maceration of the whole leaf, including the petiole, 4 = generalization to the whole plant. Virulence scores were not blinded.

Iron binding experiments. 100 µl of Ni-NTA, Zn-NTA, Cu-NTA or Fe-NTA resins equilibrated in buffer A were incubated with 10 µg of protein in the same buffer for 15 min. After centrifugation the supernatant was withdrawn and the resins were washed three times with 1 ml of buffer A. The protein was then eluted with 100 µl of 50 mM EDTA and the fractions were analysed by SDS PAGE.

UV-visible spectroscopy. UV-visible absorption spectra were obtained at 25 °C on a Nicolet Evolution 100 spectrophotometer. Purified IbpS was diluted in buffer A at a final concentration of 50-100 µM. Equivalents of Fe^{3+} (donor solution: $FeCl_3$, Fe-Citrate, Fe-NTA, Fe^{3+}-CAS) were gradually added with a volume variation below 1% step-by-step and absorption spectra were recorded from 230 to 800 nm after 5 minutes of equilibration between each metal addition. The protein was then buffer exchanged using Micro Spin columns (Pierce) before new spectra recording.

Fluorescence spectroscopy. Fluorescence quenching of IbpS was monitored between 300 and 400 nm with an excitation wavelength of 280 nm. Protein was dissolved in 50 mM Tris-HCl, 100 mM NaCl buffer (pH 7.0) to a final concentration of 70 µM. Metal ions solution was titrated stepwise into the protein solution with a volume variation below 1% and incubated for 5 min at room temperature before the analysis. Each addition was made from a 100-fold concentrated metal solution to give a final 1-fold metal concentration. Fe^{3+} ions were given by a solution of $FeCl_3$.

H_2O_2 killing tests. Bacteria grown in LB medium overnight were centrifuged, resuspended in water at an OD_{600} = 1 and diluted 1000-fold. 100 µl of this bacterial suspension were incubated for 5 min with 50 µM EDDHA or 50 µM IbpS or IbpP. 10 mM (for *D. dadantii*) or 30 mM (for *E. coli*) H_2O_2 were added. After 30 min, viable bacteria number was determined by plating serial dilutions on LB agar plates.

Enzymatic assays. ß-glucuronidase assays were performed on toluenized extracts of cells grown to exponential phase by the method of Bardonnet *et al.* [72] using *p*-nitrophenyl-ß-D-glucuronate as the substrate. ß-galactosidase assays were performed on toluenized extracts of cells grown to exponentional phase with *o*-nitrophenyl-ß-D-galactose as the substrate.

Luminescence assays. The assays were conducted in 96-well plates. The wells were filled with 200 µL of 0.4 % glucose M63 minimal media containing increasing concentrations of metals, inoculated with 106 bacteria harvested at OD_{600} of 0.6. The plate was sealed using gas-permeable Breathe Easy membrane (Sigma Aldrich) and placed into a "TECAN Infinite

Pro" plate reader equilibrated at 37 °C and programmed to measure OD_{600} and luminescence every 20 min, after a 1-min period of shaking, during 12 to 20 h. Background

OD and luminescence (values at time = 0) were subtracted to each data point. To calculate the maximal activity, for each well, the ratio (luminescence/OD) was plotted as a function of time, and the maximal value was conserved. By doing so, we took into account the eventual growth lag between two conditions

Analysis of the Ibp protein family. The closest homologs of *ibpS* and *ibpP* were searched, using PSI-BLAST [28] with the *D. dadantii* (ABF-18996) protein sequence as query, in the NCBI non-redundant (nr) database. Four iterations were done, with a threshold of $1e^{-50}$, retrieving 897 protein sequences. This threshold was chosen because, at this level of the results, there was a relatively important increase in e-values, from e^{-54} to e^{-48}, suggesting that proteins with stronger e-values do not correspond to Ibp proteins. PSI-BLAST hits, with e-value worse than the threshold, up to $1e^{-9}$, were displayed to see the proteins that were the most similar to the obtained Ibp family. These hits corresponded to hundreds of bacterial SBP, mainly from the D cluster of SPB proteins, but did not contain other eukaryotic similar sequences. The 897 proteins of the Ibp family were aligned using MAFFT with the L-INS-i algorithms and default

settings [73]. Different maximum likelihood (ML) phylogenetic trees were constructed to explore the sequence diversity, with the method detailed below for the final selected sequences, but with the approximate likelihood ratio test for branches [74] instead of bootstraps. These trees permitted the selection of a subset of 71 species representative of the diversity of the taxa, and which Ibp sequences reflected well the diversity observed among the 897 detected Ibp. For the analysis of Ibp proteins in these species, we kept the Ibp detected in the complete proteome of a unique selected strain, downloaded from an Ensembl site when available [33]. 122 sequences were thus selected and aligned with MAFFT and the L-INS-i algorithm [73]. Consensus sequences, allowing gaps, were constructed, using Seaview [75], to detect the residues strictly (100%) or strongly (≥95%) conserved.

Phylogenetic relationships between the selected Ibp proteins were inferred using Maximum Likelihood and Bayesian approaches. In both cases, regions that were suitable for phylogenetic inference were selected from the multiple alignment, using BMGE with default parameters [76]. For the ML approach, ProtTest3 was used for determination of amino acid sequence evolution best-fit model [77] According to the Akaike information criterion corrected for small sample size (AICc), the best-fit model was the LG model [78] with rate variation among sites (+G). The ML tree was then constructed with PhyML 3.0 [79] using the following parameters: the LG model, an estimated gamma distribution of rates of evolution, subtree pruning and regrafting (SPR) and five random starting trees added to the standard BioNJ starting tree. The support of the data for each internal branch of the phylogeny was estimated using non-parametric bootstraps, with 100 replicates. For the Bayesian approach, MrBayes v3.2.6 [80] was used with a mixture of models and an automatic detection of the model with highest probability as well as an estimation of the gamma distribution of the rates of evolution. The best scoring model of evolution was determined to be the WAG model with a probability of 1.0. The program was run with four chains for 1 000 000 generations and trees were sampled every 500 generations. To construct the consensus tree, 25% of the trees were eliminated following a burn-in process and posterior

probabilities were used as support for internal branches. The resulting trees were edited with Figtree v.1.4.3.

Statistical analysis. To analyse plant infection symptoms, a contingency analysis (Khi2 likelihood ratio test) was performed on symptom classes everyday. The results presented in the Figures correspond to the mean values ± standard deviation (error bars). The significance level was performed following the post test Tukey's multiple comparisons according to the method of one-way analysis of variance (ANOVA). *** represents significant differences between the two pairwise groups, otherwise ns indicates no significant difference.

References

1. Okmen B, Doehlemann G. Inside plant: biotrophic strategies to modulate host immunity and metabolism. *Cur Opin Plant Biol* **20**, 19-25 (2014).
2. Mengiste T. Plant immunity to necrotrophs. *Annu Rev Phytopathol* **50**, 267-294 (2012).
3. Koeck M, Hardham AR, Dodds PN. The role of effectors of biotrophic and hemibiotrophic fungi in infection. *Cell Microbiol* **13**, 1849-1857 (2011).
4. González-Fernández R, Valero-Galván J, Gómez-Gálvez FJ, Jorrín-Novo JV. Unraveling the *in vitro* secretome of the phytopathogen *Botrytis cinerea* to understand the interaction with its hosts. *Frontiers in Plant Science* **6**, 839 (2015).
5. Ottmann C*, et al.* A common toxin fold mediates microbial attack and plant defense. *Proc Natl Acad Sci U S A* **106**, 10359-10364 (2009).
6. Pemberton CL, Salmond GP. The Nep1-like proteins-a growing family of microbial elicitors of plant necrosis. *Mol Plant Pathol* **5**, 353-359 (2004).
7. Oome S*, et al.* Nep1-like proteins from three kingdoms of life act as a microbe-associated molecular pattern in *Arabidopsis*. *Proc Natl Acad Sci U S A* **111**, 16955-16960 (2014).

8. Mattinen L, Tshuikina M, Mae A, Pirhonen M. Identification and characterization of Nip, necrosis-inducing virulence protein of *Erwinia carotovora* subsp. *carotovora. Mol Plant Microbe Interact* **17**, 1366-1375 (2004).
9. Dodds PN, Rathjen JP. Plant immunity: towards an integrated view of plant-pathogen interactions. *Nature Rev Genet* **11**, 539-548 (2010).
10. Jones JD, Dangl JL. The plant immune system. *Nature* **444**, 323-329 (2006).
11. Camejo D, Guzman-Cedeno A, Moreno A. Reactive oxygen species, essential molecules, during plant-pathogen interactions. *Plant Physiol Bioch* **103**, 10-23 (2016).
12. Aznar A, Chen NW, Thomine S, Dellagi A. Immunity to plant pathogens and iron homeostasis. *Plant science* **240**, 90-97 (2015).
13. Fones H, Preston GM. The impact of transition metals on bacterial plant disease. *FEMS Microbiol Rev* **37**, 495-519 (2013).
14. Expert D. Withholding and exchanging iron:: interactions between *Erwinia* spp. and their plant hosts. *Annu Rev Phytopathol* **37**, 307-334 (1999).
15. Aznar A, Patrit O, Berger A, Dellagi A. Alterations of iron distribution in *Arabidopsis* tissues infected by *Dickeya dadantii*. *Mol Plant Pathol* **16**, 521-528 (2015).
16. Roschzttardtz H, Conejero G, Curie C, Mari S. Identification of the endodermal vacuole as the iron storage compartment in the *Arabidopsis* embryo. *Plant Physiol* **151**, 1329-1338 (2009).
17. Briat JF, Duc C, Ravet K, Gaymard F. Ferritins and iron storage in plants. *Biochim Biophys Acta* **1800**, 806-814 (2010).
18. Munzinger M, Budzikiewicz H, Expert D, Enard C, Meyer JM. Achromobactin, a new citrate siderophore of *Erwinia chrysanthemi*. *Z Naturforschung C* **55**, 328-332 (2000).
19. Persmark M, Expert D, Neilands JB. Isolation, characterization, and synthesis of chrysobactin, a compound with siderophore activity from *Erwinia chrysanthemi*. *J Biol Chem* **264**, 3187-3193 (1989).
20. Dellagi A*, et al.* Siderophore-mediated upregulation of *Arabidopsis* ferritin expression in response to *Erwinia chrysanthemi* infection. *Plant J* **43**, 262-272 (2005).

21. Franza T, Mahe B, Expert D. *Erwinia chrysanthemi* requires a second iron transport route dependent of the siderophore achromobactin for extracellular growth and plant infection. *Mol Microbiol* **55**, 261-275 (2005).

22. Dellagi A*, et al.* Microbial siderophores exert a subtle role in *Arabidopsis* during infection by manipulating the immune response and the iron status. *Plant Physiol* **150**, 1687-1696 (2009).

23. Aznar A*, et al.* Scavenging iron: a novel mechanism of plant immunity activation by microbial siderophores. *Plant Physiol* **164**, 2167-2183 (2014).

24. Hassan S, Shevchik VE, Robert X, Hugouvieux-Cotte-Pattat N. PelN is a new pectate lyase of *Dickeya dadantii* with unusual characteristics. *J Bacteriol* **195**, 2197-2206 (2013).

25. Hsiao PY, Cheng CP, Koh KW, Chan MT. The *Arabidopsis* defensin gene, *AtPDF1.1*, mediates defence against *Pectobacterium carotovorum* subsp. *carotovorum* via an iron-withholding defence system. *Sci Rep* **7**, 9175 (2017).

26. Charkowski A*, et al.* The role of secretion systems and small molecules in soft-rot *enterobacteriaceae* pathogenicity. *Annu Rev Phytopathol* **50**, 425-449 (2012).

27. Coulthurst SJ, Lilley KS, Hedley PE, Liu H, Toth IK, Salmond GP. DsbA plays a critical and multifaceted role in the production of secreted virulence factors by the phytopathogen *Erwinia carotovora* subsp. *atroseptica*. *J Biol Chem* **283**, 23739-23753 (2008).

28. Altschul SF*, et al.* Gapped BLAST and PSI-BLAST: a new generation of protein database search programs. *Nucleic Acids Res* **25**, 3389-3402 (1997).

29. Berntsson RP, Smits SH, Schmitt L, Slotboom DJ, Poolman B. A structural classification of substrate-binding proteins. *FEBS Lett* **584**, 2606-2617 (2010).

30. Chapelle E*, et al.* A straightforward and reliable method for bacterial in planta transcriptomics: application to the *Dickeya dadantii*/*Arabidopsis thaliana* pathosystem. *Plant J* **82**, 352-362 (2015).

31. Pedron J, Chapelle E, Alunni B, Van Gijsegem F. Transcriptome analysis of the *Dickeya dadantii* PecS regulon during the early stages of interaction with *Arabidopsis thaliana*. *Mol Plant Pathol* **19**, 647-663 (2018).

32. Hugouvieux-Cotte-Pattat N, Condemine G, Nasser W, Reverchon S. Regulation of pectinolysis in *Erwinia chrysanthemi*. *Annu Rev Microbiol* **50**, 213-257 (1996).

33. Kersey PJ, *et al.* Ensembl Genomes 2018: an integrated omics infrastructure for non-vertebrate species. *Nucleic Acids Res* **46**, D802-d808 (2018).

34. Petersen TN, Brunak S, von Heijne G, Nielsen H. SignalP 4.0: discriminating signal peptides from transmembrane regions. *Nature Methods* **8**, 785-786 (2011).

35. Bendtsen JD, Nielsen H, Widdick D, Palmer T, Brunak S. Prediction of twin-arginine signal peptides. *BMC Bioinformatics* **6**, 167 (2005).

36. Schwyn B, Neilands JB. Universal chemical assay for the detection and determination of siderophores. *Anal Biochem* **160**, 47-56 (1987).

37. Mao B, Pear MR, McCammon JA, Quiocho FA. Hinge-bending in L-arabinose-binding protein. The "Venus's-flytrap" model. *J Biol Chem* **257**, 1131-1133 (1982).

38. Holm L, Laakso LM. Dali server update. *Nucleic Acids Res* **44**, W351-355 (2016).

39. Scheepers GH, Lycklama ANJA, Poolman B. An updated structural classification of substrate-binding proteins. *FEBS Lett* **590**, 4393-4401 (2016).

40. Sit B, *et al.* Active transport of phosphorylated carbohydrates promotes intestinal colonization and transmission of a bacterial pathogen. *PLoS Pathog* **11**, e1005107 (2015).

41. Koropatkin N, Randich AM, Bhattacharyya-Pakrasi M, Pakrasi HB, Smith TJ. The structure of the iron-binding protein, FutA1, from *Synechocystis* 6803. *J Biol Chem* **282**, 27468-27477 (2007).

42. Zheng H, Cooper DR, Porebski PJ, Shabalin IG, Handing KB, Minor W. CheckMyMetal: a macromolecular metal-binding validation tool. *Acta Crystallograph D, Struct Biol* **73**, 223-233 (2017).

43. Yuan X, *et al.* The diguanylate cyclase GcpA inhibits the production of pectate lyases via the H-NS protein and RsmB regulatory RNA in *Dickeya dadantii*. *Mol Plant Pathol* (2018). doi: 10.1111/mpp.12665

44. Petit JM, van Wuytswinkel O, Briat JF, Lobreaux S. Characterization of an iron-dependent regulatory sequence involved in the transcriptional control of *AtFer1* and *ZmFer1* plant ferritin genes by iron. *J Biol Chem* **276**, 5584-5590 (2001).

45. Dellagi A, Brisset MN, Paulin JP, Expert D. Dual role of desferrioxamine in *Erwinia amylovora* pathogenicity. *Mol Plant Microbe Interact* **11**, 734-742 (1998).

46. Kong W*, et al.* Large-scale transcriptome analysis of cucumber and *Botrytis cinerea* during infection. *PLoS One* **10**, e0142221 (2015).

47. Joshi MV*, et al.* The twin arginine protein transport pathway exports multiple virulence proteins in the plant pathogen *Streptomyces scabies. Mol Microbiol* **77**, 252-271 (2010).

48. Husnik F, McCutcheon JP. Functional horizontal gene transfer from bacteria to eukaryotes. *Nat Rev Microbiol* **16**, 67-79 (2018).

49. Savory F, Leonard G, Richards TA. The role of horizontal gene transfer in the evolution of the oomycetes. *PLoS Pathog* **11**, e1004805 (2015).

50. Kumar M*, et al.* De novo transcriptome sequencing and analysis of the cereal cyst nematode, Heterodera avenae. *PLoS One* **9**, e96311 (2014).

51. Chen C*, et al.* Large-scale identification and characterization of *Heterodera avenae* putative effectors suppressing or inducing cell death in *Nicotiana benthamiana*. *Front Plant Sci* **8**, 2062 (2017).

52. Danchin EG*, et al.* Multiple lateral gene transfers and duplications have promoted plant parasitism ability in nematodes. *Proc Natl Acad Sci U S A* **107**, 17651-17656 (2010).

53. Faddeeva-Vakhrusheva A*, et al.* Coping with living in the soil: the genome of the parthenogenetic springtail *Folsomia candida*. *BMC Genomics* **18**, 493 (2017).

54. Fountain MT, Hopkin SP. *Folsomia candida* (*Collembola*): a "standard" soil arthropod. *Annu Rev Entomol* **50**, 201-222 (2005).

55. Chandrangsu P, Rensing C, Helmann JD. Metal homeostasis and resistance in bacteria. *Nat Rev Microbiol* **15**, 338-350 (2017).

56. Nicolaou SA, Fast AG, Nakamaru-Ogiso E, Papoutsakis ET. Overexpression of *fetA* (*ybbL*) and *fetB* (*ybbM*), encoding an iron exporter, enhances resistance to oxidative stress in *Escherichia coli*. *Appl Environ Microbiol* **79**, 7210-7219 (2013).

57. Yoon BY*, et al.* Direct ROS scavenging activity of CueP from *Salmonella enterica* serovar *Typhimurium*. *Mol Cells* **37**, 100-108 (2014).

58. Giner-Lamia J, Lopez-Maury L, Florencio FJ. CopM is a novel copper-binding protein involved in copper resistance in *Synechocystis* sp. PCC 6803. *MicrobiologyOpen* **4**, 167-185 (2015).

59. Giner-Lamia J, Pereira SB, Bovea-Marco M, Futschik ME, Tamagnini P, Oliveira P. Extracellular proteins: novel key components of metal resistance in cyanobacteria? *Front Microbiology* **7**, 878 (2016).

60. Antal Z*, et al.* The homeobox BcHOX8 gene in *Botrytis cinerea* regulates vegetative growth and morphology. *PLoS One* **7**, e48134 (2012).

61. Roeder DL, Collmer A. Marker-exchange mutagenesis of a pectate lyase isozyme gene in *Erwinia chrysanthemi*. *J Bacteriol* **164**, 51-56 (1985).

62. Villalba F*, et al.* Improved gene targeting in *Magnaporthe grisea* by inactivation of MgKU80 required for non-homologous end joining. *Fungal Genet Bio* **45**, 68-75 (2008).

63. Laleve A, Gamet S, Walker AS, Debieu D, Toquin V, Fillinger S. Site-directed mutagenesis of the P225, N230 and H272 residues of succinate dehydrogenase subunit B from *Botrytis cinerea* highlights different roles in enzyme activity and inhibitor binding. *Environ Microbiol* **16**, 2253-2266 (2014).

64. Kabsch W. Automatic processing of rotation diffraction data from crystals of initially unknown symmetry and cell constants. *J Appl Cryst* **26**, 795-800 (1993).

65. The CCP4 suite: programs for protein crystallography. *Acta Crystallogr D Biol Crystallogr* **50**, 760-763 (1994).

66. Adams PD*, et al.* PHENIX: building new software for automated crystallographic structure determination. *Acta Crystallogr D Biol Crystallogr* **58**, 1948-1954 (2002).

67. Emsley P, Cowtan K. Coot: model-building tools for molecular graphics. *Acta Crystallogr D Biol Crystallogr* **60**, 2126-2132 (2004).

68. Adams PD*, et al.* The Phenix software for automated determination of macromolecular structures. *Methods* **55**, 94-106 (2011).

69. Billon-Grand G, Rascle C, Droux M, Rollins JA, Poussereau N. pH modulation differs during sunflower cotyledon colonization by the two closely related necrotrophic fungi *Botrytis cinerea* and *Sclerotinia sclerotiorum*. *Mol Plant Pathol* **13**, 568-578 (2012).

70. Torres MA, Dangl JL, Jones JD. *Arabidopsis gp91phox* homologues *AtrbohD* and *AtrbohF* are required for accumulation of reactive oxygen intermediates in the plant defense response. *Proc Natl Acad Sci U S A* **99**, 517-522 (2002).

71. Lebeau A*, et al.* The GacA global regulator is required for the appropriate expression of *Erwinia chrysanthemi* 3937 pathogenicity genes during plant infection. *Environ Microbiol* **10**, 545-559 (2008).

72. Bardonnet N, Blanco C. Improved vectors for transcriptional signal screening in corynebacteria. *FEMS Microbiol Lett* **68**, 97-102 (1991).

73. Katoh K, Standley DM. MAFFT multiple sequence alignment software version 7: improvements in performance and usability. *Molecular Biol Evol* **30**, 772-780 (2013).

74. Anisimova M, Gascuel O. Approximate likelihood-ratio test for branches: A fast, accurate, and powerful alternative. *Syst Biol* **55**, 539-552 (2006).

75. Gouy M, Guindon S, Gascuel O. SeaView version 4: A multiplatform graphical user interface for sequence alignment and phylogenetic tree building. *Mol Biol Evo***27**, 221-224 (2010).

76. Criscuolo A, Gribaldo S. BMGE (Block Mapping and Gathering with Entropy): a new software for selection of phylogenetic informative regions from multiple sequence alignments. *BMC Biol Evol* **10**, 210 (2010).

77. Darriba D, Taboada GL, Doallo R, Posada D. ProtTest 3: fast selection of best-fit models of protein evolution. *Bioinformatics* **27**, 1164-1165 (2011).

78. Le SQ, Gascuel O. an improved general amino acid replacement matrix. *Mol Biol Evol* **25**, 1307-1320 (2008).

79. Guindon S, Dufayard JF, Lefort V, Anisimova M, Hordijk W, Gascuel O. New algorithms and methods to estimate maximum-likelihood phylogenies: assessing the performance of PhyML 3.0. *Syst Biol* **59**, 307-321 (2010).

80. Huelsenbeck JP, Ronquist F. MRBAYES: Bayesian inference of phylogenetic trees. *Bioinformatics* **17**, 754-755 (2001).

Acknowledgments

We thank Céline Vannoz and Florence Ruaudel for excellent technical work, members of the MAP laboratory and D. Expert for reading the manuscript. We are grateful to Elise Lacroix in charge of the greenhouse facilities of the FR BioEnvis at the University Claude Bernard, Lyon, for her assistance. We thank Dr. Didier Nurizzo and other members of the ESRF Staff for assistance in data collection and Roland Montserret for help with ITC experiments. We acknowledge the contribution of Protein Science Facility of SFR Biosciences (UMS3444/CNRS, US8/Inserm, ENS de Lyon, UCBL) for protein crystallization and mass spectrometry analysis.

Chapter II: Additional results

Materials and methods

I Biology and biochemistry materials

I.1 Bacterial strains and media

D. dadantii and *E. coli* strains used in this study are described in (Table 6). *D. dadantii* and *E. coli* cells were grown at 30 and 37°C respectively in LB medium or M63 minimal medium supplemented with a carbon source (2 g/L). When required antibiotics were added at the following concentration: ampicillin, 100 µg/L, kanamycin and chloramphenicol, 25 µg/L. Media were solidified with 1.5 g/L agar.

I.2 Reagents for phage display

– 2X YT medium (1 L): 16 g peptone, 10 g yeast, 5 g NaCl. Bring to 1 L with bidestilled water. Adjust pH to 7.0 if necessary. Autoclave and store at room temperature for up to several weeks

– 2 M glucose. Filter to sterilize

– 100 mg/mL ampicillin and 10 mg/mL kanamycin. Filter to sterilize

– Phage dilution buffer: 10 mM Tris–HCl (pH 7.5), 20 mM NaCl, 2 mM EDTA

– PEG/NaCl: 16.7% (w/v) PEG-6000, 3.3 mM NaCl. Autoclave and store at 4□

– 450 mL sterile plastic rotor flasks and conventional Erlenmeyer flasks

– Hyperphage stock (Progen Biotechnik GmbH, Heidelberg, Germany)

II Genetic and molecular biology methods

II.1 Plasmid construction

Plasmids and primers used in this study are listed in Table 6. DNA cloning and plasmid extractions were performed with the standard methods. Plasmids were transformed by the $CaCl_2$ procedure into *E. coli* (Sambrook *et al*., 1989) or by the electroporation into *D. dadantii* (Enderle and Farwell, 1998).

II.2 Construction of *ibpS* mutants by site-directed mutagenesis

Site-directed mutagenesis was performed by the Quick-change method. Pairs of complementary mutagenic primers (Table 6) containing the desired nucleotide substitutions were used to amplify the entire plasmid template pGEX-*ibpS* in a PCR using the PrimeSTAR® Max DNA Polymerase (Takara). The PCR products were treated with 1 µL of *DpnI* restriction enzyme and left to incubate at 37°C for 2 hours to eliminate the initial (non-mutated) plasmid, then check the products on agarose gel by electrophoresis. 2 µL of the products was used to transform 200 µL competent *E. coli* cells by heat-shock. The plasmids obtained from extraction by the Nucleospin plasmid kit were sent to sequence, in order to verify the incorporation of the mutations.

II.3 Protein purification

The pGEX derivatives producing the mutated proteins were introduced into *E. coli* NM522 strain. Cells were grown in LB medium to OD_{600} 0.8 and protein production was induced with 1 mM isopropylthiogalactoside (IPTG) for 3h. Cells were collected by centrifugation, resuspended in buffer A (50 mM Tris pH 7.0, 100 mM NaCl) and broken in a French cell press. Unbroken cells were eliminated by centrifugation. The fusion proteins were bound on Protino Glutathione Agarose 4B (Macherey-Nagel)

Strains	**Description**	**Reference**
D. dadantii 3937	Wild type	Laboratory collection
E. coli NM522	Δ(*lac-proAB*) *thi hsd*-5 *supE (*F' *proAB lacI*^{q} Δ *lacZ*M15)	Stratagene
Oligonucleotides used in additional experiments		
IbpS D58E+	cgtttatgccggcggcgaagtacagtcgcagcaagcg	
IbpS D58E -	cgcttgctgcgactgtacttcgccgccggcataaacg	
IbpS D193E +	taccctaacgacgacgaagcggtgctgttctgg	
IbpS D193E -	ccagaacagcaccgcttcgtcgtcgttagggta	
IbpS W268F +	accgacccgtttgtctccttcgcgcaacgcgccgccatc	
IbpS W268F -	gatggcggcgcgttgcgcgaaggagacaaacgggtcggt	
IbpS E341R +	gaccgtggcgcggtccgccgcttccgcgcacag	
IbpS E341R -	ctgtgcgcggaagcggaccgcgccacggtc	
IbpS E353A +	agcaaataccacgacttccgtatcgacaaccaa	
IbpS E353A -	ttggttgtcgatacggaagtcgtggtatttgct	

Table 6 Bacteria strains and primers used in additional experiments.

equilibrated with buffer A, washed several times with the same buffer and the proteins were liberated by addition of Prescission® protease (GE Healthcare) according to the manufacturer's protocol. The protein was incubated with 1 mM EDTA to remove any trace metal. EDTA was eliminated using PD-10 buffer exchange columns (GE Healthcare).

III Biological and biochemical methods

III.1 IbpS binding experiments on Fe-NTA resins

100 µL of Ni-NTA, Zn-NTA, Cu-NTA or Fe-NTA resins equilibrated in buffer A were incubated with 10 µg of protein in the same buffer for 15 min. After centrifugation the supernatant (F = flowthrough) was withdrawn and the resins were washed three times with 1 mL of buffer A. The protein was then eluted with 100 µL of 50 mM EDTA (E = elution) and the fractions were analysed by SDS PAGE.

III.2 Hydroxyl radical scavenging assay

Purified IbpS (50 µM) was incubated with 10 µM $FeCl_3$ or 10 µM $CuCl_2$ for 10 min, then the supercoiled pUC 19 plasmid (1 µg) and 5 mM (for $FeCl_3$) or 10 mM (for $CuCl_2$) H_2O_2 was added. After incubation for 5 min at room temperature, the mixture was immediately run on an agarose gel (0.8%) to examine the levels of intact (supercoiled) and open circle plasmid bands. The DNA was visualized by EtBr staining. Quantitative analysis of the plasmid was performed by the ChemiDoc™ MP Imaging System with software Image Lab.

III.3 Quantification of copper bound to IbpS

IbpS (800 μg) was incubated in buffer Tris-HCl-NaCl (10 mM/L Tris-HCl pH 7.5, 100 mM/L NaCl) containing 0 or 1.5 mM/L of CuSO4 in a volume of 500 μL for 10 min at room temperature; For Cu(I)- binding experiments, ascorbic acid was added to 150 mM/L final concentration to buffer Tris-HCl-NaCl, and to the copper stock solution to reduce Cu(II) to Cu(I) ions. The mixture of protein and copper was incubated for 30 min at room temperature. The mixture was loaded into a PD10 Desalting column (GE Healthcare), previously equilibrated with buffer Tris-HCl-NaCl. 1 μL was used before loading to the columns for protein determination by Nanodrop 2000. Trichloracetic acid (100% w/v) was added to a final concentration of 10%, and the reaction was placed on ice for 10 min. The tubes were then centrifuged at 14, 000g for 10 min at 4°C to separate the denatured protein. The supernatant, containing released copper ions, was then neutralized with 80 μL of 6 M/L NaOH and 100 μL of 1 M/L Tris buffer. After this, ascorbic acid was added again to 150 mM/L final concentration, in this case to reduce all copper to Cu(I) ions. BCSA (Sigma-Aldrich Chemie, Steinheim, Germany), a chromophoric Cu(I) chelator, was added to a final concentration of 0.65 mM/L to determine Cu(I)-IbpS complex concentration using the previously reported extinction coefficient, with a standard curve from 0 to 200 μM/L Cu(I). Either Cu(II)/ Cu(I) or IbpS incubated alone as a negative control and Bovine Serum Albumin (BSA) as positive copperbinding control were performed simultaneously under the same conditions.

III.4 Phage display

The *ibpS* gene without the sequence of the signal peptide was cloned in fusion with the *pIII* gene in the pSEX81 vector. The recombinant plasmid *pSEX81::ibpS-pIII* was introduced into *E. coli* NM522. A colony was grown in 50 mL 2X YT medium

supplemented with 100 mg/mL ampicillin and 100 mM glucose at 37°C overnight. 500 mL of the above medium were inoculated with 5 mL of the overnight culture, and incubated until the OD is 0.5. Hyperphage were added at a MOI of 20 for the production of recombinant phage. The culture was incubated at 37°C for 15–20 min without shaking and then shooke for 45 min with 250 rpm at 37°C. Bacteria were pelleted and resuspended in 500 mL of 2X YT medium supplemented with 100 mg/mL ampicillin and 50 mg/mL kanamycin but without glucose and shaken overnight with 230 rpm at 37°C for recombinant phage production. Bacteria were pelleted and the supernatant recovered. Phage particles were precipitated with 1/5 volume of PEG/NaCl for > 5 h on ice and centrifuged at 10, 000 x g at 4°C for 1 h. The white phage pellet was resuspended in 1/100 of the initial culture volume (5 mL) of phage dilution buffer and aliquoted into 1.5 mL Eppendorf tubes. The process of phage construction and IbpS displayed on phage surface is described below (Figure 20). Binding on Fe-NTA resin was performed as described in **III.1**.

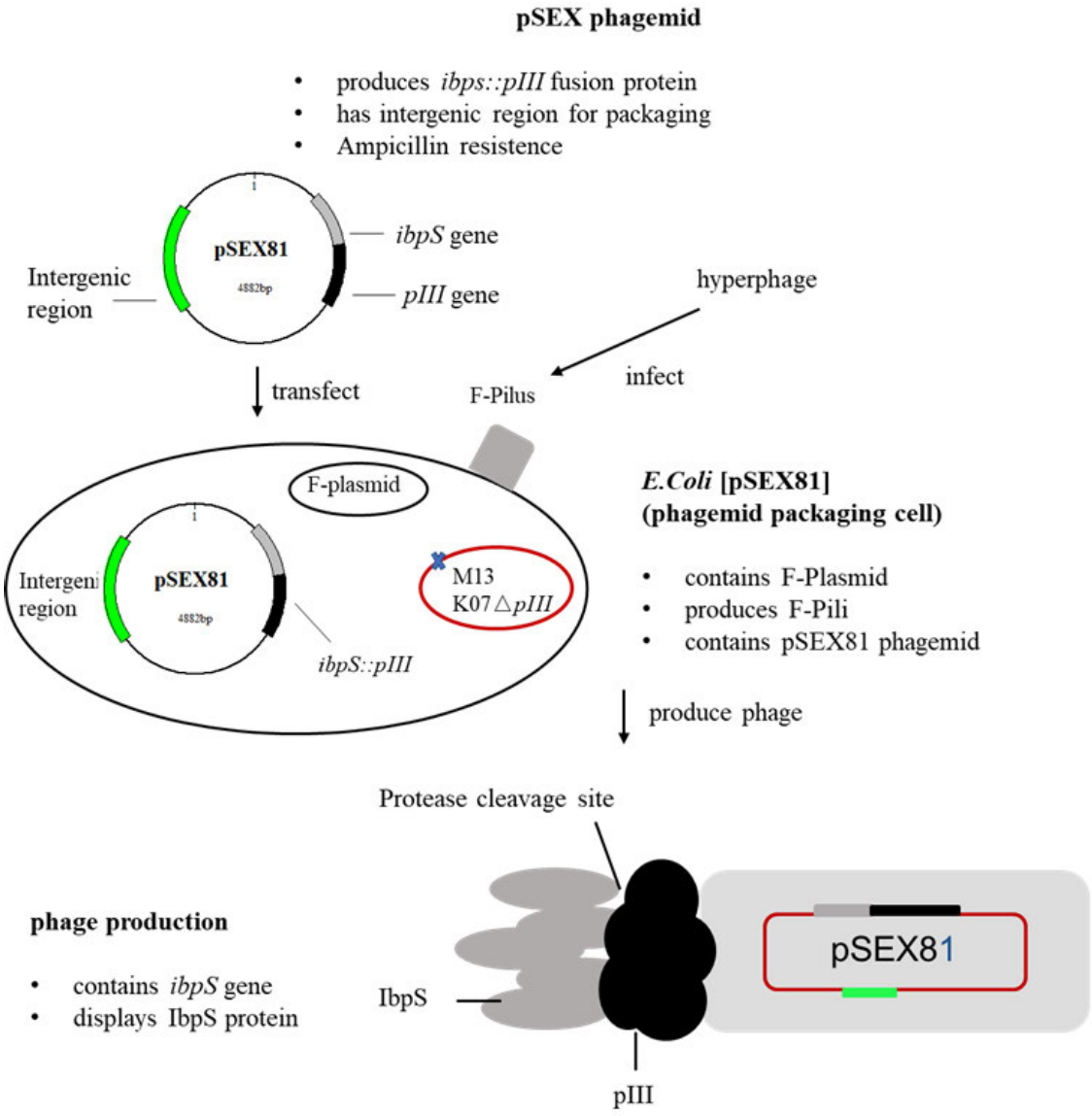

Figure 20 Process of phage construction and IbpS displayed on phage surface.

IbpS displayed on phage surface is done by fusing *ibpS* gene to the phage minor coat protein pIII of phage M13. Incorporation of this fusion protein into the mature phage coat results in the presentation of IbpS protein on the phage surface.

Results

I Construction and metal binding tests of IbpS mutants

I.1 Construction of IbpS mutants

Crystallographic data show a weak coordination of iron with IbpS. However, some residues are very conserved among all the members of the Ibp family. To check if these residues could be involved in metal binding, we selected some of these sites to construct several site-directed mutants of IbpS (Table 7). These mutants are $IbpS_{D58E}$, $IbpS_{D193E}$, $IbpS_{W268F}$, $IbpS_{E353A}$, $IbpS_{E341R}$. To produce these proteins, we chose to express them in fusion with the Glutathion-S-transferase (GST) which allows to bind the fusion protein on a glutathione resin, and to cleave the fusion between GST and IbpS with the Prescission protease. The IbpS protein produced this way is recovered as a soluble protein. However, GST-$IbpS_{E341R}$ was not produced and $IbpS_{D58E}$, $IbpS_{D193E}$ and $IbpS_{W268F}$ were not recovered after cleavage by the protease, indicating that they are insoluble (Figure 21). Only $IbpS_{E353A}$ could be purified in quantity (Figure 22).

I.2 IbpS mutant metal binding test

Production of additional IbpS mutants has been performed in the laboratory. Mutations in residues present in or near the iron binding pocket (D191, D192 and D193) often give non or poorly soluble proteins. Similarly, mutations in or deletion of the C-terminal tail that allows dimerization of IbpS lead to insoluble proteins (Table 7).

For the IbpS mutant metal binding test, we used $IbpS_{E353A}$, $IbpS_{E341R}$ and $IbpS_{W268F}$. When purified $IbpS_{E353A}$, $IbpS_{E341R}$ and $IbpS_{W268F}$ were incubated with Fe-NTA, Cu-NTA resins, the IbpS mutants bound to the matrixes, indicating that mutation in these positions do not affect the iron and copper binding function of IbpS (Figure 23).

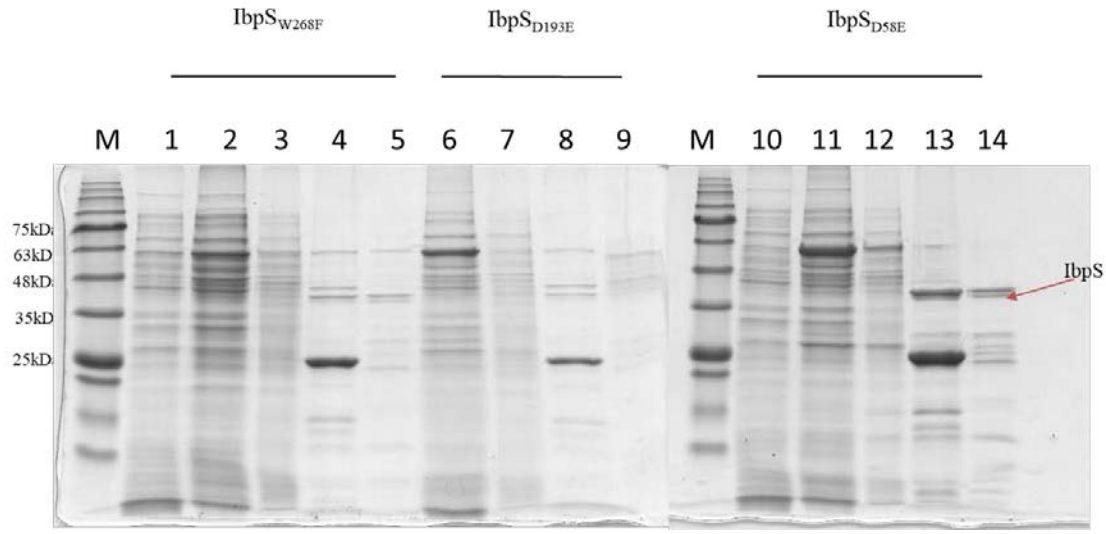

Figure 21 Production and purification of IbpS mutants.

Lane 1, 10: culture not induced; Lane 2,6,11: culture induced by 100 mM IPTG; lane 3,7,12: the supernatant after cells broken; lane 4,8,13: the resin after the elution; lane 5, 9, 14: purified IbpS mutants (2 µL+18 µL ddH_2O); M: protein marker.

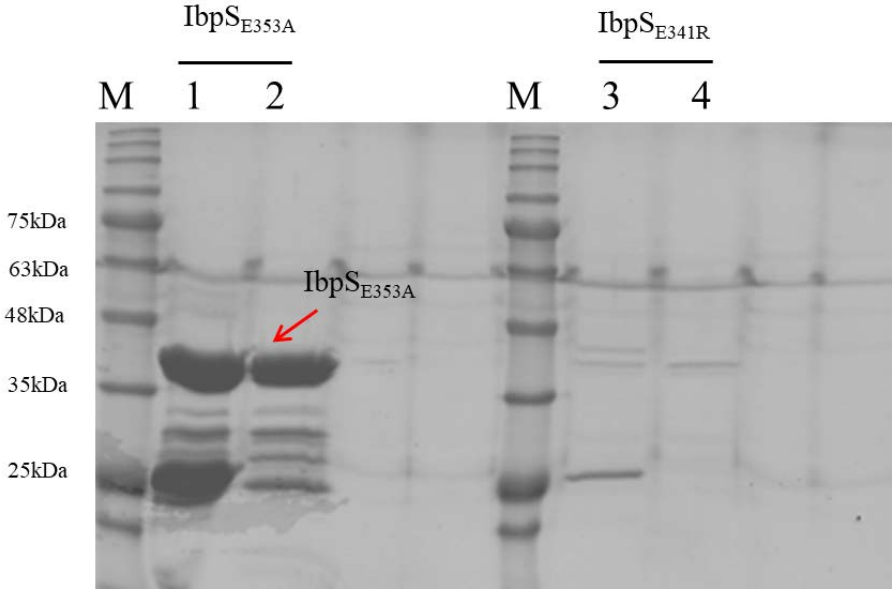

Figure 22 Production and purification of the IbpS mutants.

Lane 1,3: resine after purification; Lane 2,4: purified protein; M: protein marker.

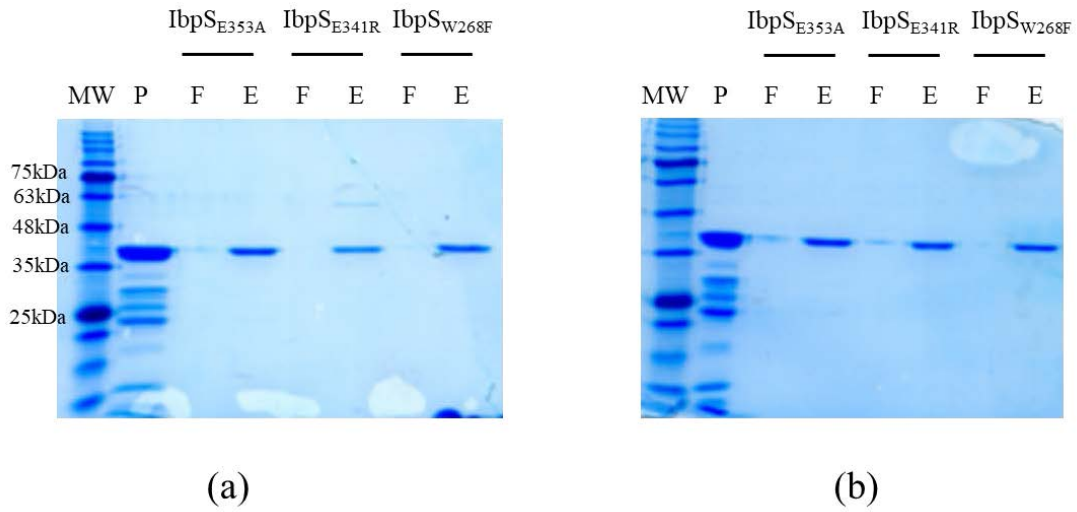

Figure 23 IbpS mutants IbpS$_{E353A}$, IbpS$_{E341R}$, IbpS$_{W268F}$ iron (a) and copper (b) binding test.

IbpS mutants protein (10 µg) in 100 µL of buffer Tris-HCl-NaCl was incubated with 100 µL of the (a) Fe-NTA or (b) Cu-NTA resins for 15 min. After centrifugation the supernatants (flowthroughs) were removed and the resins were washed three times with 1 mL of buffer A. Protein was eluted with 100 µL of 50 mM EDTA and 10 µL of the flowthrough (F) or eluate (E) was loaded onto a SDS-PAGE gel, 1 µL purified IbpS protein (P) was loaded as a control.

Mutant	Production with fusion GST	Fe fixation Residue	Dimerization Residue	Fixation on Fe-NTA	Fixation on Cu-NTA
D58E	slightly soluble			+	+
S86A	soluble			+	+
A91F	insoluble			NT	NT
D100K	soluble			+	+
Q110A	soluble			+	+
E171A	soluble			NT	NT
D191A	soluble			+	+
D191S	insoluble			NT	NT
D192A	slightly soluble			+	+
D192S	soluble			+	+
D192P	insoluble			NT	NT
D193E	insoluble			NT	NT
D193A	insoluble			NT	NT
D193N	insoluble			NT	NT
E209K	soluble			+	+
E212K	soluble			+	+
R223K	slightly soluble			+	NT
W268F	slightly soluble			+	+
E341R	slightly soluble			+	+
E353A	soluble			+	+
H366K	soluble			+	+
E368K	slightly soluble			+	+
D346-fin	insoluble			NT	NT

Table 7 Site-directed mutants of IbpS.

"+" represents the fixation of IbpS to Fe-NTA or Cu-NTA; "NT" represents "not tested". The blue labels represent the Fe fixation residue and dimerization residue of IbpS, and the details were described in Supplementary Figure 8 of the article (**Chapter I**).

A summary of all the metal binding tests of the mutants is presented on (Table 7). All the soluble mutants are able to bind iron and copper. This confirms that metals are weakly bound to IbpS and that none of the tested residue is necessary for binding. Double or multiple mutants should be constructed to have a non-binding protein.

I.3 Determination of residues involved in iron binding by "reverse phage display"

Phage display is a very powerful method to identify peptides or proteins that bind to a target of interest. Peptides or proteins are produced as fusions with the minor coat protein pIII of phage M13 and are exposed at the surface of the phage. It is possible to obtain large libraries of different hybrid proteins. Phages expressing these proteins are incubated with the immobilized target protein. Only phages expressing proteins possessing the highest affinity for the target will be retained after washing. Bound phages can be recovered from the surface, re-infected into bacteria, and thus amplified for further enrichment. This method is used to select antibodies binding with high affinity to an antigen of choice. To our knowledge, this method has never been described to isolate, starting with a protein that binds to matrix, a non-binding mutant. Since IbpS binds to a Fe-NTA matrix, we wondered whether we could isolate non-binding IbpS mutant by "reverse phage display". The first step is to construct a M13 phage expressing a IbpS-pIII fusion and to check the binding of this phage on the Fe-NTA matrix. If binding is observed, the next step would be to fuse pIII with a library of IbpS mutants and to select non-binding phages. These phages will express IbpS-pIII proteins with a

decreased affinity for iron. The physical linkage between the mutant protein and the gene that encodes it in the phage should allow the identification of the mutation.

The *ibpS* gene was cloned in frame with the *pIII* gene in the pSEX81 vector. Introduction of the plasmid in *E. coli* and infection with the Hyperphage helper phage allowed the obtention of phages. However, the low titer (about 10^6 phages/ml) did not allow to confirm the expression of IbpS by the phages by Western blot. Binding experiments to a Fe-NTA matrix were performed. The titer of phages added to the matrix or recovered after incubation was the same for the WT phages or the phages expressing IbpS-pIII, indicating that the latter did not bind the Fe-NTA matrix (Table 8). Thus, the project was not pursued. Absence of binding could be due to the low affinity of IbpS for iron or a conformation of the IbpS-pIII protein that does not allow binding to iron. The low titer could be due to the large size of IbpS.

Numbers of phages		
	Before Fe-NTA	After Fe-NTA
WT phage	$8.8x10^5$	$6x10^5$
IbpS-phage	$1.8x10^5$	$1.5x10^5$

Table 8 Titration of phage before and after incubation with the Fe-NTA matrix.

II Protection of metal-induced plasmid cleavage by IbpS

Plant defense reactions involve the production of H_2O_2 which generates highly reactive ROS, such as OH°, that will kill the pathogens in the presence of iron or copper.

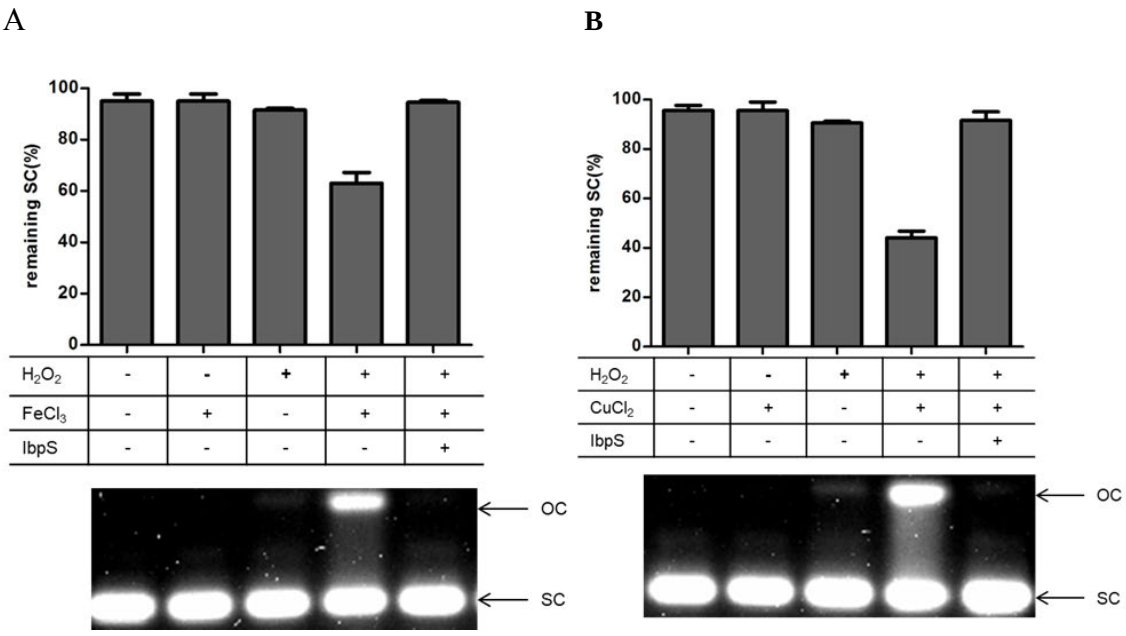

Figure 24 IbpS prevents DNA cleavage by ROS.

Hydroxyl radicals cleave the supercoiled plasmid (SC) into the open circle form (OC). After reaction of the protein IbpS (50 μM) with (10 μM) $FeCl_3$ (**A**) or (10 μM) $CuCl_2$ (**B**) for 10 min, the plasmid and 5 mM (**A**) or 10 mM H_2O_2 (**B**) were added and incubated for 5 min at room temperature and then immediately run the agarose gel electrophoresis (0.8%). The DNA was visualized by EtBr staining. Quantitative analysis of the plasmid was performed by the ChemiDoc™ MP Imaging System with software Image Lab. Values are expressed as means ± S.D. of three independent experiments. A representative agarose gel electrophoresis is shown in the bottom.

We tested whether IbpS can prevent the damage of plasmids generated by free radicals produced by the Fenton reaction in the presence of iron and copper. The IbpS protein was incubated in a reaction mixture containing supercoiled plasmids pUC19 and $FeCl_3$ or $CuCl_2$, to which H_2O_2 was added in order to trigger the Fenton reaction. Supercoiled plasmids were used to probe the generation of hydroxyl radicals in this experiment, because hydroxyl radicals, but not H_2O_2, can make a single strand breakage in the plasmid, leading to the generation of an open-circle plasmid (LES Netto *et al*., 1996). Addition of H_2O_2 alone generated only a limited cleavage of the plasmid. Addition of H_2O_2 and metal ($FeCl_3$ or $CuCl_2$) induced the cleavage of DNA. This effect was significantly reduced when IbpS was added to the mixture (Figure 24**)**. This result confirmed that IbpS can bind Fe^{3+} and Cu^{2+} and prevent ROS formation in the presence of H_2O_2.

III IbpS has affinity for Cu(I)

In our study, we determined that IbpS was a copper binding secreted protein. Due to the ability of copper to alternate between its cuprous Cu(I) and cupric Cu(II) oxidation states, as well as the ability of Cu(I) to generate ROS through Fenton-like reactions, we investigated IbpS interaction with copper, in the Cu(I) or Cu(II) forms. We determined the amount of Cu(I) and Cu(II) bound to IbpS by the BCSA colorimetric method. Our results show that one IbpS can bind 2 Cu(II) or 3 Cu(I) (Figure 25). These results are superior to that obtained by ITC. However, we have shown that IbpS can bind aspecifically metals. Other methods should be used to determine the exact stoichiometry of metal binding to IbpS.

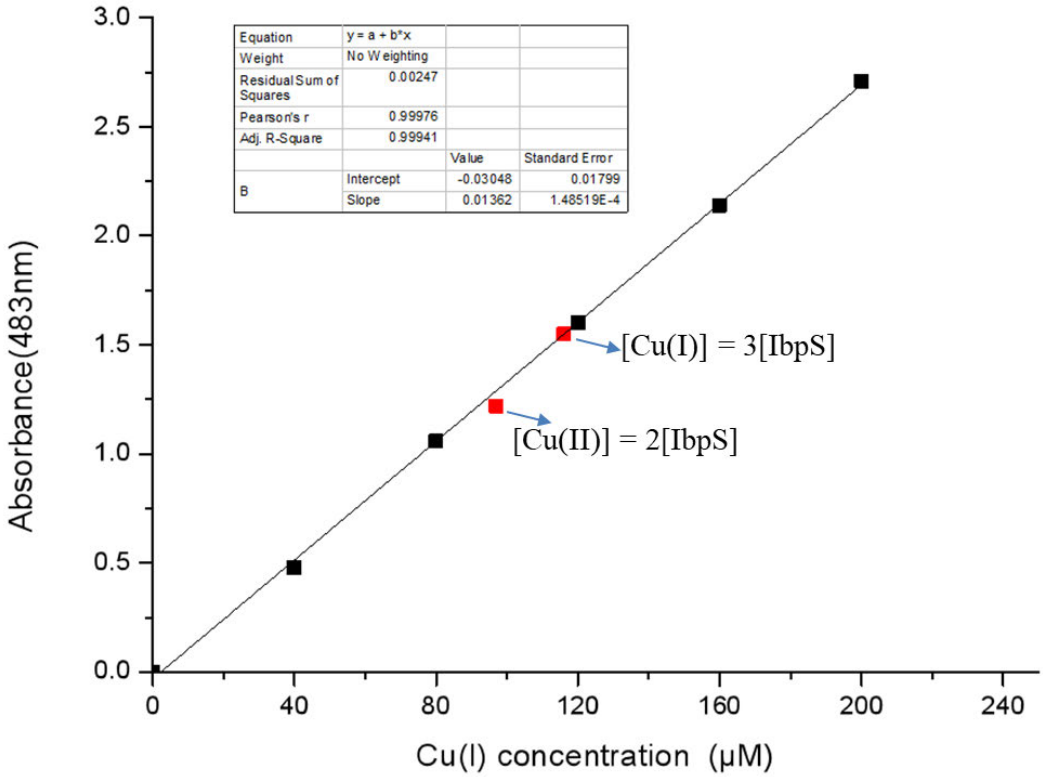

Figure 25 Affinity of IbpS to Cu(I) and Cu(II) in solution.

Purified IbpS (40 µM) protein was incubated with $CuCl_2$, the same mixture was incubated with ascorbate for 30min at room temperature to test of Cu(I) binding to IbpS. Unbound copper ions were removed by gel filtration. IbpS was denatured with TCA. After reduction with ascorbate, Cu(I) was quantified by the BCSA colorimetric assay. Quantity of Cu(I) bound to 40 µM of IbpS was determined to be 96 µM and that of Cu(II) 116µM.

Conclusion – Perspectives

In this work we have characterized IbpS, the prototype of a new family of proteins secreted by several necrotrophic plant pathogenic microorganisms. IbpS had been detected in the Out-dependent supernatant of *P. atrosepticum* grown in a medium containing polygalacturonate (Coulthurst *et al*., 2008). An analysis of the secretome of *D. dadantii* grown in the same medium failed to detect this protein (Kazemi‐Pour *et al*., 2004). Results presented here explain this result: expression of *ibpS* is not induced by polygalacturonate in *D. dadantii*. Induction of *ibpS* expression was only observed in the presence of chicory fragments. Polygalacturonate is an inducer of the expression of most of the secreted pectinases and of the Out secretion system in *D. dadantii*. However, expression of other genes encoding Out-secreted protein involved in virulence, such as *avrL* and *avrM*, is not induced by this compound but by chicory fragments, like *ibpS*. This suggests the existence of a regulon of genes induced in this condition that could play a role in *D. dadantii* virulence. Characterization of the inducing molecule(s) present in chicory and identification of the regulator that responds to this condition could be of great interest to understand the mechanisms of *D. dadantii* pathogenicity. Purification of the inducing molecule using a bio-guided approach has been initiated during this work. A strain containing an *ibpS-lacZ* fusion was used to test the inducing properties of different fractions obtained from chicory leaves. However, the induction levels were low and purification could not be completed. Other plants could be tested to find one that contains a higher concentration of the inducing molecule(s). Other reporters such as the *avrL-lacZ* or *avrM-lacZ* fusions could be used instead of the *ibpS-lacZ* fusion if they show better induction levels. Such an induction let suppose the existence of a regulator responding to this signal. To identify this regulator, two approaches can be used. A mutant in which a repressor gene is inactivated will be identified in a library of transposon insertions as a clone expressing the *ibpS-lacZ* fusion at an elevated level. An activator effect will be identified after introduction of a *D. dadantii* gene library into a strain containing the *ibpS-lacZ* fusion, as a clone expressing

the fusion at an elevated level. Then, all the genes controlled by this predicted regulator could be identified by a transcriptomic analysis of the corresponding mutant. This should allow the identification of new actors of *D. dadantii* virulence.

D. dadantii encodes a second protein of the Ibp family, IbpP. Biochemical experiments have shown that this protein is also able to bind iron and copper. However, the conditions that allow *ibpS* expression do not induce *ibpP*. IbpP seems to be not or poorly secreted. A study of the conditions of expression of *ibpP* and of the characteristics of the protein IbpP could help to explain the reason of this redundancy in *Dickeya*. Multiplicity of *ibp* genes in the same organism is observed in certain oomycetes or *Folsomia candida* but not in bacteria, except *Dickeya*. It will be interesting to analyse in these other organisms if this redundancy is caused by a difference in the properties of the Ibp proteins, or in the condition, timing and localization of their gene expression.

The role of IbpS seems to buffer the large amounts of metal released during bacterial progression in the leaf to limit the production of ROS in bacteria (Aznar *et al*., 2015). However, in later stages of infection, iron becomes limiting since it is accumulated in plant ferritin ahead of the macerated zone (Aznar *et al*., 2015) and it is also complexed by siderophores produced by *D. dadantii* when iron becomes limited (Burbank *et al*., 2015). It would be interesting to know if the plant and the bacteria can mobilize iron bound to IbpS. The low affinity of IbpS for metals and the high affinity of siderophores and ferritins for iron suggest that it is the case. This hypothesis could be confirmed experimentally. By incubating purified siderophores or plant ferritins with iron-loaded IbpS, it will be possible to see if iron can be transferred from IbpS to siderophores and ferritins. This would confirm that binding of metals to IbpS is not a dead end for metals but that they remain usable for the bacteria or the plant.

When IbpS was infiltrated into *A. thaliana* leaves, a strong induction of the PR-1

(Pathogenesis related Protein-1) gene was observed. *PR-1* expression is induced in response to a variety of pathogens or stresses (Mitsuhara *et al*., 2008). Induction could probably result from the iron deficiency. However, another hypothesis can be proposed. The strong conservation of Ibp proteins in a large number of plant pathogens distributed in three kingdoms of life could have given it a function of PAMP. Recognition of PAMPs by plant receptors induces their immune system which includes the gene *PR-1*. Confirmation of this hypothesis would give a new view on the role of Ibp proteins in plant microbe interactions.

Reference

Adeolu, M., Alnajar, S., Naushad, S., S Gupta, R., 2016. Genome-based phylogeny and taxonomy of the "Enterobacteriales": proposal for Enterobacterales ord. nov. divided into the families *Enterobacteriaceae*, *Erwiniaceae* fam. nov., *Pectobacteriaceae* fam. nov., *Yersiniaceae* fam. nov., *Hafniaceae* fam. nov., *Morganellaceae* fam. nov., and *Budviciaceae* fam. nov. Int. J. Syst. Evol. Microbiol. 66, 5575–5599. https://doi.org/10.1099/ijsem.0.001485

Agrios, G.N., 1997. Plant pathology. Academic Press, San Diego.

Alfano, J., Collmer, A., 1996. Bacterial pathogens in plants: Life up against the Wall. Plant Cell 8, 1683–1698.

Alfano, J.R., Collmer, A., 2004. Type III secretion system effector proteins: double agents in bacterial disease and plant defense. Annu Rev Phytopathol 42, 385–414. https://doi.org/10.1146/annurev.phyto.42.040103.110731

Amselem, J., Cuomo, C.A., van Kan, J.A.L., Viaud, M., Benito, E.P., Couloux, A., Coutinho, P.M., de Vries, R.P., Dyer, P.S., Fillinger, S., Fournier, E., Gout, L., Hahn, M., Kohn, L., Lapalu, N., Plummer, K.M., Pradier, J.-M., Quévillon, E., Sharon, A., Simon, A., ten Have, A., Tudzynski, B., Tudzynski, P., Wincker, P., Andrew, M., Anthouard, V., Beever, R.E., Beffa, R., Benoit, I., Bouzid, O., Brault, B., Chen, Z., Choquer, M., Collémare, J., Cotton, P., Danchin, E.G., Da Silva, C., Gautier, A., Giraud, C., Giraud, T., Gonzalez, C., Grossetete, S., Güldener, U., Henrissat, B., Howlett, B.J., Kodira, C., Kretschmer, M., Lappartient, A., Leroch, M., Levis, C., Mauceli, E., Neuvéglise, C., Oeser, B., Pearson, M., Poulain, J., Poussereau, N., Quesneville, H., Rascle, C., Schumacher, J., Ségurens, B., Sexton, A., Silva, E., Sirven, C., Soanes, D.M., Talbot, N.J., Templeton, M., Yandava, C., Yarden, O., Zeng, Q., Rollins, J.A., Lebrun, M.-H., Dickman, M., 2011. Genomic analysis of the necrotrophic fungal pathogens *Sclerotinia sclerotiorum* and *Botrytis cinerea*. PLoS Genet. 7, e1002230. https://doi.org/10.1371/journal.pgen.1002230

Armstrong, N., Gouaux, E., 2000. Mechanisms for activation and antagonism of an AMPA-sensitive glutamate receptor: crystal structures of the GluR2 ligand binding core. Neuron 28, 165–181.

Arts, J., de Groot, A., Ball, G., Durand, E., Khattabi, M.E., Filloux, A., Tommassen, J., Koster, M., 2007. Interaction domains in the *Pseudomonas aeruginosa* type II secretory apparatus component XcpS (GspF). Microbiology 153, 1582–1592. https://doi.org/10.1099/mic.0.2006/002840-0

Aznar, A., Patrit, O., Berger, A., Dellagi, A., 2015. Alterations of iron distribution in *Arabidopsis* tissues infected by *Dickeya dadantii*. Molecular Plant Pathology 16, 521–528. https://doi.org/10.1111/mpp.12208

Bally, M., Filloux, A., Akrim, M., Ball, G., Lazdunski, A., Tommassen, J., 1992. Protein secretion in *Pseudomonas aeruginosa*: characterization of seven xcp genes and processing of secretory apparatus components by prepilin peptidase. Molecular Microbiology 6, 1121–1131. https://doi.org/10.1111/j.1365-2958.1992.tb01550.x

Barrie Johnson, D., Hallberg, K.B., 2008. Carbon, Iron and sulfur metabolism in acidophilic micro-organisms, in: Poole, R.K. (Ed.), Advances in Microbial Physiology. Academic Press, pp. 201–255. https://doi.org/10.1016/S0065-2911(08)00003-9

Baxter, L., Tripathy, S., Ishaque, N., Boot, N., Cabral, A., Kemen, E., Thines, M., Ah-Fong, A., Anderson, R., Badejoko, W., Bittner-Eddy, P., Boore, J.L., Chibucos, M.C., Coates, M., Dehal, P., Delehaunty, K., Dong, S., Downton, P., Dumas, B., Fabro, G., Fronick, C., Fuerstenberg, S.I., Fulton, L., Gaulin, E., Govers, F., Hughes, L., Humphray, S., Jiang, R.H.Y., Judelson, H., Kamoun, S., Kyung, K., Meijer, H., Minx, P., Morris, P., Nelson, J., Phuntumart, V., Qutob, D., Rehmany, A., Rougon-Cardoso, A., Ryden, P., Torto-Alalibo, T., Studholme, D., Wang, Y., Win, J., Wood, J., Clifton, S.W., Rogers, J., Ackerveken, G.V. den, Jones, J.D.G., McDowell, J.M., Beynon, J., Tyler, B.M., 2010. Signatures of adaptation to obligate biotrophy in the *Hyaloperonospora arabidopsidis* genome. Science 330, 1549–1551. https://doi.org/10.1126/science.1195203

Berger, E.A., 1973. Different Mechanisms of Energy Coupling for the Active Transport of Proline and Glutamine in *Escherichia coli*. PNAS 70, 1514–1518. https://doi.org/10.1073/pnas.70.5.1514

Berntsson, R.P.-A., 2010. Structure and function of substrate-binding proteins of ABC-transporters. s.n.

Berntsson, R.P.-A., Smits, S.H.J., Schmitt, L., Slotboom, D.-J., Poolman, B., 2010. A structural classification of substrate-binding proteins. FEBS Letters, Gothenburg Special Issue: Molecules of Life 584, 2606–2617. https://doi.org/10.1016/j.febslet.2010.04.043

Biemans-Oldehinkel, E., Doeven, M.K., Poolman, B., 2006. ABC transporter architecture and regulatory roles of accessory domains. FEBS Letters, ABC Transporters 580, 1023–1035. https://doi.org/10.1016/j.febslet.2005.11.079

Bleves, S., Lazdunski, A., Filloux, A., 1996. Membrane topology of three Xcp proteins involved in exoprotein transport by *Pseudomonas aeruginosa*. Journal of Bacteriology 178, 4297–4300. https://doi.org/10.1128/jb.178.14.4297-4300.1996

Bos, M.P., Robert, V., Tommassen, J., 2007. Biogenesis of the Gram-negative bacterial outer membrane. Annual Review of Microbiology 61, 191–214. https://doi.org/10.1146/annurev.micro.61.080706.093245

Boughammoura, A., Franza, T., Dellagi, A., Roux, C., Matzanke-Markstein, B., Expert, D., 2007. Ferritins, bacterial virulence and plant defence. Biometals 20, 347. https://doi.org/10.1007/s10534-006-9069-0

Bouley, J., Condemine, G., Shevchik, V.E., 2001. The PDZ domain of OutC and the N-terminal region of OutD determine the secretion specificity of the type II out pathway of *Erwinia chrysanthemi*. 11Edited by I. B. Holland. Journal of Molecular Biology 308, 205–219. https://doi.org/10.1006/jmbi.2001.4594

Brady, C.L., Cleenwerck, I., Denman, S., Venter, S.N., Rodríguez-Palenzuela, P., Coutinho, T.A., De Vos, P., 2012. Proposal to reclassify *Brenneria quercina* (Hildebrand and Schroth 1967) Hauben *et al*. 1999 into a new genus, *Lonsdalea* gen. nov., as *Lonsdalea quercina* comb. nov., descriptions of *Lonsdalea quercina* subsp. *quercina* comb. nov., *Lonsdalea quercina* subsp. *iberica* subsp. nov. and *Lonsdalea quercina* subsp. *britannica* subsp. nov., emendation of the description of the genus *Brenneria*, reclassification of *Dickeya dieffenbachiae* as *Dickeya dadantii* subsp. *dieffenbachiae* comb. nov., and emendation of the description of *Dickeya dadantii*. International Journal of Systematic and Evolutionary Microbiology 62, 1592–1602. https://doi.org/10.1099/ijs.0.035055-0

Braud, A., Hoegy, F., Jezequel, K., Lebeau, T., Schalk, I.J., 2009. New insights into the metal

specificity of the *Pseudomonas aeruginosa* pyoverdine–iron uptake pathway. Environmental Microbiology 11, 1079–1091. https://doi.org/10.1111/j.1462-2920.2008.01838.x

Brok, R., Van Gelder, P., Winterhalter, M., Ziese, U., Koster, A.J., de Cock, H., Koster, M., Tommassen, J., Bitter, W., 1999. The C-terminal domain of the *Pseudomonas* secretin XcpQ forms oligomeric rings with pore activity. 11Edited by R. Huber. Journal of Molecular Biology 294, 1169–1179. https://doi.org/10.1006/jmbi.1999.3340

Brune, A., Urbach, W., Dietz, K.-J., 1994. Zinc stress induces changes in apoplasmic protein content and polypeptide composition of barley primary leaves. J Exp Bot 45, 1189–1196. https://doi.org/10.1093/jxb/45.9.1189

Bruns, C.M., Nowalk, A.J., Arvai, A.S., McTigue, M.A., Vaughan, K.G., Mietzner, T.A., McRee, D.E., 1997. Structure of *Haemophilus influenzae* Fe+3-binding protein reveals convergent evolution within a superfamily. Nature Structural & Molecular Biology 4, 919–924. https://doi.org/10.1038/nsb1197-919

Bullen, J.J., 1981. The significance of iron in infection. Rev Infect Dis 3, 1127–1138. https://doi.org/10.1093/clinids/3.6.1127

Burbank, L., Mohammadi, M., Roper, M.C., 2015. Siderophore-mediated iron acquisition influences motility and is required for full virulence of the xylem-dwelling bacterial phytopathogen *Pantoea stewartii* subsp. *stewartii*. Appl Environ Microbiol 81, 139–148. https://doi.org/10.1128/AEM.02503-14

Butt, A., Mousley, C., Morris, K., Beynon, J., Can, C., Holub, E., Greenberg, J.T., Buchanan-Wollaston, V., 1998. Differential expression of a senescence-enhanced metallothionein gene in *Arabidopsis* in response to isolates of *Peronospora parasitica* and *Pseudomonas syringae*. Plant J. 16, 209–221.

Campos, M., Nilges, M., Cisneros, D.A., Francetic, O., 2010. Detailed structural and assembly model of the type II secretion pilus from sparse data. PNAS 107, 13081–13086. https://doi.org/10.1073/pnas.1001703107

Castiglione, S., Franchin, C., Fossati, T., Lingua, G., Torrigiani, P., Biondi, S., 2007. High zinc concentrations reduce rooting capacity and alter metallothionein gene expression in white

poplar (*Populus alba L.* cv. *Villafranca*). Chemosphere 67, 1117–1126. https://doi.org/10.1016/j.chemosphere.2006.11.039

Chang, J.H., Urbach, J.M., Law, T.F., Arnold, L.W., Hu, A., Gombar, S., Grant, S.R., Ausubel, F.M., Dangl, J.L., 2005. A high-throughput, near-saturating screen for type III effector genes from *Pseudomonas syringae*. PNAS 102, 2549–2554. https://doi.org/10.1073/pnas.0409660102

Changela, A., Chen, K., Xue, Y., Holschen, J., Outten, C.E., O'halloran, T.V., Mondragón, A., 2003. Molecular basis of metal-ion selectivity and zeptomolar sensitivity by CueR. Science 301, 1383–1387.

Charkowski, A.O., 2018. The changing face of bacterial soft-rot diseases. Annual Review of Phytopathology 56, 269–288. https://doi.org/10.1146/annurev-phyto-080417-045906

Chen, J., 2013. Molecular mechanism of the *Escherichia coli* maltose transporter. Current Opinion in Structural Biology 23, 492–498. https://doi.org/10.1016/j.sbi.2013.03.011

Chisholm, S.T., Coaker, G., Day, B., Staskawicz, B.J., 2006. Host-microbe interactions: shaping the evolution of the plant immune Response. Cell 124, 803–814. https://doi.org/10.1016/j.cell.2006.02.008

Cianciotto, N.P., 2005. Type II secretion: a protein secretion system for all seasons. Trends Microbiol. 13, 581–588. https://doi.org/10.1016/j.tim.2005.09.005

Coaker, G., Falick, A., Staskawicz, B., 2005. Activation of a Phytopathogenic bacterial effector protein by a eukaryotic cyclophilin. Science 308, 548–550. https://doi.org/10.1126/science.1108633

Cole, S.P.C., 2014. Multidrug Resistance Protein 1 (MRP1, ABCC1), a "Multitasking" ATP-binding Cassette (ABC) Transporter. J Biol Chem 289, 30880–30888. https://doi.org/10.1074/jbc.R114.609248

Cornelis, P., Matthijs, S., 2002. Diversity of siderophore-mediated iron uptake systems in fluorescent pseudomonads: not only pyoverdines. Environmental Microbiology 4, 787–798. https://doi.org/10.1046/j.1462-2920.2002.00369.x

Cosio, C., Martinoia, E., Keller, C., 2004. Hyperaccumulation of cadmium and zinc in *Thlaspi caerulescens* and *Arabidopsis halleri* at the leaf cellular level. Plant Physiology 134, 716–725. https://doi.org/10.1104/pp.103.031948

Coulthurst, S.J., Lilley, K.S., Hedley, P.E., Liu, H., Toth, I.K., Salmond, G.P.C., 2008. DsbA plays a critical and multifaceted role in the production of secreted virulence factors by the phytopathogen *Erwinia carotovora* subsp. *atroseptica*. J. Biol. Chem. 283, 23739–23753. https://doi.org/10.1074/jbc.M801829200

Dawson, R.J.P., Locher, K.P., 2006. Structure of a bacterial multidrug ABC transporter. Nature 443, 180–185. https://doi.org/10.1038/nature05155

de Peredo, A.G., Saint-Pierre, C., Latour, J.-M., Michaud-Soret, I., Forest, E., 2001. Conformational changes of the ferric uptake regulation protein upon metal activation and DNA binding; first evidence of structural homologies with the diphtheria toxin repressor. 11Edited by G. v. Heijne. Journal of Molecular Biology 310, 83–91. https://doi.org/10.1006/jmbi.2001.4769

DebRoy, S., Thilmony, R., Kwack, Y.-B., Nomura, K., He, S.Y., 2004. A family of conserved bacterial effectors inhibits salicylic acid-mediated basal immunity and promotes disease necrosis in plants. PNAS 101, 9927–9932. https://doi.org/10.1073/pnas.0401601101

Dellagi, A., Rigault, M., Segond, D., Roux, C., Kraepiel, Y., Cellier, F., Briat, J.-F., Gaymard, F., Expert, D., 2005. Siderophore-mediated upregulation of *Arabidopsis* ferritin expression in response to *Erwinia chrysanthemi* infection. The Plant Journal 43, 262–272. https://doi.org/10.1111/j.1365-313X.2005.02451.x

Denny, T., 2006. Plant pathogenic *Ralstonia* species, in: Gnanamanickam, S.S. (Ed.), Plant-Associated Bacteria. Springer Netherlands, Dordrecht, pp. 573–644. https://doi.org/10.1007/978-1-4020-4538-7_16

Dhungana, S., Taboy, C.H., Anderson, D.S., Vaughan, K.G., Aisen, P., Mietzner, T.A., Crumbliss, A.L., 2003. The influence of the synergistic anion on iron chelation by ferric binding protein, a bacterial transferrin. PNAS 100, 3659–3664. https://doi.org/10.1073/pnas.0536897100

Douzi, B., Durand, E., Bernard, C., Alphonse, S., Cambillau, C., Filloux, A., Tegoni, M., Voulhoux, R., 2009. The XcpV/GspI pseudopilin has a central role in the assembly of a quaternary complex within the T2SS pseudopilus. J. Biol. Chem. 284, 34580–34589. https://doi.org/10.1074/jbc.M109.042366

Douzi, B., Filloux, A., Voulhoux, R., 2012. On the path to uncover the bacterial type II secretion

system. Philos. Trans. R. Soc. Lond., B, Biol. Sci. 367, 1059–1072. https://doi.org/10.1098/rstb.2011.0204

Duplessis, S., Cuomo, C.A., Lin, Y.-C., Aerts, A., Tisserant, E., Veneault-Fourrey, C., Joly, D.L., Hacquard, S., Amselem, J., Cantarel, B.L., Chiu, R., Coutinho, P.M., Feau, N., Field, M., Frey, P., Gelhaye, E., Goldberg, J., Grabherr, M.G., Kodira, C.D., Kohler, A., Kües, U., Lindquist, E.A., Lucas, S.M., Mago, R., Mauceli, E., Morin, E., Murat, C., Pangilinan, J.L., Park, R., Pearson, M., Quesneville, H., Rouhier, N., Sakthikumar, S., Salamov, A.A., Schmutz, J., Selles, B., Shapiro, H., Tanguay, P., Tuskan, G.A., Henrissat, B., Peer, Y.V. de, Rouzé, P., Ellis, J.G., Dodds, P.N., Schein, J.E., Zhong, S., Hamelin, R.C., Grigoriev, I.V., Szabo, L.J., Martin, F., 2011. Obligate biotrophy features unraveled by the genomic analysis of rust fungi. PNAS 108, 9166–9171. https://doi.org/10.1073/pnas.1019315108

Durand, É., Bernadac, A., Ball, G., Lazdunski, A., Sturgis, J.N., Filloux, A., 2003. Type II protein secretion in *Pseudomonas aeruginosa*: the pseudopilus is a multifibrillar and adhesive structure. Journal of Bacteriology 185, 2749–2758. https://doi.org/10.1128/JB.185.9.2749-2758.2003

Enard, C., Diolez, A., Expert, D., 1988. Systemic virulence of *Erwinia chrysanthemi* 3937 requires a functional iron assimilation system. Journal of Bacteriology 170, 2419–2426. https://doi.org/10.1128/jb.170.6.2419-2426.1988

Enderle, P.J., Farwell, M.A., 1998. Electroporation of freshly plated *Escherichia coli* and *Pseudomonas aeruginosa* cells. BioTechniques 25, 954–956, 958. https://doi.org/10.2144/98256bm05

Escolar, L., Pérez-Martín, J., Lorenzo, V. de, 1999. Opening the iron box: transcriptional metalloregulation by the fur protein. Journal of Bacteriology 181, 6223–6229.

Espagne, E., Lespinet, O., Malagnac, F., Da Silva, C., Jaillon, O., Porcel, B.M., Couloux, A., Aury, J.-M., Ségurens, B., Poulain, J., Anthouard, V., Grossetete, S., Khalili, H., Coppin, E., Déquard-Chablat, M., Picard, M., Contamine, V., Arnaise, S., Bourdais, A., Berteaux-Lecellier, V., Gautheret, D., de Vries, R.P., Battaglia, E., Coutinho, P.M., Danchin, E.G., Henrissat, B., Khoury, R.E., Sainsard-Chanet, A., Boivin, A., Pinan-Lucarré, B., Sellem, C.H., Debuchy, R., Wincker, P., Weissenbach, J., Silar, P., 2008. The genome sequence of

the model ascomycete fungus *Podospora anserina*. Genome Biology 9, R77. https://doi.org/10.1186/gb-2008-9-5-r77

Espinosa, A., Alfano, J.R., 2004. Disabling surveillance: bacterial type III secretion system effectors that suppress innate immunity. Cell. Microbiol. 6, 1027–1040. https://doi.org/10.1111/j.1462-5822.2004.00452.x

Estela Silva-Stenico, M., Pacheco, F.T.H., Rodrigues, J.L.M., Carrilho, E., Tsai, S.M., 2005. Growth and siderophore production of *Xylella fastidiosa* under iron-limited conditions. Microbiological Research 160, 429–436. https://doi.org/10.1016/j.micres.2005.03.007

Expert, D., 1999. Withholding and exchanging iron: interactions between *Erwinia* spp. and their plant hosts. Annual Review of Phytopathology 37, 307–334. https://doi.org/10.1146/annurev.phyto.37.1.307

Expert, D., Franza, T., Dellagi, A., 2012. Iron in plant–pathogen interactions, in: molecular aspects of iron metabolism in pathogenic and symbiotic plant-microbe associations. Springer, pp. 7–39.

Expert, D., Neema, C., Pierre Laulhère, J., Sauvage, C., Masclaux, C., Mahé, B., 1994. Iron and plant pathogenesis: the systemic soft rot disease induced by *Erwinia chrysanthemi* 3937 on *saintpaulia* plants, in: Kado, C.I., Crosa, J.H. (Eds.), Molecular Mechanisms of Bacterial Virulence, Developments in Plant Pathology. Springer Netherlands, Dordrecht, pp. 161–171. https://doi.org/10.1007/978-94-011-0746-4_11

Felder, C.B., Graul, R.C., Lee, A.Y., Merkle, H.-P., Sadee, W., 1999. The venus flytrap of periplasmic binding proteins: An ancient protein module present in multiple drug receptors. AAPS PharmSci 1, 7–26. https://doi.org/10.1208/ps010202

Felix, G., Boller, T., 2003. Molecular sensing of bacteria in plants. The highly conserved RNA-binding motif RNP-1 of bacterial cold shock proteins is recognized as an elicitor signal in tobacco. J. Biol. Chem. 278, 6201–6208. https://doi.org/10.1074/jbc.M209880200

Ferrandez, Y., Condemine, G., 2008. Novel mechanism of outer membrane targeting of proteins in Gram-negative bacteria. Mol. Microbiol. 69, 1349–1357. https://doi.org/10.1111/j.1365-2958.2008.06366.x

Filloux, A., 2004. The underlying mechanisms of type II protein secretion. Biochimica et Biophysica

Acta (BBA) - Molecular Cell Research, Protein Export/Secretion in Bacteria 1694, 163–179. https://doi.org/10.1016/j.bbamcr.2004.05.003

Fones, H., Preston, G.M., 2013. The impact of transition metals on bacterial plant disease. FEMS Microbiol Rev 37, 495–519. https://doi.org/10.1111/1574-6976.12004

Fones, H., Preston, G.M., 2012. Reactive oxygen and oxidative stress tolerance in plant pathogenic *Pseudomonas*. FEMS Microbiol Lett 327, 1–8. https://doi.org/10.1111/j.1574-6968.2011.02449.x

Franza, T., Mahé, B., Expert, D., 2005. *Erwinia chrysanthemi* requires a second iron transport route dependent of the siderophore achromobactin for extracellular growth and plant infection. Molecular Microbiology 55, 261–275. https://doi.org/10.1111/j.1365-2958.2004.04383.x

Fritz-Laylin, L.K., Krishnamurthy, N., Tör, M., Sjölander, K.V., Jones, J.D.G., 2005. Phylogenomic analysis of the receptor-like proteins of *Rice* and *Arabidopsis*. Plant Physiology 138, 611–623. https://doi.org/10.1104/pp.104.054452

Fukami-Kobayashi, K., Tateno, Y., Nishikawa, K., 1999. Domain dislocation: a change of core structure in periplasmic binding proteins in their evolutionary history. J. Mol. Biol. 286, 279–290. https://doi.org/10.1006/jmbi.1998.2454

Fulyani, F., Schuurman-Wolters, G.K., Žagar, A.V., Guskov, A., Slotboom, D.-J., Poolman, B., 2013. Functional Diversity of Tandem Substrate-Binding Domains in ABC Transporters from Pathogenic Bacteria. Structure 21, 1879–1888. https://doi.org/10.1016/j.str.2013.07.020

Garnier, L., Simon Plas, F., Thuleau, P., Agnel, J.-P., Blein, J.-P., Ranjeva, R., Montillet, J.-L., 2006. Cadmium affects tobacco cells by a series of three waves of reactive oxygen species that contribute to cytotoxicity. Plant, Cell & Environment 29, 1956–1969. https://doi.org/10.1111/j.1365-3040.2006.01571.x

Glasner, J.D., Yang, C.-H., Reverchon, S., Hugouvieux-Cotte-Pattat, N., Condemine, G., Bohin, J.-P., Van Gijsegem, F., Yang, S., Franza, T., Expert, D., Plunkett, G., San Francisco, M.J., Charkowski, A.O., Py, B., Bell, K., Rauscher, L., Rodriguez-Palenzuela, P., Toussaint, A., Holeva, M.C., He, S.Y., Douet, V., Boccara, M., Blanco, C., Toth, I., Anderson, B.D., Biehl, B.S., Mau, B., Flynn, S.M., Barras, F., Lindeberg, M., Birch, P.R.J., Tsuyumu, S., Shi, X., Hibbing, M., Yap, M.-N., Carpentier, M., Dassa, E., Umehara, M., Kim, J.F., Rusch, M.,

Soni, P., Mayhew, G.F., Fouts, D.E., Gill, S.R., Blattner, F.R., Keen, N.T., Perna, N.T., 2011. Genome sequence of the plant-pathogenic bacterium *Dickeya dadantii* 3937. J Bacteriol 193, 2076–2077. https://doi.org/10.1128/JB.01513-10

Glazebrook, J., 2005. Contrasting mechanisms of defense against biotrophic and necrotrophic pathogens. Annu Rev Phytopathol 43, 205–227. https://doi.org/10.1146/annurev.phyto.43.040204.135923

Gonin, S., Arnoux, P., Pierru, B., Lavergne, J., Alonso, B., Sabaty, M., Pignol, D., 2007. Crystal structures of an Extracytoplasmic Solute Receptor from a TRAP transporter in its open and closed forms reveal a helix-swapped dimer requiring a cation for α-keto acid binding. BMC Structural Biology 7, 11. https://doi.org/10.1186/1472-6807-7-11

Govrin, E.M., Levine, A., 2000. The hypersensitive response facilitates plant infection by the necrotrophic pathogen *Botrytis cinerea*. Current Biology 10, 751–757. https://doi.org/10.1016/S0960-9822(00)00560-1

Greenberg, J.T., 1997. Programmed cell death in plant-pathogen interactions. Annual Review of Plant Physiology and Plant Molecular Biology 48, 525–545. https://doi.org/10.1146/annurev.arplant.48.1.525

Grinter, R., Josts, I., Zeth, K., Roszak, A.W., McCaughey, L.C., Cogdell, R.J., Milner, J.J., Kelly, S.M., Byron, O., Walker, D., 2014. Structure of the atypical bacteriocin pectocin M2 implies a novel mechanism of protein uptake. Molecular Microbiology 93, 234–246. https://doi.org/10.1111/mmi.12655

Hammer, N.D., Skaar, E.P., 2012. The impact of metal sequestration on *Staphylococcus aureus* metabolism. Current Opinion in Microbiology, Host—microbe interactions: bacteria 15, 10–14. https://doi.org/10.1016/j.mib.2011.11.004

Hancock, J.G., Huisman, O.C., 1981. Nutrient movement in host-pathogen systems. Annual Review of Phytopathology 19, 309–331. https://doi.org/10.1146/annurev.py.19.090181.001521

Hanikenne, M., 2003. *Chlamydomonas reinhardtii* as a eukaryotic photosynthetic model for studies of heavy metal homeostasis and tolerance. New Phytologist 331–340. https://doi.org/10.1046/j.1469-8137.2003.00788.x@10.1111/(ISSN)1469-8137.HeavymetalsandplantsAug2003

Hantke, K., 2001. Iron and metal regulation in bacteria. Current Opinion in Microbiology 4, 172–177. https://doi.org/10.1016/S1369-5274(00)00184-3

Hassan, S., Hugouvieux-Cotte-Pattat, N., 2011. Identification of Two Feruloyl Esterases in *Dickeya dadantii* 3937 and Induction of the Major Feruloyl Esterase and of Pectate Lyases by Ferulic Acid. Journal of Bacteriology 193, 963–970. https://doi.org/10.1128/JB.01239-10

Hauck, P., Thilmony, R., He, S.Y., 2003. A *Pseudomonas syringae* type III effector suppresses cell wall-based extracellular defense in susceptible *Arabidopsis* plants. PNAS 100, 8577–8582. https://doi.org/10.1073/pnas.1431173100

Haydon, M.J., Cobbett, C.S., 2007. A novel major facilitator superfamily protein at the tonoplast influences zinc tolerance and accumulation in *Arabidopsis*. Plant Physiology 143, 1705–1719. https://doi.org/10.1104/pp.106.092015

He, P., Chintamanani, S., Chen, Z., Zhu, L., Kunkel, B.N., Alfano, J.R., Tang, X., Zhou, J.-M., 2004. Activation of a COI1-dependent pathway in *Arabidopsis* by *Pseudomonas syringae* type III effectors and coronatine. The Plant Journal 37, 589–602. https://doi.org/10.1111/j.1365-313X.2003.01986.x

Heath, M.C., 2000. Hypersensitive response-related death, in: Lam, E., Fukuda, H., Greenberg, J. (Eds.), Programmed Cell Death in Higher Plants. Springer Netherlands, Dordrecht, pp. 77–90. https://doi.org/10.1007/978-94-010-0934-8_6

Heide, T. van der, Poolman, B., 2002. ABC transporters: one, two or four extracytoplasmic substrate binding sites? EMBO reports 3, 938–943. https://doi.org/10.1093/embo-reports/kvf201

Henry, G., Thonart, P., Ongena, M., 2012. PAMPs, MAMPs, DAMPs and others: an update on the diversity of plant immunity elicitors. Biotechnol. Agron. Soc. Environ, ISSN: 1370-6233.

Higgins, C.F., 1992. ABC Transporters: From Microorganisms to Man. Annual Review of Cell Biology 8, 67–113. https://doi.org/10.1146/annurev.cb.08.110192.000435

Higgins, C.F., Hiles, I.D., Salmond, G.P.C., Gill, D.R., Downie, J.A., Evans, I.J., Holland, I.B., Gray, L., Buckel, S.D., Bell, A.W., Hermodson, M.A., 1986. A family of related ATP-binding subunits coupled to many distinct biological processes in bacteria. Nature 323, 448–450. https://doi.org/10.1038/323448a0

Higgins, C.F., Linton, K.J., 2004. The ATP switch model for ABC transporters. Nature Structural

&Molecular Biology 11, 918–926. https://doi.org/10.1038/nsmb836

Hobbs, M., Mattick, J.S., 1993. Common components in the assembly of type 4 fimbriae, DNA transfer systems, filamentous phage and protein-secretion apparatus: a general system for the formation of surface-associated protein complexes. Molecular Microbiology 10, 233–243. https://doi.org/10.1111/j.1365-2958.1993.tb01949.x

Hollenstein, K., Frei, D.C., Locher, K.P., 2007. Structure of an ABC transporter in complex with its binding protein. Nature 446, 213–216. https://doi.org/10.1038/nature05626

Huang, H.-E., Ger, M.-J., Chen, C.-Y., Yip, M.-K., Chung, M.-C., Feng, T.-Y., 2006. Plant ferredoxin-like protein (PFLP) exhibits an anti-microbial ability against soft-rot pathogen *Erwinia carotovora* subsp. *carotovora* in vitro and in vivo. Plant Science 171, 17–23. https://doi.org/10.1016/j.plantsci.2006.01.007

Hugouvieux-Cotte-Pattat, N., Condemine, G., Nasser, W., Reverchon, S., 1996. Regulation of pectinolysis in *Erwinia Chrysanthemi*. Annual Review of Microbiology 50, 213–257. https://doi.org/10.1146/annurev.micro.50.1.213

Hugouvieux Cotte Pattat, N., Condemine, G., Shevchik, V.E., 2014. Bacterial pectate lyases, structural and functional diversity. Environmental Microbiology Reports 6, 427–440. https://doi.org/10.1111/1758-2229.12166

Iriti, M., Castorina, G., Vitalini, S., Mignani, I., Soave, C., Fico, G., Faoro, F., 2010. Chitosan-induced ethylene-independent resistance does not reduce crop yield in bean. Biological Control 54, 241–247. https://doi.org/10.1016/j.biocontrol.2010.05.012

Jin, M.S., Oldham, M.L., Zhang, Q., Chen, J., 2012. Crystal structure of the multidrug transporter P-glycoprotein from *Caenorhabditis elegans*. Nature 490, 566–569. https://doi.org/10.1038/nature11448

Johnson, T.L., Abendroth, J., Hol, W.G.J., Sandkvist, M., 2006. Type II secretion: from structure to function. FEMS Microbiol Lett 255, 175–186. https://doi.org/10.1111/j.1574-6968.2006.00102.x

Jones, J.D.G., Dangl, J.L., 2006. The plant immune system. Nature 444, 323–329. https://doi.org/10.1038/nature05286

Karamanoli, K., Bouligaraki, P., Constantinidou, H.-I.A., Lindow, S.E., 2011. Polyphenolic

compounds on leaves limit iron availability and affect growth of epiphytic bacteria. Annals of Applied Biology 159, 99–108. https://doi.org/10.1111/j.1744-7348.2011.00478.x

Kazemi Pour, N., Condemine, G., Hugouvieux Cotte Pattat, N., 2004. The secretome of the plant pathogenic bacterium *Erwinia chrysanthemi*. PROTEOMICS 4, 3177–3186. https://doi.org/10.1002/pmic.200300814

Khare, D., Oldham, M.L., Orelle, C., Davidson, A.L., Chen, J., 2009. Alternating access in maltose transporter mediated by rigid-body rotations. Molecular Cell 33, 528–536. https://doi.org/10.1016/j.molcel.2009.01.035

Koch, E., Slusarenko, A., 1990. *Arabidopsis* is susceptible to infection by a downy mildew fungus. Plant Cell 2, 437–445. https://doi.org/10.1105/tpc.2.5.437

Kombrink, E., Schmelzer, E., 2001. The hypersensitive response and its role in local and systemic disease resistance. European Journal of Plant Pathology 107, 69–78. https://doi.org/10.1023/A:1008736629717

Korotkov, K.V., Gonen, T., Hol, W.G.J., 2011. Secretins: dynamic channels for protein transport across membranes. Trends in Biochemical Sciences 36, 433–443. https://doi.org/10.1016/j.tibs.2011.04.002

Korotkov, K.V., Hol, W.G.J., 2008. Structure of the GspK–GspI–GspJ complex from the enterotoxigenic *Escherichia coli* type 2 secretion system. Nature Structural & Molecular Biology 15, 462–468. https://doi.org/10.1038/nsmb.1426

Korotkov, K.V., Sandkvist, M., Hol, W.G.J., 2012. The type II secretion system: biogenesis, molecular architecture and mechanism. Nat. Rev. Microbiol. 10, 336–351. https://doi.org/10.1038/nrmicro2762

Kraepiel, Y., Barny, M.-A., 2016. Gram-negative phytopathogenic bacteria, all hemibiotrophs after all? Molecular Plant Pathology 17, 313–316. https://doi.org/10.1111/mpp.12345

Krämer, M., Jäkel, O., Haberer, T., Kraft, G., Schardt, D., Weber, U., 2000. Treatment planning for heavy-ion radiotherapy: physical beam model and dose optimization. Phys. Med. Biol. 45, 3299. https://doi.org/10.1088/0031-9155/45/11/313

Kunkel, B.N., Brooks, D.M., 2002. Cross talk between signaling pathways in pathogen defense. Current Opinion in Plant Biology 5, 325–331. https://doi.org/10.1016/S1369-

5266(02)00275-3

Kunze, G., Zipfel, C., Robatzek, S., Niehaus, K., Boller, T., Felix, G., 2004. The N terminus of bacterial Elongation factor Tu elicits innate immunity in *Arabidopsis* Plants. The Plant Cell 16, 3496–3507. https://doi.org/10.1105/tpc.104.026765

Küpper, H., Mijovilovich, A., Meyer-Klaucke, W., Kroneck, P.M.H., 2004. Tissue- and age-dependent differences in the complexation of cadmium and zinc in the cadmium/zinc hyperaccumulator *Thlaspi caerulescens* (Ganges Ecotype) Revealed by X-Ray Absorption Spectroscopy. Plant Physiology 134, 748–757. https://doi.org/10.1104/pp.103.032953

Küpper, H., Zhao, F.J., McGrath, S.P., 1999. Cellular compartmentation of zinc in leaves of the hyperaccumulator *Thlaspi caerulescens*. Plant Physiology 119, 305–312. https://doi.org/10.1104/pp.119.1.305

Laluk, K., Mengiste, T., 2010. Necrotroph attacks on plants: wanton destruction or covert extortion? *Arabidopsis* Book 8. https://doi.org/10.1199/tab.0136

Lamb, C., Dixon, R.A., 1997. The oxidative burst in plant disease resistance. Annual Review of Plant Physiology and Plant Molecular Biology 48, 251–275. https://doi.org/10.1146/annurev.arplant.48.1.251

Lasat, M.M., Baker, A., Kochian, L.V., 1996. Physiological characterization of root zn2+ absorption and translocation to shoots in zn hyperaccumulator and nonaccumulator species of *Thlaspi*. Plant Physiology 112, 1715–1722. https://doi.org/10.1104/pp.112.4.1715

LES Netto, null, Chae, H.Z., Kang, S.W., Rhee, S.G., Stadtman, E.R., 1996. Removal of hydrogen peroxide by thiol-specific antioxidant enzyme (TSA) is involved with its antioxidant properties. TSA possesses thiol peroxidase activity. J. Biol. Chem. 271, 15315–15321.

Lewinson, O., Lee, A.T., Locher, K.P., Rees, D.C., 2010. A distinct mechanism for the ABC transporter BtuCD–BtuF revealed by the dynamics of complex formation. Nature Structural & Molecular Biology 17, 332–338. https://doi.org/10.1038/nsmb.1770

Li, J., Jaimes, K.F., Aller, S.G., 2014. Refined structures of mouse P-glycoprotein. Protein Science 23, 34–46. https://doi.org/10.1002/pro.2387

Liochev, S.I., Fridovich, I., 2002. The Haber-Weiss cycle—70 years later: an alternative view. Redox Report 7, 55–57. https://doi.org/10.1179/135100002125000190

Locher, K.P., 2016. Mechanistic diversity in ATP-binding cassette (ABC) transporters. Nature Structural & Molecular Biology 23, 487–493. https://doi.org/10.1038/nsmb.3216

Locher, K.P., Lee, A.T., Rees, D.C., 2002. The *E. coli* BtuCD structure: a framework for ABC transporter architecture and mechanism. Science 296, 1091–1098. https://doi.org/10.1126/science.1071142

Loo, T.W., Clarke, D.M., 2005. Recent progress in understanding the mechanism of p-glycoprotein-mediated drug efflux. J Membrane Biol 206, 173–185. https://doi.org/10.1007/s00232-005-0792-1

Mao, B., Pear, M.R., McCammon, J.A., Quiocho, F.A., 1982. Hinge-bending in L-arabinose-binding protein. The "Venus's-flytrap" model. J. Biol. Chem. 257, 1131–1133.

Marciniak, S.J., Yun, C.Y., Oyadomari, S., Novoa, I., Zhang, Y., Jungreis, R., Nagata, K., Harding, H.P., Ron, D., 2004. CHOP induces death by promoting protein synthesis and oxidation in the stressed endoplasmic reticulum. Genes Dev. 18, 3066–3077. https://doi.org/10.1101/gad.1250704

Marschner, H., Römheld, V., Kissel, M., 1986. Different strategies in higher plants in mobilization and uptake of iron. Journal of Plant Nutrition 9, 695–713. https://doi.org/10.1080/01904168609363475

Martínez, J.L., Herrero, M., de Lorenzo, V., 1994. The organization of intercistronic regions of the aerobactin operon of *pCoIV-K30* may account for the differential expression of the *iucABCD iutA* genes. Journal of Molecular Biology 238, 288–293. https://doi.org/10.1006/jmbi.1994.1290

Masclaux, C., Expert, D., 1995. Signalling potential of iron in plant—microbe interactions: the pathogenic switch of iron transport in *Erwinia chrysanthemi*. The Plant Journal 7, 121–128. https://doi.org/10.1046/j.1365-313X.1995.07010121.x

Massé, E., Arguin, M., 2005. Ironing out the problem: new mechanisms of iron homeostasis. Trends in Biochemical Sciences 30, 462–468. https://doi.org/10.1016/j.tibs.2005.06.005

Massé, E., Gottesman, S., 2002. A small RNA regulates the expression of genes involved in iron metabolism in *Escherichia coli*. PNAS 99, 4620–4625. https://doi.org/10.1073/pnas.032066599

Mbengue, M., Navaud, O., Peyraud, R., Barascud, M., Badet, T., Vincent, R., Barbacci, A., Raffaele, S., 2016. Emerging trends in molecular interactions between plants and the broad host range fungal pathogens *Botrytis cinerea* and *Sclerotinia sclerotiorum*. Front Plant Sci 7. https://doi.org/10.3389/fpls.2016.00422

McDevitt, C.A., Ogunniyi, A.D., Valkov, E., Lawrence, M.C., Kobe, B., McEwan, A.G., Paton, J.C., 2011. A molecular mechanism for bacterial susceptibility to zinc. PLOS Pathogens 7, e1002357. https://doi.org/10.1371/journal.ppat.1002357

Mendgen, K., Hahn, M., 2002. Plant infection and the establishment of fungal biotrophy. Trends in Plant Science 7, 352–356. https://doi.org/10.1016/S1360-1385(02)02297-5

Mengiste, T., 2012. Plant immunity to necrotrophs. Annu Rev Phytopathol 50, 267–294. https://doi.org/10.1146/annurev-phyto-081211-172955

Michel, G., Bleves, S., Ball, G., Lazdunski, A., Filloux, A., 1998. Mutual stabilization of the XcpZ and XcpY components of the secretory apparatus in *Pseudomonas aeruginosa*. Microbiology 144, 3379–3386. https://doi.org/10.1099/00221287-144-12-3379

Miethke, M., Marahiel, M.A., 2007. Siderophore-based iron acquisition and pathogen control. Microbiol. Mol. Biol. Rev. 71, 413–451. https://doi.org/10.1128/MMBR.00012-07

Mila, I., Scalbert, A., Expert, D., 1996. Iron withholding by plant polyphenols and resistance to pathogens and rots. Phytochemistry 42, 1551–1555. https://doi.org/10.1016/0031-9422(96)00174-4

Mishra, A.K., Sharma, K., Misra, R.S., 2009. Purification and characterization of elicitor protein from *Phytophthora colocasiae* and basic resistance in *Colocasia esculenta*. Microbiological Research 164, 688–693. https://doi.org/10.1016/j.micres.2008.09.001

Misono, K.S., 2002. Natriuretic peptide receptor: Structure and signaling. Mol Cell Biochem 230, 49–60. https://doi.org/10.1023/A:1014257621362

Mitsuhara, I., Iwai, T., Seo, S., Yanagawa, Y., Kawahigasi, H., Hirose, S., Ohkawa, Y., Ohashi, Y., 2008. Characteristic expression of twelve rice PR1 family genes in response to pathogen infection, wounding, and defense-related signal compounds (121/180). Mol Genet Genomics 279, 415–427. https://doi.org/10.1007/s00438-008-0322-9

Montesano, M., Brader, G., Palva, E.T., 2003. Pathogen derived elicitors: searching for receptors in

plants. Molecular Plant Pathology 4, 73–79. https://doi.org/10.1046/j.1364-3703.2003.00150.x

Mosbahi, K., Wojnowska, M., Albalat, A., Walker, D., 2018. Bacterial iron acquisition mediated by outer membrane translocation and cleavage of a host protein. PNAS 115, 6840–6845. https://doi.org/10.1073/pnas.1800672115

Mulligan, C., Geertsma, E.R., Severi, E., Kelly, D.J., Poolman, B., Thomas, G.H., 2009. The substrate-binding protein imposes directionality on an electrochemical sodium gradient-driven TRAP transporter. PNAS 106, 1778–1783. https://doi.org/10.1073/pnas.0809979106

Münzinger, M., Budzikiewicz, H., Expert, D., Enard, C., Meyer, J.-M., 2014. Achromobactin, a new citrate siderophore of *Erwinia chrysanthemi*. Zeitschrift für Naturforschung C 55, 328–332. https://doi.org/10.1515/znc-2000-5-605

Nairz, M., Schroll, A., Sonnweber, T., Weiss, G., 2010. The struggle for iron – a metal at the host–pathogen interface. Cellular Microbiology 12, 1691–1702. https://doi.org/10.1111/j.1462-5822.2010.01529.x

Neema, C., Laulhere, J.P., Expert, D., 1993. Iron deficiency induced by chrysobactin in *Saintpaulia* leaves inoculated with *Erwinia chrysanthemi*. Plant Physiology 102, 967–973. https://doi.org/10.1104/pp.102.3.967

Neilands, J.B., 1995. Siderophores: Structure and function of microbial iron transport compounds. J. Biol. Chem. 270, 26723–26726. https://doi.org/10.1074/jbc.270.45.26723

Nicaise, V., Roux, M., Zipfel, C., 2009. Recent advances in PAMP-triggered immunity against bacteria: pattern recognition receptors watch over and raise the alarm. Plant Physiology 150, 1638–1647. https://doi.org/10.1104/pp.109.139709

Nies, D.H., Brown, N.L., 1998. Two-Component Systems in the Regulation of Heavy Metal Resistance, in: Silver, S., Walden, W. (Eds.), Metal Ions in Gene Regulation, Chapman & Hall Microbiology Series. Springer US, Boston, MA, pp. 77–103. https://doi.org/10.1007/978-1-4615-5993-1_4

Nomura, K., Melotto, M., He, S.-Y., 2005. Suppression of host defense in compatible plant–*Pseudomonas syringae* interactions. Current Opinion in Plant Biology, Biotic interactions

8, 361–368. https://doi.org/10.1016/j.pbi.2005.05.005

Nouwen, N., Ranson, N., Saibil, H., Wolpensinger, B., Engel, A., Ghazi, A., Pugsley, A.P., 1999. Secretin PulD: Association with pilot PulS, structure, and ion-conducting channel formation. PNAS 96, 8173–8177. https://doi.org/10.1073/pnas.96.14.8173

Nunn, D., 1999. Bacterial Type II protein export and pilus biogenesis: more than just homologies? Trends in Cell Biology 9, 402–408. https://doi.org/10.1016/S0962-8924(99)01634-7

Nunn, D.N., Lory, S., 1993. Cleavage, methylation, and localization of the *Pseudomonas aeruginosa* export proteins XcpT, -U, -V, and -W. Journal of Bacteriology 175, 4375–4382. https://doi.org/10.1128/jb.175.14.4375-4382.1993

Oancea, G., O'Mara, M.L., Bennett, W.F.D., Tieleman, D.P., Abele, R., Tampé, R., 2009. Structural arrangement of the transmission interface in the antigen ABC transport complex TAP. PNAS 106, 5551–5556. https://doi.org/10.1073/pnas.0811260106

Ökmen, B., Doehlemann, G., 2014. Inside plant: biotrophic strategies to modulate host immunity and metabolism. Current Opinion in Plant Biology, SI: Biotic interactions 20, 19–25. https://doi.org/10.1016/j.pbi.2014.03.011

Ong, S.T., Shan Ho, J.Z., Ho, B., Ding, J.L., 2006. Iron-withholding strategy in innate immunity. Immunobiology 211, 295–314. https://doi.org/10.1016/j.imbio.2006.02.004

Orelle, C., Alvarez, F.J.D., Oldham, M.L., Orelle, A., Wiley, T.E., Chen, J., Davidson, A.L., 2010. Dynamics of α-helical subdomain rotation in the intact maltose ATP-binding cassette transporter. PNAS. https://doi.org/10.1073/pnas.1006544107

Palmer, C.-L., Skinner, W., 2002. *Mycosphaerella graminicola*: latent infection, crop devastation and genomics. Molecular Plant Pathology 3, 63–70. https://doi.org/10.1046/j.1464-6722.2002.00100.x

Palmgren, M.G., Nissen, P., 2011. P-Type ATPases. Annual Review of Biophysics 40, 243–266. https://doi.org/10.1146/annurev.biophys.093008.131331

Parkinson, N., DeVos, P., Pirhonen, M., Elphinstone, J., 2014. *Dickeya aquatica* sp. nov., isolated from waterways. International Journal of Systematic and Evolutionary Microbiology 64, 2264–2266. https://doi.org/10.1099/ijs.0.058693-0

Payne, S.M., 1993. Iron acquisition in microbial pathogenesis. Trends in Microbiology 1, 66–69.

https://doi.org/10.1016/0966-842X(93)90036-Q

Pemberton, C.L., Salmond, G.P.C., 2004. The Nep1-like proteins-a growing family of microbial elicitors of plant necrosis. Mol. Plant Pathol. 5, 353–359. https://doi.org/10.1111/j.1364-3703.2004.00235.x

Persmark, M., Expert, D., Neilands, J.B., 1989. Isolation, characterization, and synthesis of chrysobactin, a compound with siderophore activity from *Erwinia chrysanthemi*. J. Biol. Chem. 264, 3187–3193.

Persmark, M., Neilands, J.B., 1992. Iron(III) complexes of chrysobactin, the siderophore of *Erwinia chrysanthemi*. Biometals 5, 29–36. https://doi.org/10.1007/BF01079695

Pollard, A.J., Powell, K.D., Harper, F.A., Smith, J.A.C., 2002. The Genetic Basis of Metal Hyperaccumulation in Plants. Critical Reviews in Plant Sciences 21, 539–566. https://doi.org/10.1080/0735-260291044359

Preston, G.M., 2000. *Pseudomonas syringae* pv. tomato: the right pathogen, of the right plant, at the right time. Mol. Plant Pathol. 1, 263–275. https://doi.org/10.1046/j.1364-3703.2000.00036.x

Pugsley, A.P., 1993. The complete general secretory pathway in gram-negative bacteria. Microbiology and Molecular Biology Reviews 57, 50–108.

Pugsley, A.P., Chapon, C., Schwartz, M., 1986. Extracellular pullulanase of *Klebsiella pneumoniae* is a lipoprotein. Journal of Bacteriology 166, 1083–1088. https://doi.org/10.1128/jb.166.3.1083-1088.1986

Py, B., Loiseau, L., Barras, F., 2001. An inner membrane platform in the type II secretion machinery of Gram negative bacteria. EMBO reports 2, 244–248. https://doi.org/10.1093/embo-reports/kve042

Quiocho, F.A., Ledvina, P.S., 1996. Atomic structure and specificity of bacterial periplasmic receptors for active transport and chemotaxis: variation of common themes. Mol. Microbiol. 20, 17–25.

Ratledge, C., Dover, L.G., 2000. Iron Metabolism in Pathogenic Bacteria. Annual Review of Microbiology 54, 881–941. https://doi.org/10.1146/annurev.micro.54.1.881

Rauscher, L., Expert, D., Matzanke, B.F., Trautwein, A.X., 2002. Chrysobactin-dependent Iron

Acquisition in *Erwinia chrysanthemi* functional study of a homolog of the *escherichia coli* ferric enterobactin esterase. J. Biol. Chem. 277, 2385–2395. https://doi.org/10.1074/jbc.M107530200

Rea, P.A., 1999. MRP subfamily ABC transporters from plants and yeast. Journal of Experimental Botany 50, 895–913.

Rea, P.A., Li, Z.-S., Lu, Y.-P., Drozdowicz, Y.M., Martinoia, E., 1998. From Vacuolar Gs-X Pumps to Multispecific Abc Transporters. Annual Review of Plant Physiology and Plant Molecular Biology 49, 727–760. https://doi.org/10.1146/annurev.arplant.49.1.727

Reuber, T.L., Plotnikova, J.M., Dewdney, J., Rogers, E.E., Wood, W., Ausubel, F.M., 1998. Correlation of defense gene induction defects with powdery mildew susceptibility in *Arabidopsis* enhanced disease susceptibility mutants. Plant J. 16, 473–485.

Reymond, P., Farmer, E.E., 1998. Jasmonate and salicylate as global signals for defense gene expression. Current Opinion in Plant Biology 1, 404–411. https://doi.org/10.1016/S1369-5266(98)80264-1

Rico, A., McCraw, S.L., Preston, G.M., 2011. The metabolic interface between *Pseudomonas syringae* and plant cells. Current Opinion in Microbiology, Host–microbe interactions 14, 31–38. https://doi.org/10.1016/j.mib.2010.12.008

Ridge, P.G., Zhang, Y., Gladyshev, V.N., 2008. Comparative genomic analyses of copper transporters and cuproproteomes reveal evolutionary dynamics of copper utilization and its link to oxygen. PLOS ONE 3, e1378. https://doi.org/10.1371/journal.pone.0001378

Ritter, C., Dangl, J.L., 1996. Interference between two specific pathogen recognition events mediated by distinct plant disease resistance genes. The Plant Cell 8, 251–257. https://doi.org/10.1105/tpc.8.2.251

Rondelet, A., Condemine, G., 2013. Type II secretion: the substrates that won't go away. Research in Microbiology, Bacterial secretion systems: function and structural biology 164, 556–561. https://doi.org/10.1016/j.resmic.2013.03.005

Samanovic, M.I., Ding, C., Thiele, D.J., Darwin, K.H., 2012. Copper in microbial pathogenesis: meddling with the metal. Cell Host & Microbe 11, 106–115. https://doi.org/10.1016/j.chom.2012.01.009

Sambrook, J., Fritsch, E.F., Maniatis, T., 1989. Molecular cloning: a laboratory manual. Molecular cloning: a laboratory manual.

Samson, R., Legendre, J.B., Christen, R., Fischer-Le Saux, M., Achouak, W., Gardan, L., 2005. Transfer of *Pectobacterium chrysanthemi* (Burkholder *et al*. 1953) Brenner *et al*. 1973 and *Brenneria paradisiaca* to the genus *Dickeya* gen. nov. as *Dickeya chrysanthemi* comb. nov. and *Dickeya paradisiaca* comb. nov. and delineation of four novel species, *Dickeya dadantii* sp. nov., *Dickeya dianthicola* sp. nov., *Dickeya dieffenbachiae* sp. nov. and *Dickeya zeae* sp. nov. Int. J. Syst. Evol. Microbiol. 55, 1415–1427. https://doi.org/10.1099/ijs.0.02791-0

Sauna, Z.E., Kim, I.-W., Nandigama, K., Kopp, S., Chiba, P., Ambudkar, S.V., 2007. Catalytic Cycle of ATP Hydrolysis by P-Glycoprotein: Evidence for Formation of the E·S Reaction Intermediate with ATP-γ-S, a Nonhydrolyzable Analogue of ATP. Biochemistry 46, 13787–13799. https://doi.org/10.1021/bi701385t

Sauvonnet, N., Vignon, G., Pugsley, A.P., Gounon, P., 2000. Pilus formation and protein secretion by the same machinery in *Escherichia coli*. The EMBO Journal 19, 2221–2228. https://doi.org/10.1093/emboj/19.10.2221

Scheepers, G.H., Nijeholt, J.A.L. a, Poolman, B., 2016. An updated structural classification of substrate-binding proteins. FEBS Letters 590, 4393–4401. https://doi.org/10.1002/1873-3468.12445

Senior, A.E., Al-Shawi, M.K., Urbatsch, I.L., 1995. The catalytic cycle of P-glycoprotein. FEBS Letters 377, 285–289. https://doi.org/10.1016/0014-5793(95)01345-8

Shah, J., Zeier, J., 2013. Long-distance communication and signal amplification in systemic acquired resistance. Front Plant Sci 4. https://doi.org/10.3389/fpls.2013.00030

Sharom, F.J., 2011. The P-glycoprotein multidrug transporter. Essays Biochem. 50, 161–178. https://doi.org/10.1042/bse0500161

Shevchik, V.E., Robert Baudouy, J., Condemine, G., 1997. Specific interaction between OutD, an *Erwinia chrysanthemi* outer membrane protein of the general secretory pathway, and secreted proteins. The EMBO Journal 16, 3007–3016. https://doi.org/10.1093/emboj/16.11.3007

Shiu, S.-H., Bleecker, A.B., 2001. Receptor-like kinases from *Arabidopsis* form a monophyletic gene family related to animal receptor kinases. PNAS 98, 10763–10768. https://doi.org/10.1073/pnas.181141598

Siarheyeva, A., Liu, R., Sharom, F.J., 2010. Characterization of an asymmetric occluded state of P-glycoprotein with two bound nucleotides: Implications for catalysis. J. Biol. Chem. jbc.M109.047290. https://doi.org/10.1074/jbc.M109.047290

Simmons, C.R., Fridlender, M., Navarro, P.A., Yalpani, N., 2003. A maize defense-inducible gene is a major facilitator superfamily member related to bacterial multidrug resistance efflux antiporters. Plant Mol. Biol. 52, 433–446.

Skelton, A.P.F., Robinson, N.J., Goldsbrough, P.B., 1998. Metallothionein-like Genes and Phytochelatins in Higher Plants, in: Silver, S., Walden, W. (Eds.), Metal Ions in Gene Regulation, Chapman & Hall Microbiology Series. Springer US, Boston, MA, pp. 398–430. https://doi.org/10.1007/978-1-4615-5993-1_15

Soanes, D.M., Alam, I., Cornell, M., Wong, H.M., Hedeler, C., Paton, N.W., Rattray, M., Hubbard, S.J., Oliver, S.G., Talbot, N.J., 2008. Comparative Genome Analysis of Filamentous Fungi Reveals Gene Family Expansions Associated with Fungal Pathogenesis. PLOS ONE 3, e2300. https://doi.org/10.1371/journal.pone.0002300

Spanu, P.D., 2012. The genomics of obligate (and nonobligate) biotrophs. Annual review of phytopathology 50, 91–109. https://doi.org/10.1146/annurev-phyto-081211-173024

Spanu, P.D., Abbott, J.C., Amselem, J., Burgis, T.A., Soanes, D.M., Stüber, K., Themaat, E.V.L. van, Brown, J.K.M., Butcher, S.A., Gurr, S.J., Lebrun, M.-H., Ridout, C.J., Schulze-Lefert, P., Talbot, N.J., Ahmadinejad, N., Ametz, C., Barton, G.R., Benjdia, M., Bidzinski, P., Bindschedler, L.V., Both, M., Brewer, M.T., Cadle-Davidson, L., Cadle-Davidson, M.M., Collemare, J., Cramer, R., Frenkel, O., Godfrey, D., Harriman, J., Hoede, C., King, B.C., Klages, S., Kleemann, J., Knoll, D., Koti, P.S., Kreplak, J., López-Ruiz, F.J., Lu, X., Maekawa, T., Mahanil, S., Micali, C., Milgroom, M.G., Montana, G., Noir, S., O'Connell, R.J., Oberhaensli, S., Parlange, F., Pedersen, C., Quesneville, H., Reinhardt, R., Rott, M., Sacristán, S., Schmidt, S.M., Schön, M., Skamnioti, P., Sommer, H., Stephens, A., Takahara, H., Thordal-Christensen, H., Vigouroux, M., Weßling, R., Wicker, T., Panstruga, R., 2010.

Genome expansion and gene loss in powdery mildew fungi reveal tradeoffs in extreme parasitism. Science 330, 1543–1546. https://doi.org/10.1126/science.1194573

Spurlino, J.C., Lu, G.Y., Quiocho, F.A., 1991. The 2.3-A resolution structure of the maltose- or maltodextrin-binding protein, a primary receptor of bacterial active transport and chemotaxis. J. Biol. Chem. 266, 5202–5219.

Staskawicz, B.J., Mudgett, M.B., Dangl, J.L., Galan, J.E., 2001. Common and Contrasting Themes of Plant and Animal Diseases. Science 292, 2285–2289. https://doi.org/10.1126/science.1062013

Stohs, S.J., Bagchi, D., 1995. Oxidative mechanisms in the toxicity of metal ions. Free Radical Biology and Medicine 18, 321–336. https://doi.org/10.1016/0891-5849(94)00159-H

Tam, R., Saier, M.H., 1993. Structural, functional, and evolutionary relationships among extracellular solute-binding receptors of bacteria. Microbiology and Molecular Biology Reviews 57, 320–346.

Tang, C., Schwieters, C.D., Clore, G.M., 2007. Open-to-closed transition in apo maltose-binding protein observed by paramagnetic NMR. Nature 449, 1078–1082. https://doi.org/10.1038/nature06232

Theodoulou, F.L., 2000. Plant ABC transporters. Biochimica et Biophysica Acta (BBA) - Biomembranes 1465, 79–103. https://doi.org/10.1016/S0005-2736(00)00132-2

Thieme, D., Neubauer, P., Nies, D.H., Grass, G., 2008. Sandwich hybridization assay for sensitive detection of dynamic changes in mrna transcript levels in crude *Escherichia coli* cell extracts in response to copper ions. Appl. Environ. Microbiol. 74, 7463–7470. https://doi.org/10.1128/AEM.01370-08

Thomma, B.P.H.J., Tierens, K.F.M., Penninckx, I.A.M.A., Mauch-Mani, B., Broekaert, W.F., Cammue, B.P.A., 2001. Different micro-organisms differentially induce *Arabidopsis* disease response pathways. Plant Physiology and Biochemistry 39, 673–680. https://doi.org/10.1016/S0981-9428(01)01282-7

Tian, Y., Zhao, Y., Yuan, X., Yi, J., Fan, J., Xu, Z., Hu, B., De Boer, S.H., Li, X., 2016. *Dickeya fangzhongdai* sp. nov., a plant-pathogenic bacterium isolated from pear trees (*Pyrus pyrifolia*). International Journal of Systematic and Evolutionary Microbiology 66, 2831–

2835. https://doi.org/10.1099/ijsem.0.001060

Tomii, K., Kanehisa, M., 1998. A comparative analysis of ABC transporters in complete microbial genomes. Genome Res. 8, 1048–1059. https://doi.org/10.1101/gr.8.10.1048

Toth, I.K., van der Wolf, J.M., Saddler, G., Lojkowska, E., Hélias, V., Pirhonen, M., Tsror Lahkim, L., Elphinstone, J.G., 2011. *Dickeya* species: an emerging problem for potato production in Europe: *Dickeya* spp. on potato in Europe. Plant Pathology 60, 385–399. https://doi.org/10.1111/j.1365-3059.2011.02427.x

Touati, D., 2000. Iron and oxidative stress in bacteria. Archives of Biochemistry and Biophysics 373, 1–6. https://doi.org/10.1006/abbi.1999.1518

Venisse, J.-S., Gullner, G., Brisset, M.-N., 2001. Evidence for the involvement of an oxidative stress in the initiation of infection of pear by *Erwinia amylovora*. Plant Physiology 125, 2164–2172. https://doi.org/10.1104/pp.125.4.2164

Vogel, J., Somerville, S., 2000. Isolation and characterization of powdery mildew-resistant *Arabidopsis* mutants. Proc. Natl. Acad. Sci. U.S.A. 97, 1897–1902. https://doi.org/10.1073/pnas.030531997

Voulhoux, R., Ball, G., Ize, B., Vasil, M.L., Lazdunski, A., Wu, L.-F., Filloux, A., 2001. Involvement of the twin arginine translocation system in protein secretion via the type II pathway. The EMBO Journal 20, 6735–6741. https://doi.org/10.1093/emboj/20.23.6735

Walton, J.D., 1996. Host-selective toxins: agents of compatibility. Plant Cell 8, 1723–1733.

Ward, A., Reyes, C.L., Yu, J., Roth, C.B., Chang, G., 2007. Flexibility in the ABC transporter MsbA: Alternating access with a twist. PNAS 104, 19005–19010. https://doi.org/10.1073/pnas.0709388104

Weinberg, E.D., 1993. The development of awareness of iron-withholding defense. Perspectives in Biology and Medicine 36, 215–221. https://doi.org/10.1353/pbm.1993.0063

Whitby, P.W., VanWagoner, T.M., Springer, J.M., Morton, D.J., Seale, T.W., Stull, T.L., 2006. *Burkholderia cenocepacia* utilizes ferritin as an iron source. Journal of Medical Microbiology 55, 661–668. https://doi.org/10.1099/jmm.0.46199-0

Wilkens, S., 2015. Structure and mechanism of ABC transporters. F1000Prime Rep 7. https://doi.org/10.12703/P7-14

Wojtaszek, P., 1997. Oxidative burst: an early plant response to pathogen infection. Biochemical Journal 322, 681–692. https://doi.org/10.1042/bj3220681

Wolpert, T.J., Dunkle, L.D., Ciuffetti, L.M., 2002. Host-selective toxins and avirulence determinants: what's in a name? Annu Rev Phytopathol 40, 251–285. https://doi.org/10.1146/annurev.phyto.40.011402.114210

Yuan, M., Chu, Z., Li, X., Xu, C., Wang, S., 2010. The Bacterial Pathogen *Xanthomonas oryzae* overcomes rice defenses by regulating host copper redistribution. The Plant Cell 22, 3164–3176. https://doi.org/10.1105/tpc.110.078022

Yuan, M., Li, X., Xiao, J., Wang, S., 2011. Molecular and functional analyses of COPT/Ctr-type copper transporter-like gene family in rice. BMC Plant Biol. 11, 69. https://doi.org/10.1186/1471-2229-11-69

Zaini, P.A., Fogaça, A.C., Lupo, F.G.N., Nakaya, H.I., Vêncio, R.Z.N., Silva, A.M. da, 2008. The iron stimulon of *Xylella fastidiosa* includes genes for Type IV Pilus and Colicin V-Like Bacteriocins. Journal of Bacteriology 190, 2368–2378. https://doi.org/10.1128/JB.01495-07

Zhu, W., Yang, B., Chittoor, J.M., Johnson, L.B., White, F.F., 1998. AvrXa10 contains an acidic transcriptional activation domain in the functionally conserved C terminus. MPMI 11, 824–832. https://doi.org/10.1094/MPMI.1998.11.8.824

Zipfel, C., 2009. Early molecular events in PAMP-triggered immunity. Current Opinion in Plant Biology, Biotic Interactions 12, 414–420. https://doi.org/10.1016/j.pbi.2009.06.003

Zipfel, C., Kunze, G., Chinchilla, D., Caniard, A., Jones, J.D.G., Boller, T., Felix, G., 2006. Perception of the bacterial PAMP EF-Tu by the receptor EFR restricts Agrobacterium-mediated transformation. Cell 125, 749–760. https://doi.org/10.1016/j.cell.2006.03.037